NRL Report 5669

PROJECT CLINKER REPORT NO. 10

[UNCLASSIFIED TITLE]

R. E. Carroll, H. L. Clark,
C. T. McComb, and E. B. McInturff

Applied Optics Branch
Optics Division

October 18, 1961

U. S. NAVAL RESEARCH LABORATORY
Washington, D.C.

NRL Report 5669

PROJECT CLINKER REPORT NO. 10

[UNCLASSIFIED TITLE]

DEVELOPMENT AND PERFORMANCE OF THE AN/AAR-23(XB-1) AIRBORNE PASSIVE SUBMARINE-DETECTION SYSTEM

[CONFIDENTIAL TITLE]

R. E. Carroll, H. L. Clark,
C. T. McComb, and E. B. McInturff

Applied Optics Branch
Optics Division

October 18, 1961

U. S. NAVAL RESEARCH LABORATORY
Washington, D.C.

CONTENTS

ABSTRACT

[redacted]
(unclass)

The AN/AAR-23(XB-1) equipment, an airborne passive detection system for use in airships, is designed to detect the surface scars from completely submerged submarines. This system, developed by NRL, is sensitive to 8-to-13-micron radiation and can passively detect changes in the radiation from the surface of the sea of less than ten parts per million. Tests conducted by NRL showed that this equipment can detect, at night, the scars from submarines operating down to keel depths of 400 ft in sea states up to 5 or 6 for periods up to three hours after the passage of the submarine. Subsequent improvement in detector-element performance should permit this capability from high-speed, fixed-wing aircraft.

PROBLEM STATUS

This is an interim report on one phase of the problem; work on this and other phases is continuing.

AUTHORIZATION

NRL Problem N03-01
BuWeps Task Nos. RUDC-4B-203-F001-05-002,
RUDC-4B-000-652-1/F001-05-002

Manuscript submitted June 27, 1961.

DEVELOPMENT AND PERFORMANCE OF THE AN/AAR-23(XB-1) AIRBORNE PASSIVE SUBMARINE-DETECTION SYSTEM

[[redacted] Title]

Unclass

INTRODUCTION

Project Objectives

Project Clinker is a program of applied research whose purpose is the determination of (a) the radiometric properties of the surface scars produced by completely submerged submarines, (b) the mechanisms involved in the generation of these scars, and (c) the influence of the sea environment upon the detectability of these scars. The program presently consists of studies, from aircraft and surface vessels of actual submarine wakes at sea and one-sixth scale measurements on the midget submarine (SSX-1) operating in Chesapeake Bay.

Background

In 1948, NRL determined that it was possible to detect from the air, with thermal detectors, the invisible surface wakes from completely submerged submarines (1). During the next three years, attempts were made to improve this detection technique on an exploratory basis (2-4) with some degree of success. As this work progressed, it became apparent that an orderly investigation of the basic properties of these wakes was required if this method of detection was to be fully exploited in a reasonable length of time. In the fall of 1950, NRL proposed to the Bureau of Aeronautics a study which required the development and use of a 100-in.-diameter radiometer mounted in the ZPM-4 airship. This radiometer was put in service in November 1954. Shortly thereafter a general opinion developed within the Navy Department that this method of detection held little promise. This feeling was intensified by the lack of success of the AN/AAR-3 equipment, a submarine wake detector developed under contract by the Bureau of Aeronautics for use in fixed-wing aircraft and by a similar lack of success overseas with the British equivalent which had been developed under Project Yellow Duckling. Funding and fleet support difficulties ensued.

Finally though, the first basic measurements of the parameters of the wakes from completely submerged submarines were made in the Oriente Deep off Cuba in the spring of 1956 (5). With these data and increased backing from the Bureau of Aeronautics, the AN/AAR-23(XB-1) was developed by NRL during the next 14 months. The first sea trials were conducted in the North Atlantic during the months of September and October 1958 with the AN/AAR-23(XB-1) mounted in a ZPG-2 airship. Although successful detections were made against submarines operating down to keel depths of 400 ft in sea states up to 5 and 6, aerodynamic difficulties necessitated an eventual redesign of the entire equipment. Sea trials were resumed twelve months later, in October 1959. Successful exercises were conducted during the subsequent two months against submarines operating at keel depths down to 400 ft in both the North Atlantic and Gulf of Mexico. On Dec. 14, 1959, the AN/AAR-23(XB-1) was transferred to the Operational Test and Evaluation Force for evaluation by the Fleet (6,7).

[redacted]

BASIC CONSIDERATIONS

Submarine Signatures

When an airborne radiometer views the surface of the ocean, it sees

1. Radiation emitted by the water
2. Radiation emitted by the intervening atmosphere
3. Radiation emitted by the sky and reflected from the water.

The amounts of each available to the radiometer at a given altitude are determined by their respective temperatures, the transmission of the atmosphere, and the mean angle at which the water facets are viewed. However, by itself the radiometer cannot differentiate; it merely responds to the total radiation available to it.

A completely submerged submarine, proceeding at keel depths down to 600 ft, alters the magnitude of the radiation reaching the radiometer by a detectable amount as the result of modifications to the surface of the water (7). These modifications appear to the radiometer as surface scars above and behind the submarine, from which the total radiation has either increased or decreased by as little as ten parts per million. Detections in sea states up to 5 or 6 have been achieved. Under some conditions the most persistent of the scars has been detected for periods as long as four hours after the passage of the submarine (7).

This performance has been achieved with the NRL-developed AN/AAR-23(XB-1) equipment, which is a scanning radiometer of the differential type sensitive to small radiometric perturbations in the 8-to-13-micron portion of the electromagnetic spectrum. Because of the opacity of sea water in this wavelength region, the choice of design parameters for this equipment was governed by a careful consideration of all of the known or predictable effects which are produced at the air-water interface by a completely submerged submarine and of the best known methods for detecting these changes both actively and passively.

A summary of the known or easily predictable surface effects and the related subsurface effects which are produced by a completely submerged submarine while underway is shown in Fig. 1. These effects are as follows.

Turbulence - Immediately astern the submarine and extending back several thousand yards is a zone of turbulence and bubbles. This zone has been investigated with acoustic gear, bubble detectors, and temperature probes (8-11), and the dispersion of this volume of water has been examined optically behind scale models (12). There is little in all of these data to indicate that the turbulent wake reaches the surface of the water within the first hour, if at all.

Joule Effect - The shaft horsepower of a submarine is expended eventually in the form of heat within the water. Direct temperature measurements made behind one boat utilizing 1600 shp showed the presence of a tube of heated water which measured three feet vertically and which was elevated $0.3^{\circ}F$ at the age of 71 minutes (13). This tube remained in line with the submarine's screws and showed no sign of rising to the surface.

Bernoulli Effect - On the surface of the water and directly over the submarine there exists a hydrodynamic depression followed by a hump. The dimensions of this depression

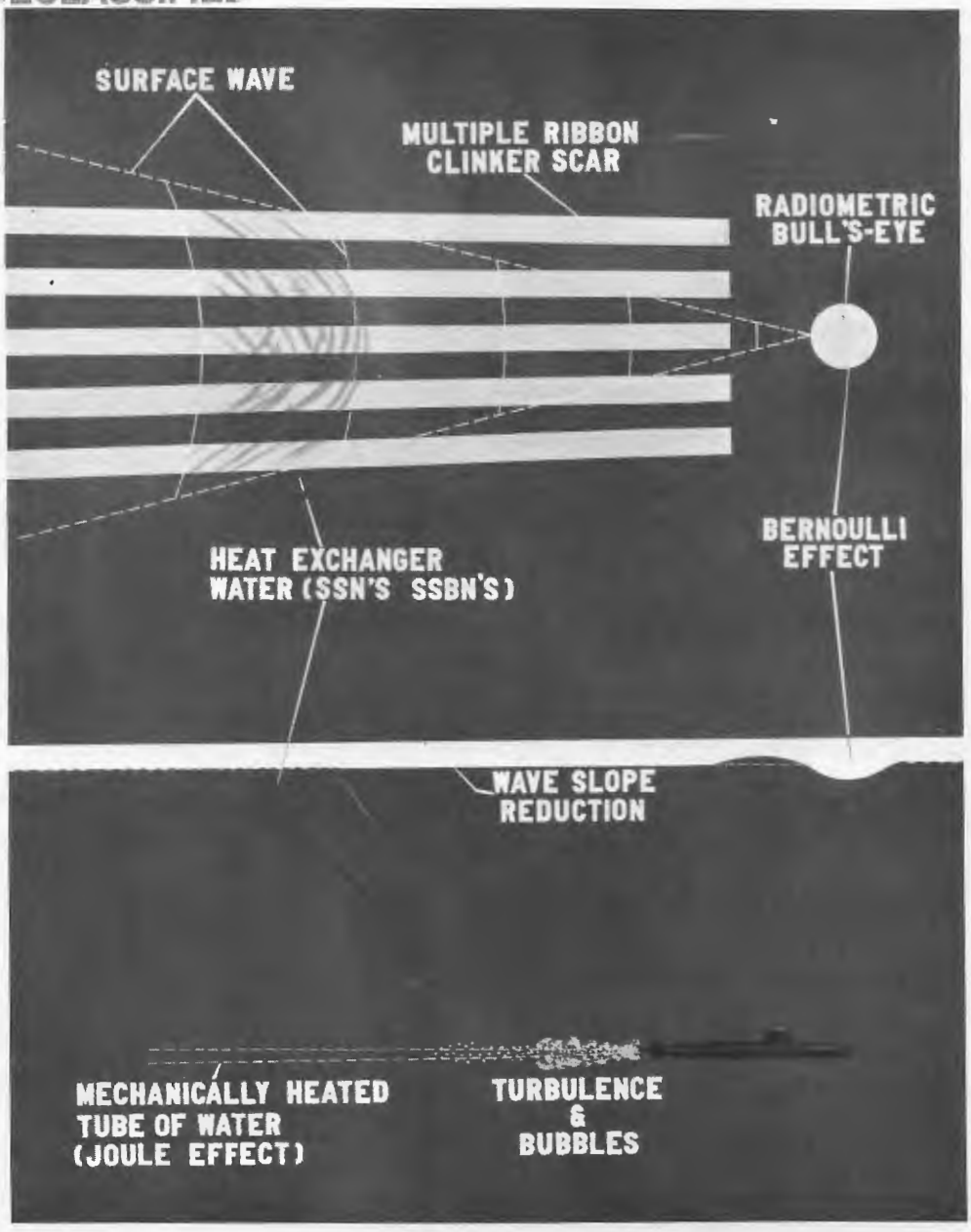

Fig. 1 - Some effects produced by a completely submerged submarine ([redacted])
(unclass)

have been predicted theoretically (14,15), and it has been observed from time to time by Naval aviators. Under certain conditions it can be detected from the air with a radiometer, because its sloping sides radiate and reflect differently than does the surrounding water. Other than serving as an occasionally detectable bullseye directly over the submerged submarine, it is of little value for general long-range target search with passive equipment.

Surface Smoothing - It has been observed visually that a completely submerged Guppy submarine operating on battery power at 6 knots with its conning tower and periscope approximately 15 ft below the surface of the water smooths the surface water above it. The smoothing action extends aft several boat lengths and involves a reduction in the angles of the wave facets of as much as eight degrees (16). This effect is observable under limited conditions when the sea state is approximately one and, like the Bernoulli effect, is useful for pinpointing the target.

Surface Waves - In addition to smoothing out the natural wave pattern on the surface, the completely submerged submarine produces a triangular pattern of transverse waves there also. The magnitude and distribution of the waves in this pattern have been predicted theoretically (14,17), and direct measurements have been made using a scale model (17). Visual and photographic observations of the waves generated by Fleet submarines have been made also. The apex of the surface wave from the USS NAUTILUS proceeding at full speed at keel depths down to 200 ft in hurricane weather has been detected radiometrically and mapped. Detection was possible because the radiation from the slopes of the transverse waves appeared in recognizable geometrical patterns. Theoretically, the amplitude of the transverse waves increases approximately as the cube of the submarine's speed, decreases exponentially with depth, and deteriorates as the square root of the distance astern. Hence it would appear that radiometric detection would be limited to the apex of patterns generated by high speed boats proceeding at not too great depths.

Knuckles - If a submarine accelerates or decelerates in a straight line or makes a sharp turn, a knuckle is generated which produces a radiometric scar at the surface of the water either on or alongside the Clinker track. A turn places the scar alongside the track on the outside of the turn, whereas a change in speed in a straight line places the scar on the track, modifying it. A deceleration, for example, may weaken the radiometric magnitude of the Clinker track. The net result is information in the search aircraft with respect to the submarine's maneuvers.

Heat-Exchanger Water - Submarines with nuclear power employ constantly circulating sea water to cool their heat exchangers. During this process, the water is elevated in temperature and is then put back into the sea. The USS NAUTILUS pumps out 10,000 gallons per minute at an average increase in temperature of $12^{\circ}F$ above the intake temperature. Because of the higher temperature, the discharged water diffuses to the surface after a period of time, the length of which is determined by the depth of the boat (18). A rise period of less than two minutes has been calculated from radiometric data obtained with the USS NAUTILUS operating at a keel depth of 60 ft.

Precursors - Radiometric data obtained by NRL with the AN/AAR-23(XB-1) indicates the possible existence of a surface disturbance which precedes the submarine by as much as three or four miles. However, these data are inadequate either to prove or disprove the definite existence of such an effect.

Clinker Effect - Of all of the known surface effects produced by a completely submerged submarine, the most persistent is the Clinker scar. This is an invisible surface pattern which appears in the area immediately above the submarine and extends aft for a

considerable distance. The lifetime of this scar is determined by the state of the sea, and it may persist as long as four hours. The predominant characteristic of this scar appears to be a multiple, ribbon-like structure (19) depicted in Fig. 1. To an airborne radiometer, the scar appears to consist of a strong center ribbon paralleled symmetrically on either side by ribbons of decreasing magnitude. In most cases, the center ribbon appears colder than the undisturbed water. The bordering ribbons on either side of the center ribbon appear warmer than the undisturbed water but are of smaller radiometric magnitude than the center ribbon. The next pair appears colder and of smaller magnitude; the next, warmer and still smaller, and so on until the edges of the scar are lost in the normal background clutter. As the submarine goes deeper, the radiometric magnitude of the entire scar decreases slowly, the side ribbons become lost in the background noise, and the entire pattern becomes simpler. Because of the persistence of the pattern, the detection and tracking of the Clinker scar was selected as the prime function for which the system was designed.

Radiometric Properties

The total radiation N available to an airborne radiometer which views the surface of the sea may be expressed as (20):

$$N = t(1 - r)\, N_{sea} + t' r N_{sky} + N_{atmos} w/cm^2 - \Omega \qquad (1)$$

where

N_{sea} = self radiation from surface of sea measured at zero distance from surface (watts per sq cm per steradian), dependent on temperature and wavelength

N_{sky} = self radiation from sky measured from sea level (watts per sq cm per steradian), dependent on temperature, water-vapor content, cloud distribution, zenith angle, and wavelength

N_{atmos} = radiation at radiometer from entire atmospheric path between radiometer and surface of the sea (watts per sq cm per steradian), dependent on temperature, water vapor content, and wavelength

t = transmittance of path between sea and radiometer for radiation emitted by sea (fraction), dependent on wavelength

t' = transmittance of path between sea and radiometer for sky radiation reflected from the sea (fraction), dependent on wavelength

r = reflectance of sea (fraction), dependent on angle of depression of radiometer, angles of wave facets or roughness, and wavelength

Ω = solid angle (steradians).

The production of a Clinker scar on the surface of the sea by a completely submerged submarine results in an incremental change in the total radiation available to the radiometer from the scar area. Positive or negative changes as small as ten parts per million have been observed. The individual contributions by the atmosphere, sea, and sky have yet to be determined accurately and completely by direct measurements.

[redacted]

Sea Radiation - When viewed at normal incidence, a dead-calm sea appears to radiate as a gray body (Fig. 2), with an emissivity of approximately 98 percent. The bulk of this radiation originates in the first 0.03 mm of the surface layer. This fact can be deduced from Fig. 3, which shows the measured transmittance of liquid water versus wavelength and pathlength (21). For pathlengths greater than 0.03 mm, less than 20 percent of the radiation over the entire spectral band is transmitted. Hence, the bulk of the radiation viewed by an airborne radiometer must originate at depths of less than 0.03 mm in order to be transmitted properly. This radiation is temperature dependent and can be expressed as

$$N_{sea} = \frac{\sigma T^4}{\pi} \quad w/cm^2 - \Omega \tag{2}$$

where

σ = Stefan-Boltzman's constant

T = Absolute temperature (^{0}K)

π = 3.1416.

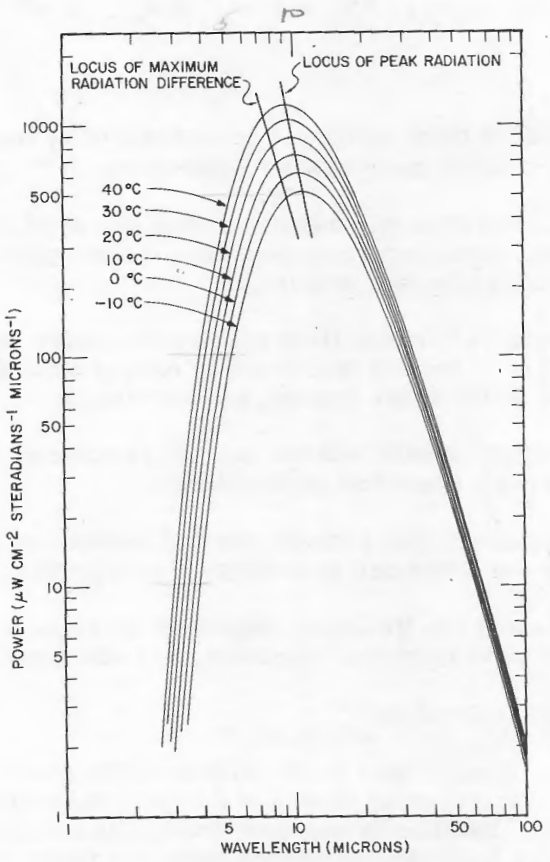

Fig. 2 - Spectral radiation from a gray body with an emissivity of 98 percent (Unclassified)

[redacted]

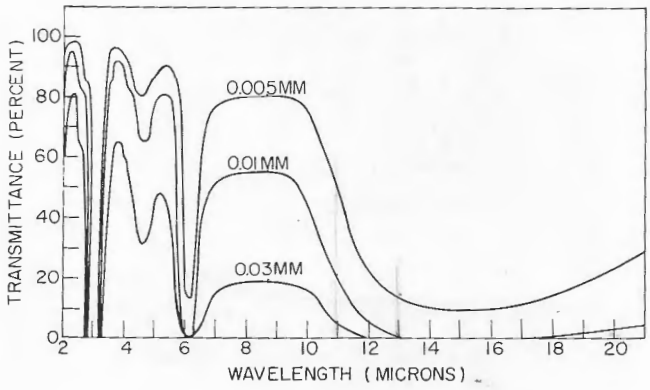

Fig. 3 - Transmittance of pure liquid water (21) (Unclassified)

If the passage of the submarine produces an incremental temperature change at the surface of the sea, a corresponding incremental change takes place in the radiation from the surface layer. A comparison of the spectral-radiation curves of Fig. 2 shows that the greatest change takes place in the wavelength interval where the radiation curve itself peaks, a conclusion that can be reached by comparing the differences in ordinates between adjacent curves. Sea temperatures vary from approximately $-10^{\circ}C$ to $+40^{\circ}C$ and, as shown in Fig. 2, the corresponding spectral curves peak in the wavelength interval between 8 and 13 microns. Because both the ambient radiation and the temperature-produced radiation increments are maximum in this wavelength interval, airborne wake detectors should be designed to operate there.

An approximate expression for the fractional change in the total radiation which is produced by a temperature change can be obtained by differentiating Eq. (2) with respect to temperature and normalizing with respect to the ambient temperature, giving

$$\frac{\Delta N}{N_{sea}} = 4\frac{\Delta T}{T}. \qquad (3)$$

Thus a change of ten parts per million in the radiation from a $20^{\circ}C$ sea could be produced by a temperature change of slightly less than $\pm 0.001^{\circ}C$. Direct measurements at sea of the temperature changes produced within 14 in. of the surface (22) by completely submerged submarines of the conventional type have shown that these changes are inadequate to explain the entire Clinker scar. Other mechanisms appear to be involved. Because of this fact, the design of an airborne wake detector should be based on the radiometric rather than the temperature profiles of the scar.

Sky Radiation - The amount of sky radiation reaching the airborne radiometer by way of reflection from the sea varies with the angle of incidence on the water and the sky gradient itself. Figure 4 is a plot of the reflectivity of pure water versus the angle of incidence (23); Fig. 5 is a plot of apparent sky temperature versus zenith angle for the extremes of sky conditions; clear and overcast (23). If the radiometer views the surface of a dead-calm sea at an angle of 60 degrees, as does the AN/AAR-23(XB-1), it encounters a 6-percent reflective surface which allows it to "see" the sky at a zenith angle of 60 degrees

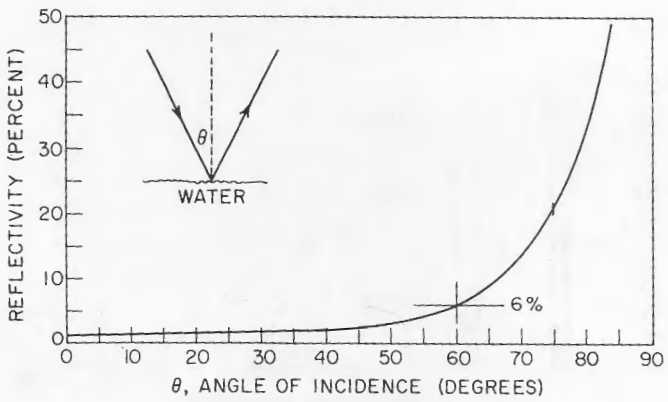

Fig. 4 - Reflectivity of pure liquid water (23) (Unclassified)

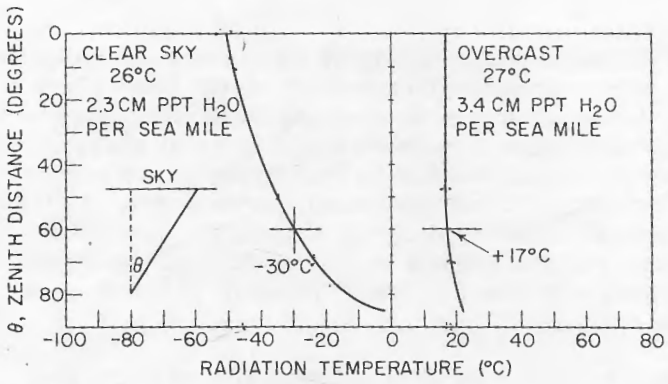

Fig. 5 - Measured radiometric temperatures of the night sky for clear and overcast conditions (23) (Unclassified)

also. At this point in the sky the radiation temperature may vary from $-30^{\circ}C$ to $+17^{\circ}C$. When the sea gets rough, it becomes a diffuse reflector and exposes the radiometer to a band, rather than a point, of sky, the extent of which is determined by the angles of the wave facets. Because the magnitude of the sky radiation varies with wavelength (24) (Fig. 6), the amount reaching the radiometer can be controlled with optical filters to some extent.

An examination of the reflectivity curve (Fig. 4) reveals that the slope of the curve at 60 degrees is 0.5 percent per degree of angle. At that angle of incidence both the reflected sky radiation and the sea radiation will change by 0.5 percent also. One will increase while the other will decrease, or vice versa, in accordance with Eq. (1). The appearance of one-degree wave facets on a dead calm sea, for example, might produce this change. With a clear sky and a dead calm sea, a change in total surface radiation of ten parts per million could be produced by changes in the slopes of the wave facets of less than 0.01 degree. Usually, however, the sea is covered with some form of wave structure, capillary or larger. Hence a broad band of sky is viewed, and the effect of the

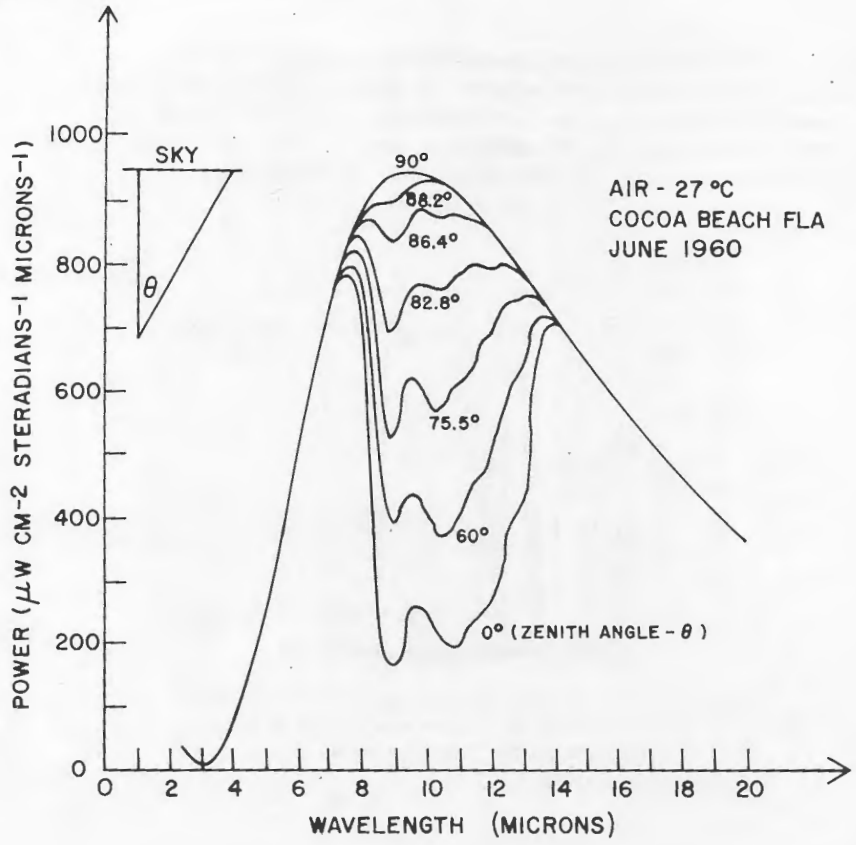

Fig. 6 - Spectral radiation from a clear sky observed at various zenith angles (24) (Unclassified)

change in wave slope is not as pronounced. Nonetheless, it is possible under some conditions to detect with a radiometer the surface-smoothing action, the Bernoulli depression, and the transverse surface waves which are produced by completely submerged submarines. It is conceivable, also, that the passage of the submerged submarine might alter the chemical content of the surface layer and hence its optical properties, so that the reflectivity is changed. Such an alteration would change the proportions of sea and sky radiation reaching the radiometer with the same effect as a change in wave slope. Therefore, the role played by sky radiation is important in the consideration of the design of a radiometric detector, particularly in regard to its spectral response.

Atmospheric Radiation - The role which the atmosphere between the surface of the sea and the airborne radiometer plays in the detection of submerged submarines has not been investigated completely. It is known that the atmosphere absorbs the self radiation from the sea together with the reflected sky radiation in different amounts depending, in each case, on the total water-vapor content in the path, and then reradiates in all directions. It is known, also, that this portion of atmosphere itself radiates as a function of water-vapor content and temperature. It is not known whether the passage of a completely submerged submarine affects the atmosphere in the immediate vicinity of the air-water interface in any way. Hence the design of the airborne detector involves a consideration of

only the absorbent properties of the atmosphere in establishing a sensitivity level which will accommodate the transmission losses. A typical transmission curve for an atmospheric path containing 1.4 centimeters of precipitable water (25) is shown in Fig. 7. It is apparent from this curve that the atmospheric window with the greatest transmission and the widest spectral span is the one between 8 and 13 microns.

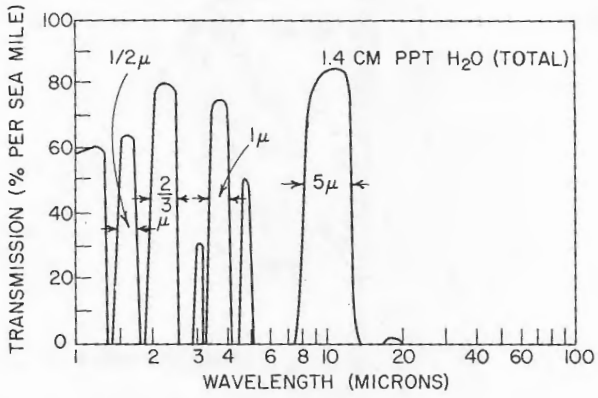

Fig. 7 - Average transmission of atmosphere over a path containing a total of 1.4 centimeters precipitable water (25) (Unclassified)

Physical Properties

Because of its durability and resulting long length, the Clinker scar is the easiest of the submarine-produced surface scars to detect. Some natural slicks and freighter wakes fall into this category also, thus providing false targets. At the present time, the differences in radiometric microstructure between the Clinker scar and these false targets has not been determined accurately and completely enough to be of value for discrimination. Hence the only alternative is to design an airborne wake detector for maximum target-signal to equipment-noise level. This procedure was followed in designing the system.

The first step in the design was a consideration of target size. In order to maximize the target-signal to equipment-noise level, it is necessary to have the radiometer view as much of the target as possible. For this reason target dimensions are important. Figure 8 shows a typical measured profile (19) and a suggested model which could be employed in equipment design. The relative radiometric amplitudes appear to vary with the shape of the submarine's hull, its depth, and the wind force. Thus a submarine with a large conning tower may produce a scar with a very strong center ribbon, increasing depth results in the loss of the minor lobes, and a strong wind will cant the pattern downwind with a smearing action. Therefore, it was decided to design the system to detect the center ribbon only and to ignore the remainder of the scar. For this purpose measurements of the width of the predominant portion of the Clinker scar were made in the Oriente Deep (5) in 1956. The results are summarized in Fig. 9. Instrumentation deficiencies prevented measurements on targets below a keel depth of 100 ft. With these data, it was concluded that the system should be designed to detect scars varying in width from 400 to 2000 ft.

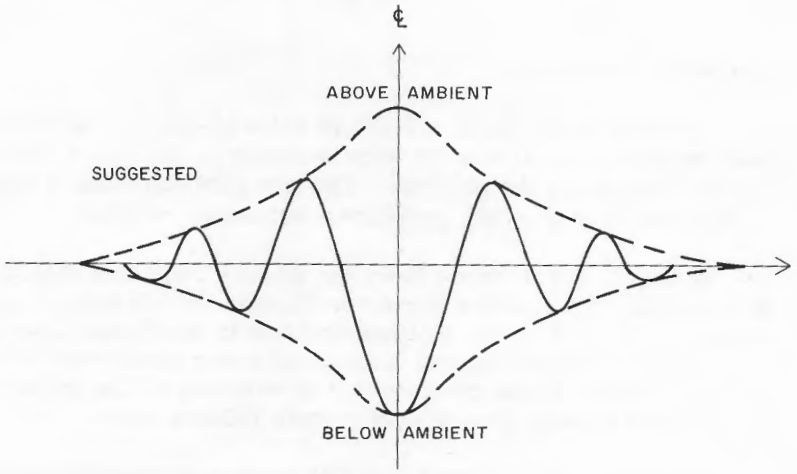

Fig. 8 - Radiometric cross section of a multiple-ribbon Clinker scar (19) ([redacted]) (unclass)

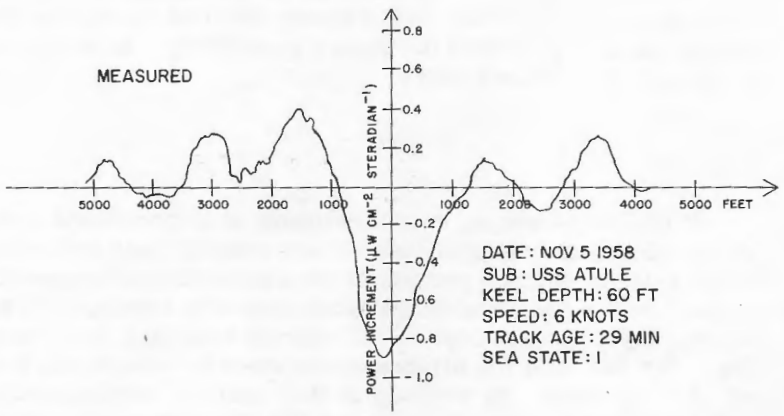

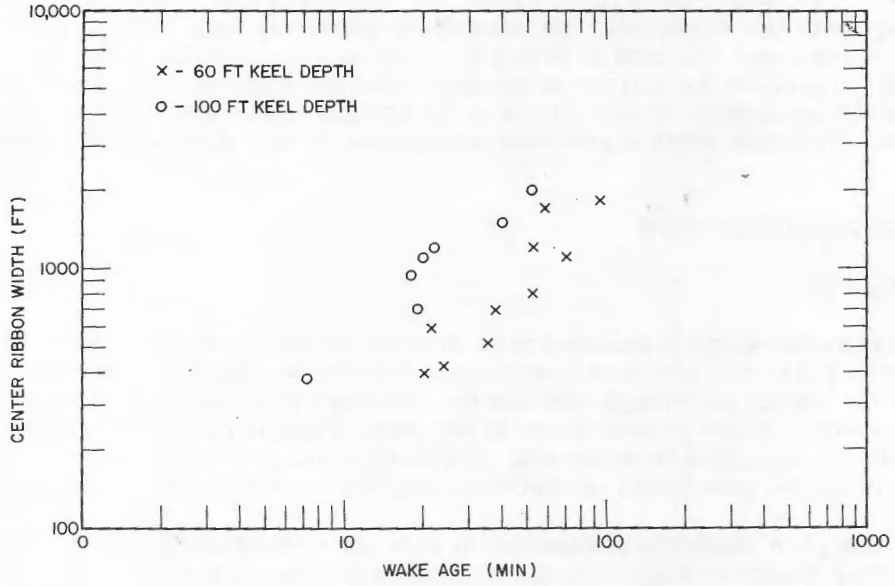

Fig. 9 - Wake widths observed with radiometer viewing sea at an angle of 45 degrees (5) ([redacted]) (unclass)

[redacted]

Celestial Interference

Because of the large amount of 8-to-13-micron radiation in both sun glints and sun's path on the water, it has not been possible to operate a sensitive radiometer successfully against the sea in the daytime. The sun glints provide a high random background noise level, and the sun's path provides a saturating signal.

At night, interference from the moon's radiation reflected from the water provides a wake-like signal under some conditions. Interference from the moon is at minimum when it is in its first or last quarter and is positioned low on the horizon. Maximum interference is experienced from a full moon positioned 20 degrees or higher above the horizon. Under these conditions, the intensity of the moon's path on the water may be 10 to 20 times greater than that of a weak Clinker scar.

In the past, it has been possible to operate radiometers at night in the presence of most lunar interference. Satisfactory daytime operation has not been achieved yet, although considerable hope exists for such a possibility. In view of this, the system was designed to operate in darkness only.

Summary

From the foregoing considerations, it is concluded that the surface scars produced by completely submerged submarines exhibit their radiometric properties most strikingly in the 8-to-13-micron portion of the electromagnetic spectrum. This is true regardless of whether the radiometric perturbations are produced by a temperature change in the surface layer or a change in reflectance resulting in a reapportionment of the sky radiation. The fact that the atmosphere transmits well in the 8-to-13-micron region strengthens the argument. By working in this spectral region at night, it is possible to detect with a passive radiometer not only the multiple-ribbon Clinker scar, but also the Bernoulli depression, the transverse surface waves, the heat-exchanger water, and any surface smoothing above the submarine. Because of the relatively long lifetime of the Clinker scar, the system was designed to detect it. With an internal noise level equivalent to a change in radiation at the surface of the sea of ten parts per million, it was tailored to detect the 400-to-2000-ft center ribbon of the Clinker scar. In operation it proved that it could accommodate these scars from submarines at keel depths down to 600 ft (7).

GENERAL REQUIREMENTS

Spatial Stability

A radiometer which is mounted in an aircraft so that it can view the surface of the sea is subjected to roll and pitch and changes in altitude. All three motions increase or decrease the optical path length between the radiometer and the sea, resulting in corresponding changes in the transmittance of the path. This, in turn, produces a variation in the radiation transmitted from the sea. A change of ten parts per million corresponds to a change in optical path length of approximately 6 in. under normal conditions.

Roll and pitch cause the radiometer to view the surface of the sea at varying angles. The resulting change in angle of incidence allows a different portion of the sky to be viewed and, as in the case of the tilting wave facets, angles as small as 0.01 degree are detectable. In actual practice, the tilting of the radiometer produces both a change in angle of incidence and in optical path length. The combined effect is illustrated in Fig. 10,

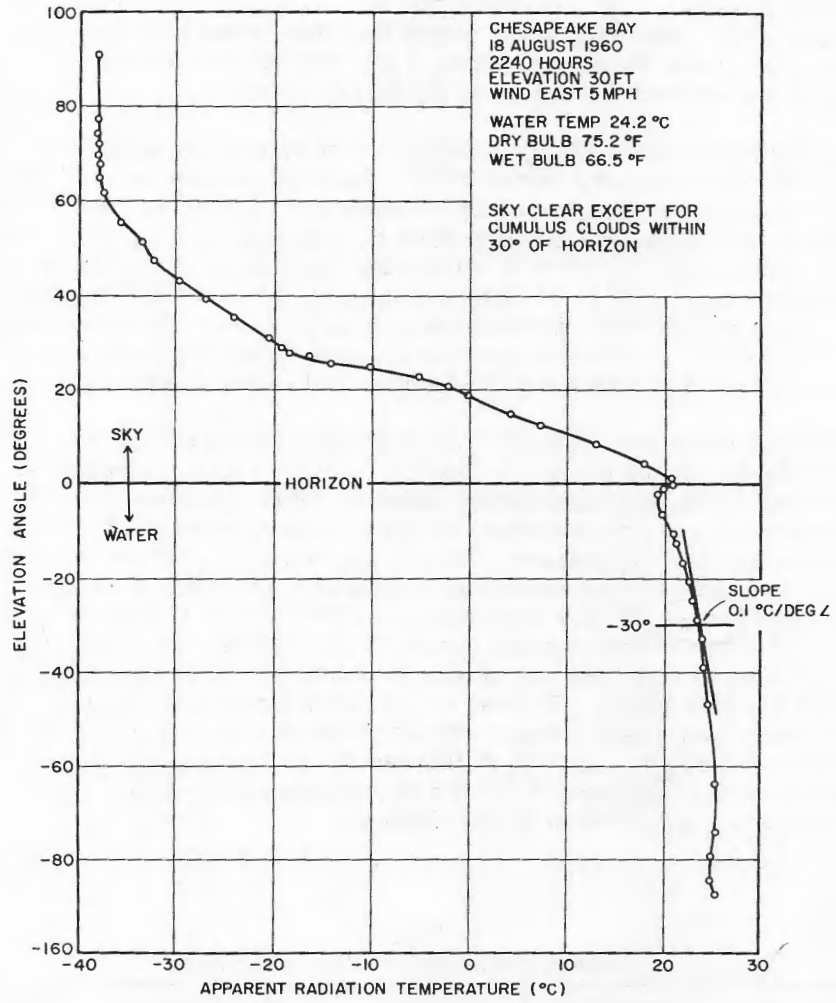

Fig. 10 - Apparent radiometric temperature of the surface of the water plus the intervening atmosphere as a function of viewing angle with the radiometer 30 ft above the surface (26) (Unclassified)

which shows the results of tilting a radiometer while holding it at a fixed distance above the water (26). It will be noted that at an angle of 60 degrees, the slope of this curve is approximately $0.1^{\circ}C$ per degree of angle. From this curve, it is apparent that a radiometer, which can detect a change in surface radiation of ten parts per million, or less than $0.001^{\circ}C$, will be bothered by angular instability of as little as 0.01 degree of arc.

From the foregoing considerations, it is concluded that the airborne radiometer must be gyrostabilized against roll and pitch with an error of less than ±0.01 degree. However, stabilization does not eliminate the effects of the changes in aircraft altitude. A survey of the dynamic characteristics of various Naval ASW aircraft reveals that the flight-stability constants are comparable with the on-target time during a right-angle crossing of a Clinker scar; hence a high false-target ratio will result. The solution to this problem is to allow

the radiometer to scan so that its sweep rate on the water is much greater than the ground speed of the aircraft. Experience has shown that this sweep rate (feet per second) should be no less than 50 times the ground speed of the aircraft in order to permit proper discrimination between aircraft motion and the target crossings.

The angular sensitivity of the radiometer dictates that the scan be a conical one around a circle of constant reflectivity on the water. In order to keep the conical scan on a circle of constant reflectivity within the required limits of ±0.01 degree, both the static and dynamic errors in the gyrostabilization must be less than this amount. Canting of the scan axis as the result of static error will permit the generation of signals of scan frequency as the radiometer describes an eccentric pattern on the water and departs from its chosen circle of constant reflectivity. Dynamic errors will produce spurious signals of the error frequency. Of the two, the static error can be most troublesome because of the close proximity of the scan frequency and the fundamental target frequency.

Because of the size and slow speed of response of the radiometer, the Navy's ZPG-2 airship was selected as the vehicle to carry it. This airship cruises at 40 to 50 knots in still air and exhibits the characteristics listed in Table 1 in turbulent air. Because of these characteristics, it was necessary to select a scan speed of 280,000 ft/min on the surface of the water for the scanner. This is approximately 50 times the ground speed of the airship and satisfies the minimum requirement for discrimination between airship motion and true targets. At this scan speed, a 1000-ft-wide Clinker scan is swept in 0.21 sec, which is 28 times faster than the period of the airship. This provided sufficient frequency separation to permit the use of simple electronic filters to suppress the effects of changes in optical path length. The use of gyrostabilization to minimize the effect of changes in viewing angle on the water was determined impractical for the scanner because of its huge size and weight. Instead, a differential optical configuration plus heavy electronic filtering were employed and proved effective against roll and pitch angles up to ±5 degrees, but at some sacrifice in signal fidelity.

Table 1
Characteristics of ZPG-2 Airship

Turbulence (ft/sec)	Amplitude (degrees)	Rate (degrees/sec)	Acceleration (degrees/sec^2)	Period (seconds)
30 (extreme)	18	15	6	7.5
20 (moderate)	10.8	9	3.6	7.5
10 (light)	5.4	4.5	1.8	7.5

Roll, pitch, and yaw characteristic are essentially the same.
(Goodyear Aircraft Corp. data.)

Circular Scan

The general configuration of the circular scan is shown in Fig. 11. In this figure, let

D = diameter of radiometer aperture (cm)

F = focal length of radiometer optics (cm)

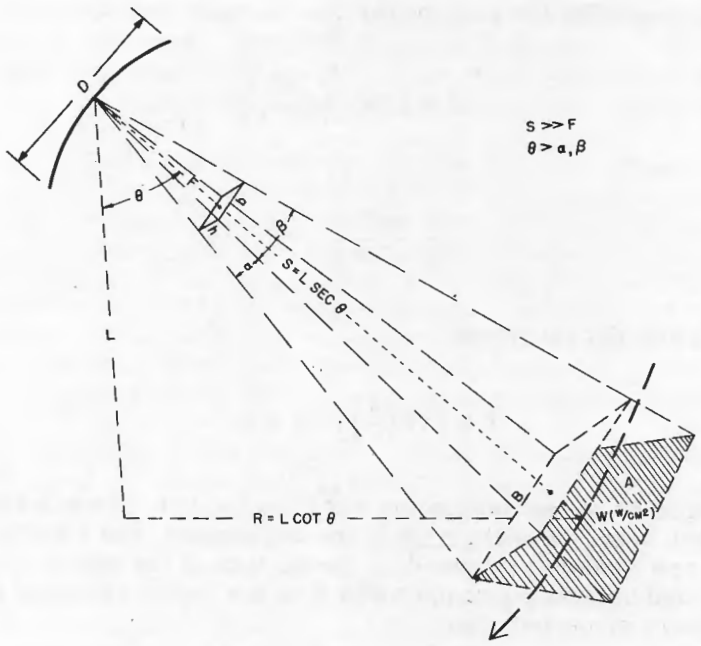

Fig. 11 - Parameters of the circular scan
([redacted])
(unclass)

E = efficiency of optics (fraction)

α = vertical dimension of field of view (radians)

β = horizontal dimension of field of view (radians)

h = height of sensitive element (cm)

b = width of sensitive element (cm)

θ = angle of inclination of radiometer (radians)

L = altitude of radiometer (cm)

R = radius of scan (cm)

S = optical path length to water (cm)

A = area of water viewed (cm^2)

W = radiant intensity of water (watts/cm^2), $W = \pi N$

t = transmittance of atmosphere (fraction)

π = 3.1416.

At the entrance to the radiometer, the flux H is approximately

$$H \approx (t)\left(\frac{WA\cos\theta}{\pi S^2}\right) \tag{4}$$

$$\approx (t)\left(\frac{WA\cos^3\theta}{\pi L^2}\right) \text{ w/cm}^2. \tag{5}$$

[redacted]

The area of water viewed by the radiometer can be expressed approximately as

$$A \approx (\beta S) \left(\frac{\alpha S}{\cos \theta}\right) \tag{6}$$

$$\approx \frac{\alpha\beta L^2}{\cos^3 \theta} \text{ cm}^2. \tag{7}$$

Combining Eq. (5) and Eq. (7) yields

$$H \approx (t) \left(\frac{W}{\pi}\right) (\alpha\beta) \text{ w/cm}^2. \tag{8}$$

The angular dimensions of the radiometer's optical field of view are determined by the width of the Clinker scar, the inclination of the radiometer, and its altitude. Because the submarine scars are randomly oriented on the surface of the sea, a projected field of view whose width and breadth equal the width B of the center ribbon of the scar is preferred. For a square projected area,

$$\alpha \approx \beta \cos \theta \text{ radians.} \tag{9}$$

If the projected dimensions equal the scar width B, then

$$\beta \approx \frac{B \cos \theta}{L} \text{ radians} \tag{10}$$

and

$$\alpha \approx \frac{B \cos^2 \theta}{L} \text{ radians.} \tag{11}$$

Replacing the values of α and β in Eq. (8) with those of Eqs. (10) and (11) gives

$$H \approx (t) \left(\frac{W}{\pi}\right) \left(\frac{B^2 \cos^3 \theta}{L^2}\right) \text{ w/cm}^2, \tag{12}$$

which states that a radiometer whose projected field of view is tailored to the width of the scar receives the largest flux when at zero altitude and zero inclination angle. Operationally, these values are not practical, and a compromise must be made.

The search aircraft must fly at a reasonable altitude and must allow the radiometer to sweep out as large a scan circle as possible for maximum coverage. The data plotted in Fig. 10, indicates that for angles of inclination greater than 70 degrees, the effects of angular instability will increase rapidly. Therefore, an angle of inclination of 70 degrees to the vertical was chosen initially for the optics of the system. This was reduced subsequently to 60 degrees in order to solve the aerodynamic fairing problem on the aircraft.

With a fixed inclination angle, the only remaining way to increase the radius of scan is to increase the operating altitude. This is possible as long as the radiometer remains below cloud cover. Not only do clouds offer a high degree of attenuation, with some being completely opaque, but they form a very noisy background when scanned over from above. Hence the radiometer must remain below all clouds, including the light, wispy ones. Reference to the Hydrographic Charts for the North Atlantic Ocean reveals that clouds can be expected at altitudes as low as 1500 ft approximately 70 percent of the time. Therefore, an operating altitude of 1500 ft was chosen. In terms of the foregoing reasoning, the choice of the last two parameters automatically established the scanning speed of the equipment at 15 rpm and the dimensions of the optical field of view at 6 degrees high by 20 degrees wide.

Sensitivity

The steady radiation from the surface of the sea which is transmitted through the atmosphere to the radiometer is given by Eq. (8). Differentiating both sides of Eq. (8), replacing the differentials with the increments, and transposing gives

$$\frac{\Delta H}{\alpha\beta} \approx (t)\left(\frac{\Delta W}{\pi}\right) \quad w/cm^2 - \Omega \tag{13}$$

where

$$\Delta H << H \text{ and } \Delta W << W.$$

For a 20°C sea, a normal atmosphere, and a submarine-induced radiometric change on the surface of the sea of ten parts per million,

$$t = 0.3 \tag{14}$$

$$\Delta W = 4.2 \times 10^{-7} \quad w/cm^2. \tag{15}$$

Thus

$$\frac{\Delta H}{\alpha\beta} \approx 4 \times 10^{-8} \quad w/cm^2 - \Omega, \tag{16}$$

which is the change in flux at the radiometer produced by a surface change of ten parts per million. Experience has shown that the airborne radiometer should detect 4×10^{-8} watts per square centimeter per steradian with a signal-to-noise ratio of unity or better in order to be operationally useful.

Of the steady flux available at the radiometer (Eq. 8), that collected by it and focused on its sensitive element is

$$P \approx (t)\ (W)\ (\alpha\beta)\left(\frac{D^2}{4}\right)(E) \quad \text{watts.} \tag{17}$$

Differentiating both sides of Eq. (17) and replacing the differential with the corresponding increments, as before, gives

$$\Delta P \approx (t)\ (\Delta W)\ (\alpha\beta) \left(\frac{D^2}{4}\right)(E) \quad \text{watts} \tag{18}$$

where

$$\Delta P << P \text{ and } \Delta W << W.$$

By definition, the Jones' D^* is:

$$D^* = \frac{(a\Delta f)^{1/2}}{NEP} \quad \text{cm} - \text{cps}^{1/2}/\text{watts} \tag{19}$$

where

a = area of sensitive element

Δf = bandwidth of associated electronics (cps)

NEP = Noise Equivalent Power for signal-to-noise ratio of unity.

From Fig. 11,

$$a = hb \approx \alpha\beta F^2 \text{ cm}^2. \tag{20}$$

Combining Eq. (19) and Eq. (20) and transposing gives

$$NEP \approx \frac{(F)\ (\alpha\beta)^{1/2}\ (\Delta f)^{1/2}}{D^*} \quad \text{watts}. \tag{21}$$

The ratio of ΔP and NEP is the signal-to-noise ratio, or

$$\frac{S}{N} \approx \left(\frac{tE}{4}\right)(\Delta W)\ (\alpha\beta)^{1/2}\ \frac{D^2}{F}\ \frac{D^*}{\Delta f^{1/2}}. \tag{22}$$

For a 20°C sea, a normal atmosphere, a typical optical system, and a submarine-induced radiometric change on the surface of ten parts per million,

$$t = 0.3$$

$$E = 0.5$$

$$\Delta W = 4.2 \times 10^{-7} \text{ watts/cm}^2.$$

Thus

$$\frac{S}{N} \approx (1.6 \times 10^{-8})\ (\alpha\beta)^{1/2}\ \frac{D^2}{F}\ \frac{D^*}{(\Delta f)^{1/2}}. \tag{23}$$

It has been shown that for a parabolic optical system, the optimum ratio of focal length to diameter is approximately 0.7 (27), the value chosen for the optics of the system. Equation (23) reduces therefore to

$$\frac{S}{N} \approx (2.2 \times 10^{-8})\ (\alpha\beta)^{1/2}\ (D)\ \frac{D^*}{(\Delta f)^{1/2}}. \tag{24}$$

For the system, with its projected field of view "matched" to the 1000-ft-wide scar,

$$\alpha = 6° = 0.105 \text{ radians} \tag{25}$$

$$\beta = 20° = 0.35 \text{ radians} \tag{26}$$

and hence

$$\frac{S}{N} \approx (4.2 \times 10^{-9})\ (D)\ \frac{D^*}{(\Delta f)^{1/2}}. \tag{27}$$

While scanning, the optical axis of the system sweeps across a 1000-ft-wide scar in 0.21 sec, for a total on-target time of 0.42 sec. Under these conditions, the required bandwidth is approximately 10 cps. Hence

$$\frac{S}{N} \approx 1.3 \times 10^{-9}\ DD^*. \tag{28}$$

For a signal-to-noise ratio of unity, the required mirror diameter is approximately:

$$D \approx \frac{10^9}{D^*} \text{ cm}. \tag{29}$$

From Eq. (29), it is apparent that the more sensitive the detector element, the smaller the required mirror diameter.

For the system, a special radiation thermopile was developed which had a D^* of approximately 10^8 cm/w-cps. With such a detector, the mirror diameter would have to be 10 cm, in accordance with Eq. (20). However, a mirror diameter of 30 in. (76 cm) was chosen, giving a calculated signal-to-noise ratio of 7.6 times for a radiometric change of ten parts per million on the surface of the sea. This selection was made to cover other factors which the calculations did not include. In actual use, in the presence of aircraft vibration and aerodynamic turbulence, the operational noise level of the system proved to be equivalent to less than the specified radiometric change of ten parts per million on the surface of the sea.

Information Rate

Not only must the airborne radiometer provide 100-percent coverage of the search area, it also must examine the target sufficiently often to show any violent evasive maneuver on the part of the submerged submarine. For example, if the submarine were to

make a sharp 90-degree turn, thus producing an L-shaped scar, the airborne radiometer must sample this scar sufficiently to show that it is a turn-off and not a simple termination with the target resting on the bottom. For this reason, it has been determined empirically that the Clinker scar should be sampled every 100 ft of its length.

To do this with the system scanning at 15 rpm while being flown at 40 to 50 knots requires six samples per scan, or one sample every 2/3 sec. This requirement was met by employing six separate optical systems in a single frame which rotated as an integral unit at 15 rpm. Thus the AN/AAR-23(XB-1) became a six-channel system.

Aerodynamics

An airborne radiometer with an 8-to-13-micron spectral sensitivity must operate in a very stable thermal environment in order to keep the background noise level at a minimum. In an aircraft, this condition is achievable by employing a special aerodynamic fairing. This fairing must provide (a) dead air around the radiometer, and (b) laminar air flow across the optical path of the radiometer.

Dead Air - Dead air around the radiometer offers three advantages. The first is that it produces no mechanical loading on the radiometer, a necessity if the unit is gyrostabilized. The second is that it helps insure a uniform air temperature around the radiometer and minimizes the possibility of generating a large signal of scan frequency or higher if the unit were forced to "look" through air of varying temperature as it rotates. Last, the absence of turbulence prevents the random heating and cooling of the radiometer's housing and window. Insulation helps keep the interior of the radiometer thermally stable; however, the window cannot be insulated. If the window transmitted 100 percent, its emissivity would be zero, and there would be no radiation from its backside. Most window materials have emissivities which are two percent or more, resulting in small changes in self radiation as the window temperature varies. Thus turbulent air must not strike the radiometer's window.

Laminar Flow - Laminar air flow beneath the aircraft in the radiometer's optical path is required. Lack of uniformity would cause spurious signals of scan frequency or higher to be generated as the radiometer scanned over the nonuniform air. In this connection, it is essential that the radiometer not be mounted on the aircraft where the hot air and exhaust gases from the aircraft's engines can pass through the radiometer's optical path and produce both random noise and attenuation.

A major effort was spent on the development of fairing for the system by the Airship Test and Development Department, U. S. Naval Air Station, Lakehurst (28). Starting with an APS-20B radome without a bottom, they added fairing in an exploratory manner until the desired performance was attained. Since that time, the state of the art has been advanced by the David Taylor Model Basin through the use of scale models in a wind tunnel (29,30).

Summary

It is concluded that an airborne radiometer which is capable of detecting a change in the total radiation at the surface of the sea of ten parts per million must, when installed in a suitable ASW aircraft, be gyrostabilized against rool and pitch with an angular error of less than ± 0.01 degree and must sweep the surface of the water with a conical scan at a rate greater than 50 times the ground speed of the aircraft. These requirements must

be met in order to minimize the spurious background signals generated by incremental changes in the radiometer's viewing angle and optical path length. The radiometer should be flown below existing cloud cover at a nominal altitude of 1500 ft with its optic axis inclined at an angle of from 60 to 70 degrees to the vertical. This is a compromise between providing reasonable search coverage and obtaining an adequate target signal. The radiometer's optical field of view should be either a square or a circle when projected on the water with a width or diameter equal to the width of the radiometric scar to be detected. This configuration provides for maximum signal strength while accommodating the random orientation of the target. Last, the radiometer should have an operational noise level equivalent to less than 4×10^{-8} watts cm^{-2} $steradians^{-1}$, and, with this detectability, it should examine the target at intervals of no greater than 100 ft along its length to prevent loss of target by evasive action.

DESCRIPTION OF THE AN/AAR-23(XB-1)

Major Components

The AN/AAR-23(XB-1) is a six-channel detection system which consists of three major components (Fig. 12).* These components are (a) a circular scanner which contains six idential optical units, (b) a final amplifier which consists of six identical channels of filtering, amplification, and signal processing, and (c) a three-coordinate mapper which is servo-driven by the scanner and which prints an instantaneous and continuous radiometric map of the area being searched.

General Principle of Operation

The system was designed to be flown at an altitude of 1500 ft and at ground speeds up to 60 knots. From that altitude, it scans, at 15 rpm, the periphery of a 2000-yd-diameter circle on the surface of the sea which is centered about an axis normal to that surface (Fig. 13). Thermal radiation in the wavelength band between 8 and 13 microns, which consists of self radiation from the water, sky radiation reflected from the water, and radiation from the intervening atmosphere, is collected by each of the six optical units in the scanner array and focused on a pair of thermopiles mounted in the focal plane of each mirror. Here it is converted into a voltage which consists of a dc component due to steady radiation plus pulses due to the scans over the target. Because of the manner in which the thermopiles in each pair are connected electrically, the dc component is eliminated, leaving only the target pulses at the output terminals of each pair of thermopiles. These signal pulses are amplified in separate preamplifiers and fed through slip rings to a six-channel final amplifier.

At the final amplifier, the signal pulses are filtered, amplified, dissected, and amplified again. The dissection separates the positive and negative lobes of each signal pulse; these are then equalized, amplified, and fed to the three-coordinate mapper through separate channels. Thus the original six channels become six double channels at the final amplifier.

At the three-coordinate mapper, the signals are separated further by printing those generated during the forward half of the scan independently from those generated during the back half. The combined result of the dissection and separation is a set of four instantaneous and continuous thermal maps printed on electrochemical paper and showing in

*All subsequent figures appear consecutively at the end of the text.

varying tones of gray the positive and negative lobes for each of the two halves of the scan. Because of the relationship between the magnitude of the radiation from the surface scar relative to that from the adjacent water and the polarity of the resulting electrical signal, the two strip maps on the left side of the three-coordinate mapper are referred to as "hot," and the two on right are referred to as "cold." If a surface scar's radiation is less than that from the surrounding water, the predominant part of its signal appears on the fore and aft "cold" maps, with its secondary or complementary features appearing on the fore and aft "hot" maps. If the scar's radiation is greater, the predominant characteristic appears on the "hot" maps, with the complementary portions showing on the "cold" maps. The fact that not only do scars of both polarities exist but that a single scar can change polarity along its length makes it necessary to present the signals of both polarity with maximum contrast; hence, the "hot" and "cold" strip maps.

Overall System Sensitivity

Over the normal range of airship speeds (up to 60 knots), the motion of the aircraft results in a continuous 2000-yd swath being swept out on the water along the aircraft's line of flight. Target samples are taken from a given spot at the rate of six bits every four seconds. Under normal conditions, when the roll and pitch of the aircraft is less than ±5 degrees, the inherent noise level of each of the system's six channels is equivalent to a signal flux of 2×10^{-8} watts per square centimeter per steradian at the equipment. In the presence of random noise, visual integration by the observer at the recorder makes it possible to detect signals that are smaller than the noise. However, under most conditions, thermal discontinuities on the water, such as natural slicks, provide the limiting noise level and prevent the use of full sensitivity. On the other hand, there are occasions when maximum sensitivity can be employed, and it is for the latter situations that the system was designed.

Signal Fidelity

The particular internal electrical connections which are made in each thermopile and which result in the cancellation of the dc signal due to the steady radiation from the surface of the water are primarily to reduce the spurious radiometric signals generated by the roll, pitch, and changes in altitude of the radiometer. This arrangement produces the projected field of view shown in Fig. 13 for each optical unit. The two center sections in each projection, together, are tailored approximately to match the width of a 1000-ft-wide Clinker scar and have the principal function of deriving a signal therefrom. This signal is positive if the scar is colder than the surrounding water. The projection on each side of the center serves the secondary purpose of providing compensation and produces a negative signal. Because the total projected area of the compensating sections equals that of the total area of the center sections, the net signal from a radiometrically uniform sea is zero, provided all of the receivers in each thermopile array are of equal sensitivity.

When one of these arrays scans across a scar of varying width, electrical signals similar to those shown in Fig. 14 are generated. For scar widths equal to or less than 1000 ft, the center section of each field of view produces a signal whose magnitude is proportional to the radiometric magnitude of the scar. The compensating sections add signals also and, for that reason, the latter are removed electronically so that the former can be printed on the system's recorder by itself. There is a pronounced lack of resolution, as can be seen from Fig. 14; the same width signal is produced from scars of any width up to 1000 ft. For scars greater in width than 1000 ft, the compensating sections, acting with the center sections, optically differentiate the signal and produce the second differential therefrom.

Because the effects of the radiometer's roll, pitch, and altitude changes are not completely minimized by the thermopile configuration, electronic filtering is employed to accommodate angular changes up to ±5 degrees. Unfortunately, this filtering eliminates some of the lower subharmonics in the signal, with the result that it is distorted somewhat, with the addition of a small overshoot. If the small overshoot is ignored, the signal from the center of the optical field of view can be considered as still being representative of the radiometric magnitude of the target's scar, provided that the latter's width does not exceed 1000 ft. For target widths in excess of 1000 ft, the equipment produces the second differential of the signal.

At the three-coordinate mapper, where the four strip maps are produced, the fore and aft "cold" maps show the slightly distorted signal from the center section of each field of view together with the small overshoot if the target's track is "cold." The signals from the two compensating sections are printed on the "hot" maps. Should the target's scar be warmer than the surrounding water, the predominant part of the signal appears on the "hot" maps, with the compensating signals on the "cold" map. The predominant part of the signal from a scar 1000 ft or less in width can be identified by its companion overshoot which always trails it. However, when the scar width exceeds 1000 ft, the map becomes quite complicated and serves only to indicate that a target scar is under the aircraft.

Equipment Details

Of the system's three major components – scanner, final amplifier, and recorder – the scanner represents the greatest developmental effort. Three different versions of the scanner were constructed before a satisfactory model was secured. The end result was a compromise between the desire to secure a maximum radiometric signal-to-noise ratio and the operational need for a large search coverage. The problem was complicated further by the aerodynamic problems associated with the installation on the aircraft. Because the designs of the final amplifier and recorder were supplemental to that of the scanner, these too had to be changed with each scanner modification. The various units are described below (31).

Scanner Assembly - The frame of the scanner was constructed of high-tensile-strength aircraft tubing so as to provide a light-weight but yet extremely rigid structure on which all six optical units could be mounted equally spaced around its periphery. Some of the details of the construction are shown in Figs. 15 and 16. The ability of this frame to support the weight of the six optical units offered no problem. However, serious difficulties did arise in providing sufficient rigidity so that the natural frequencies of vibration and flexure of the array were much higher than those of the target signal. Vibration and flexure in the frequency pass band of the system not only created a serious microphonic problem but also allowed each optical unit to scan the water independently with a small amplitude and thereby generate troublesome background signals. This problem was compounded by the requirement that the diameter of the frame be sufficiently great to permit the optical units to be mounted facing inward and downward, so that the required optical clearance hole in the bottom of the surrounding aerodynamic enclosure could be kept as small as possible. The use of a truss-like structure with relatively heavy gussets at all joints helped considerably. Nonetheless, it was found necessary to reduce the scanner's rotation velocity from an initial speed of 30 rpm to 15 rpm in order to reduce the magnitude of vibration. Isolation from the higher-frequency aircraft vibration was provided by having the scanner rotate about a rigid center post (Fig. 17) while being supported on six polyurethane wheels rolling on a smooth, 6-ft-diameter, inclined track (Fig. 18). This isolation was made more effective by driving the scanner with a toothed rubber belt (Fig. 19). The motor drive unit

itself (Fig. 20), which consists of a 28-volt dc aircraft motor coupled to a special gear box, was designed so that none of its parts rotated at, or generated, frequencies in the electronic pass band of the system's signal amplifiers. Consequently, as a result of these and other precautions, the internal noise level of the system in flight is not substantially different from what it is on the ground (Fig. 21).

All six optical units in the scanner array are of identical construction. The main components – mirror, thermopiles and preamplifier, mechanical modulator, and window – are supported by a welded tubular framework which is enclosed in an aluminum skin lined with insulation. A complete optical unit is shown in Fig. 22. The same unit, disassembled, is shown in Fig. 23.

The operation of an optical unit is depicted in Fig. 24. Steady radiation plus signals pass through the polyethylene window and thence through the rotating blades of a "venetian-blind" modulator which chops them at 14 cps. The chopped radiation falls on the collecting mirror, which focuses it on the thermopile receivers. Here the radiation is converted into a 14-cps electrical signal which has most of the dc component due to the steady radiation removed. The signal is amplified by the associated preamplifier and synchronously demodulated by a mechanical rectifier attached to the mechanical choppers. Then it is partially filtered to remove the remaining dc component and is fed out of the optical unit. From there it goes through the scanner's slip rings, through the final amplifier, and to the recorder.

Because of the large size of the optical unit's aperture, polethylene was selected for the window material. It is cheap and easy to handle, considerations which are important when frequent replacement is necessary due to exposure to the minor sandblasting which is encountered during aircraft takeoffs and landings. The polyethylene is 0.004 in. thick and has an average transmission of 70 percent in the 8-to-13-micron region. It is mounted on a ring (Fig. 25) which, in turn, is mounted on the removable front section of the optical enclosure, where it is pulled down and stretched tightly over an elliptical ridge and cruciform. The design of the ridge and cruciform are such as to make the natural vibration frequency of the window very much higher (approximately 200 cps) than the frequency pass band of the detection system. Otherwise the window vibrations, which alter the angle of incidence to the incoming radiation, would produce interfering noise modulation on the radiation which is transmitted.

The "venetian-blind" shutters (Fig. 26), which chop the incoming radiation at 14 cps after it passes through the polyethylene window, do so by rotating continuously in one direction at 7 cps. Two closings and two openings per revolution produce the 14-cps modulation. The blades of the shutter are aluminum and are mechanically coupled with Teflon-coated gears. The entire assembly is driven by two motors, rather than one, for reliability.

The mirror which collects the chopped radiation and focuses it onto the thermopile receivers is a front-surface parabola with a 30-in. diameter and 21-in. focal length. It is pressed from aluminum alloy, polished, and covered with a protective coating of silicon monoxide. Because of the high optical absorption of silicon monoxide (Fig. 27), a coating only 0.5 micron thick is used (32). The optical circle of confusion of the mirror with the coating is less than 0.3 in. in diameter, which is small compared with the off-axis comatic flare.

Located in the focal plane of the mirror are two radiation thermopiles mounted on a common preamplifier (Figs. 28 and 29), for ease in handling. The sensitive area of each thermopile measures 3×8 in. and consists of a multiplicity of thermocouples

[redacted]

connected electrically in a parallel-series arrangement so that, overall, each unit acts as two 3 × 4 in. units in electrical opposition. Each 3 × 8 in. unit is mounted on the preamplifier, so that the 3 × 4 in. portions, which produce a positive voltage when exposed to a relatively cool target, are adjacent and form a 3 × 8 in. total positive receiving area in the center. The negative 3 × 4 in. sections are at each end. It is the optical projection of this array which forms the field of view shown on the water in Fig. 13.

The details of the construction of the thermopile are shown in Fig. 30. Wedges of alternate positive and negative thermoelectric material are stacked side by side with insulating mica sheets between. The positive material is 90-percent antimony and 10-percent bismuth; the negative, 65-percent antimony and 35-percent zinc. To these wedges are spot-welded one-micron-thick gold foils on which is evaporated gold black. The entire array is mounted in an evacuated enclosure capped by a 1/2-in.-thick silver chloride window. Each side of this window is coated with Eastman Kodak 230-S filter material. A protective layer of polystyrene is deposited on the outer window surface. The dc resistance of each 3 × 4 in. section is approximately 1.5 ohms, and the sensitivity is 0.1 volt per watt per square centimeter at 14 cps. The value of D^* for each section at 14 cps is approximately 10^8 cm-cps$^{1/2}$ watt^{-1}. All four sections are connected in series across the primary winding of the preamplifier input transformer. These thermopiles are extremely rugged and exhibit no microphonism under normal conditions of aircraft vibration.

When compared with the performance of the 8-to-13-micron photoconductors which are available today, the performance of the thermopiles used in the system is poor. However, circumstances which existed at the time of the inception of the system development forced their selection. Originally it was intended to employ photoconductors, and the development of a system which utilized them was initiated (33). All of the components for this system were completed except the photoconductor receiver, which never became available. Therefore the entire photoconductor detection system was abandoned, and energy was concentrated on the development of the thermopile.* The use of this particular thermopile rather than a photoconductor necessitated larger optics to compensate for the lower sensitivity and resulted in the huge size of the system's scanner array. However, if other types of receivers readily available at the time had been used, the resulting system would have been either much larger or less reliable or both.

The common preamplifier on which both thermopiles are mounted and to which they are connected electrically is a simple transformer-input, push-pull, RC-coupled, low-signal-level amplifier. The wiring diagram is shown in Fig. 31, and the frequency response is shown in Fig. 32. It has an operational noise level equivalent to 2×10^{-9} volts rms at the input and an overall gain of 2×10^7, which is sufficient to permit operation down to the thermal-agitation noise level of the thermopiles. The dynamic range of the preamplifier allows signal-voltage swings of up to 40 volts at the output without appreciable distortion. Considerable effort was spent on the development of the input transformer for this preamplifier. The problem of providing adequate shielding to keep the induced voltages due to vibration and flexure in the earth's magnetic field at a minimum proved to be a difficult one. A special vibration table had to be constructed, and each design had to be tested on it. The problem was solved by potting the transformer inside a nest of four cylindrical, Mumetal cans with end covers and bringing out the signal leads through staggered holes. This assembly was in turn potted in a very rigid aluminum housing into which was built a nest of seven more cylindircal shields. This structure was bolted securely in place on to a very rigid aluminum casting which formed the base of the preamplifier housing. The

*This work was sponsored by the U. S. Naval Research Laboratory at the Charles M. Reeder Company of Detroit, Michigan.

arrangement is shown in Figs. 33 and 34. Signal leads from the thermopiles to the transformer were made extremely rigid and were clamped at both ends. Other electronic components were mounted with equal care, particularly those associated with the first vacuum-tube stage of amplification. Power for the preamplifier is supplied from a regulated power supply mounted inside the aircraft which, because it had to be fed through the scanner's slip rings, required additional regulation in each preamplifier so supplied. Both B+ and filament voltage-regulating circuits are built into each preamplifier to remove any electrical "hash" which the slip rings might introduce.

After amplification by the preamplifier, the signal is fed in push-pull fashion to the mechanical synchronous rectifier which is mounted on the shaft of one of the blades of the "venetian-blind" chopper. The details of the rectifier are shown in Fig. 35. Coin silver segments, imbedded in an epoxy insulator and mounted on an aluminum hub, rotate with the chopper. Signal application and pickoff are provided by silver graphite brushes. Correct signal phasing is secured by positioning the assembly on the shaft at the proper angle.

The demodulated signals are then fed from the synchronous rectifier back to the preamplifier, where filtering removes the dc component. From there the signal goes to the scanner's slip-ring assembly, along with those from the other five preamplifiers.

The overall characteristics of each optical unit are summarized in Figs. 36 through 38. Figure 36 shows the spectral response of one of the 3×8 in. thermopiles mounted behind a 0.004-in. polyethylene window. Figure 37 is a horizontal cross section of the optical field of view, and Fig. 38 is the vertical cross section. The measured on-axis response to 100^{0}C black-body radiation was found to be 1.8×10^{-9} watts cm^{-2} for a signal-to-noise ratio of unity as observed with the preamplifier's 43-cps bandwidth. The calculated noise equivalent intensity for the two 8.5×6 degree center sections of the field of view combined is, therefore, 5.6×10^{-8} watts cm^{-2} $steradians^{-1}$. Electronic filtering and processing in the final amplifier reduces this to approximately 10^{-8} watts cm^{-2} $steradians^{-1}$. As shown in Fig. 21, the inherent noise levels of the optical units increases slightly in flight; therefore the operational noise equivalent intensity calculated from laboratory measurements is approximately 2×10^{-8} watts cm^{-2} $steradians^{-1}$.

Great care was taken in the design and construction of the scanner's slip rings (Figs. 39 and 40), to insure that the sliding-contact noise which they generate is kept at a minimum. Because the power to, and the signals from, each optical unit are carried by these rings, this noise had to be kept down. Coin silver rings with silver-graphite brushes mounted three per ring are employed. The danger of coupling or leakage between circuits was eliminated by shielding and proper spacing with good insulation between components. As a result, the slip rings have given trouble-free performance.

Positions information is supplied from the scanner to the three-coordinate mapper. A type 15CXa synchro transmitter is used to provide the mapper with angular position information; the mapper is thereby kept synchronized with the scanner. For convenience, the synchro is mounted on the slip-ring assembly. In order to check the servo alignment between the mapper and scanner, a microswitch, closed momentarily when the number one optical unit looks forward of the aircraft, is employed. The mounting arrangement is shown in Fig. 41. The use of this device and others is the result of the desire to make it possible to check out the entire system in flight if necessary.

Final Amplifier - The final amplifier, which is shown in Figs. 42-45, contains six identical processing channels, one for each of the six optical units in the scanner array. The schematic is shown in Fig. 46, and the functions of the various stages are depicted in Fig. 47.

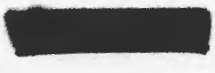

When the signal arrives at the final amplifier from the preamplifier, it is passed first through a low-frequency cutoff filter, then through a high-frequency cutoff filter, and finally through a rejection filter. The low-frequency cutoff filter eliminates the 1/4-cps signal produced by the 15-rpm rotation of the scanner when its axis is not vertical, and the 1/10-cps signal produced by the roll and pitch of the airship. The high-frequency cutoff filter eliminates the 28-cps rectification ripple. Initially, this amount of filtering proved adequate. However, it was found that the "venetian-blind" choppers on the optical units could generate a strong 7-cps signal as they rotated if one side of each blade became dirtier than the other side or if the assembly were improperly mounted, causing the shutters to bind and hence to vary in speed during each revolution. To eliminate the resultant 7-cps signal, a parallel-T RC rejection filter was added to the filter section of each channel. The resultant overall frequency response is shown in Fig. 48.

The change in the shape of the signal pulse as it passes through the final amplifier is shown in Fig. 47. The details of the signal pulse before and after filtering are shown in Fig. 49 for the case of a cold scar of relatively small width. Filtering has left the first and second lobes of the signal pulse relatively unchanged but has increased the size of the third lobe and has added a small fourth lobe. The fourth lobe is an overshoot due to the lack of adequate low-frequency response of the filter. However, the need for sufficient attenuation at the 1/4-cps rotational frequency of the scanner necessitated the compromise in signal fidelity. Of course, had it been practical to gyrostabilize the scanner to prevent canting of the rotational axis and thereby minimize the magnitude of the scan-generated signal, less filtering and hence better signal fidelity could have been achieved.

After filtering, the signal is amplified and dissected as shown in Fig. 47. The positive lobes are separated from the negative lobes, and both are treated independently throughout the remainder of the system. After dissection, the signal lobes are amplified again and are fed to the three-coordinate mapper. The final amplification is accomplished by chopping the signal at 400 cps, amplifying it, then rectifying it. This procedure results in a saving in weight and size of components and permits both negative and positive signal lobes to emerge in their respective channels with negative polarity for use, without further processing, by the styli in the three-coordinate mapper.

Three-Coordinate Mapper - The three-coordinate mapper derives its name from the fact that it prints a two-dimensional map in varying tones of gray whose intensity is proportional to the amplitude of the applied signal. A front view of the mapper is shown in Fig. 50; an interior view, in Fig. 51. The mapper employs electrochemical paper which passes through the recorder from top to bottom at a rate proportional to the ground speed of the aircraft. On this paper are printed four strip maps side by side. One pair of strip maps shows only the positive lobes of each signal pulse, and the other pair the negative lobes. In each pair the signals from the forward half of the scan are printed on one strip, and those from the back half of the scan on the other strip. If the target's scar on the water is "cold," the predominant part of the signal plus its small overshoot are printed on the right, or cold, side of the recorder as indicated in Fig. 52, with the supplementary portions being printed on the left, or "hot," side. If the target's scar is warm, the positions are reversed. In this case the predominant part of the signal appears on the left side, and the supplementary portions on the right. Controls for the recorder include a paper speed adjustment calibrated directly in knots ground speed, a six-gang sensitivity control, and a crab-angle compensator which permits the signals to be printed with respect to the airship's true course rather than its crabbed heading.

The electrochemical paper was developed by NRL (34). It is different from other papers in that it contains all of the chemicals necessary for the printing process and does not produce stylus erosion when the signal current flows. In addition it allows the

presentation of more steps on the gray scale than is possible to achieve by any other method of signal recording. The three-coordinate mapper employs this paper in 24-in. widths and in 400-ft rolled lengths.*

The mechanical arrangement for printing the four strip maps is shown in Fig. 52. The electrochemical paper passes between a heavy glass door, on which are mounted four platinum-iridium crescents, and four servo-driven drums, on each of which are mounted six platinum-iridium styli. The action of a crescent-drum combination is depicted in Fig. 53. Signals are fed from the final amplifier to the styli through segmented commutators and thence through the electrochemical paper to the crescent. The combined action of the commutator segments and the crescent is to allow each stylus to print only during a half revolution of each complete rotation of the scanner. The commutator segments and styli are positioned on the drum to permit sequential printing, and the crescent is shaped to allow nesting of these printings without overlap. Figure 54 shows the details of the stylus construction. This is an adaptation of the type used by NRL underwater sound studies (35). The multifinger design allows the paper fibers to be accommodated independently without lifting the entire array off the paper and thereby permits the production of a uniformly printed line. Each stylus prints a 1/8-in.-wide band on a 5-in.-diameter circle. Together, six of these styli on any drum print a continuous map without blank spaces for all normal ground speeds and practical altitudes of the airship. The results of the printing action are depicted in Fig. 55.

The printing drums in the mapper are rotated in synchronism with the scanner by means of a Lear servoamplifier and motor (Fig. 51). Electrical signals from the synchro transmitter at the scanner are fed to the servo combination through a differential transmitter mounted on the mapper's control panel. Manual rotation of the differential's rotor provides crab-angle compensation. From there, the signals are treated in a conventional manner by the servo unit to provide the continuous follow up.

A switch is provided on the mapper's control panel which when depressed places a mark on the extreme left strip map. This mark corresponds to a dead-ahead signal from the number one optical unit in the scanner array. This mark is triggered by a momentarily closing microswitch at the scanner and appears in the top center of the strip map if the mapper is properly synchronized with the scanner. If not, the proper adjustments can be made while in flight to secure proper synchronization.

Adjustment of the paper speed is secured by means of a potentiometer which feeds a variable amount of dc current into a simple magnetic power amplifier which, in turn, controls a Mark 16 servo motor geared to the paper-drive rollers. Stability is provided by negative feedback from a tachometer generator attached to the servo motor.

Once the initial adjustments – paper speed, sensitivity, and crab angle – have been made, the operation of the mapper is automatic and instantaneous. The problem is the operator's boredom and resulting inattentiveness. Because of this, the mapper was designed with a large, orange, transparent door through which the last ten miles of track can be viewed with maximum contrast. Thus if the operator misses the initial contact with the target during a crossing, he may see it later and, since the scar will remain on the water for some time, he can request another pass for additional details or for tracking purposes.

*In order to provide an adequate supply of paper for the AN/AAR-23(XB-1), NRL contracted with Ricbet Industries of Merchantville, New Jersey to produce it with government-owned equipment.

Power Supplies – In order to insure maximum reliability, the power for the system is distributed as shown in Fig. 56. The prime source of power is the airship's 28-volt dc line. Separate circuit breakers are provided for the scanner drive and for the equipment's electronic units.

Power is fed to the scanner's drive motor through a starter box which, because of the scanner's mass, is applied slowly through a series dropping resistor. After ten seconds, a time-delay removes this resistor and applies full power, bringing the huge scanner smoothly up to speed. Emergency shutdown is possible at the three-coordinate mapper or at the circuit breakers.

Single-phase, 120-volt, 400-cps power is utilized by the electronic units. In order to secure adequate regulation, it was necessary to employ a standard, military, 1500-VA inverter followed by an electronic regulator. The highly regulated 400-cps power from the regulator is supplied to the preamplifier's power supply and to the final amplifier's power supply.

The power supply for the six preamplifiers is shown in Figs. 57-59. This unit contains two 300-volt dc regulated supplies and six dc filament supplies. It is wired so that one 300-volt supply powers the even-numbered preamplifiers, while the other powers the odd-numbered ones. In this way, failure of one power supply deactivates only half of the preamplifiers. Monitoring meters for voltage and current are provided and can be inserted into the supply lines to each preamplifier in sequence by means of a selector switch. The schematic is shown in Fig. 60.

The power supply for the final amplifier is shown in Figs. 61-63. It contains two 300-volt dc regulated supplies for the filter and amplifier sections in the odd and even channels respectively, two 440-volt dc supplies for the driver stages in the odd and even channels, six 220-volt dc supplies for the power stages in each channel, and six 6.3-volt ac filament supplies for each channel. Failure of any supply will deactivate only a portion of the system. Voltmeters and a selector switch are provided for monitoring each supply line to the final amplifier in sequence. The schematic is shown in Fig. 64.

Aircraft Installation

The system was installed in the ZPG-2 airship, No. 141561 (Fig. 65), at the Naval Air Station, Lakehurst, New Jersey. The three-coordinate mapper and the electronic units were installed in the ASW compartment (Fig. 66), the inverter in the engine compartment (Fig. 67), the starter box in the bilge area (Fig. 68), and the circuit breakers in the mechanic's compartment Fig. 69.

The scanner was mounted in the airship's APS-20B radome, with the bottom left off. Because the airship normally flies in a 4-degree nose-up condition, the installation was made with the scan axis inclined 4 degrees aft so that it would be vertical in flight. The first model of the scanner was never installed in the airship because of its poor vibration characteristics. A second model, which had the optical units inclined 70 degrees to the vertical, was installed. However, when it became apparent that aerodynamic fairing had to be added to the radome, a third and final model was constructed with the optical units inclined 60 degrees to the vertical so that they could "see under" the fairing. This final model was completely enclosed in an aluminum skin of its own, which included a saucer-like annular ring, or skirt, around its lower periphery. This enclosure was rigidly attached to the scanner and rotated with it inside of the modified radome. The combination of external and internal fairing solved the aerodynamic problems associated with the earlier model

and made it possible to operate successfully, provided that the airship did not nose up more than a total of 9 degrees from horizontal. Beyond this angle, the enclosure scooped cold air which resulted in the generation of a spurious dead-ahead signal. The external fairing is shown in Fig. 70. Figure 71 shows the aerodynamic skirt attached to the scanner.

Calibration

All six optical units were checked and calibrated in the laboratory prior to installation in the airship, as were the final amplifier and three-coordinate mapper. Once installed, a second method of calibration, which did not necessitate removal of equipment, was employed. For this purpose a special calibrator, which can be hung over the aperture of each optical unit, was developed. Figure 72 shows the calibrator mounted in calibrating position. The essential parts of this device are a 30-in.-diameter, f/0.7, parabolic mirror in the focal plane of which is mounted a thermal signal generator (Fig. 73). Radiation from the generator is focused at infinity through a 50:1 mesh attenuator (Fig. 74). The details of the signal generator itself are shown in Figs. 75 and 76. A temperature-controlled black-body radiator is mounted on an endless belt which moves through the mirror's focal plane behind a curved field stop which compensates for the vignetting produced by the mirror housing. The size of the black-body radiator and its linear speed along the belt are equivalent to the actual scan, in flight, of an optical unit across a 500-ft-wide thermal scar on the water. By mounting and operating the thermal calibrator on one unit at a time, all six channels of the system can be completely calibrated in sequence in less than 20 minutes. Typical signals are shown in Fig. 49. The first is the output of the pre-amplifier as observed through an auxiliary 0.01-to-5-cps bandwidth filter. The second is the filtered signal, and the third is the current through the electrochemical paper in the three-coordinate mapper.

With this calibrator, it has been possible to maintain the system with ease. Calibrations have been made on the average of every two months during the past 18 months and have shown that the entire equipment is remarkably stable.

TEST FLIGHTS WITH 70-DEGREE MODEL

A total of five tests were made against submerged submarines using the original model of the AN/AAR-23(XB-1), in which the optical units viewed the water at an angle of incidence of 70 degrees. Two of these tests were made with the Guppy submarines BLENNY and GROUPER, and three with the nuclear submarine NAUTILUS. Some of the results obtained from these tests are shown in Charts 1-5. In all cases, the submarines operated in deep water in the area designated 39°N by 71°W, off the Continental Shelf approximately 150 miles due east of Atlantic City, New Jersey. After diving, each submarine proceeded on a straight-line course perpendicular to the prevailing wind, releasing special marker buoys (36) at prescribed intervals. All runs were made at night during the period of Sept. 23 through Oct. 30, 1958. On Sept. 29, hurricane Helene went through the area and afforded a chance to observe the operation of the system in rough weather. Detections were made during all five tests in spite of the fact that the enclosure around the system's scanner proved aerodynamically unsatisfactory.

Chart 1 shows a portion of the Clinker scar behind the USS GROUPER underway at 6 knots and a keel depth of 100 ft. The airship, with the system aboard, approached the submarine from ahead and crossed her scar at an angle of approximately 45 degrees. After traveling approximately 5000 yd, the airship turned off to starboard. When this record was obtained, the sea was almost dead calm and there were numerous slicks in

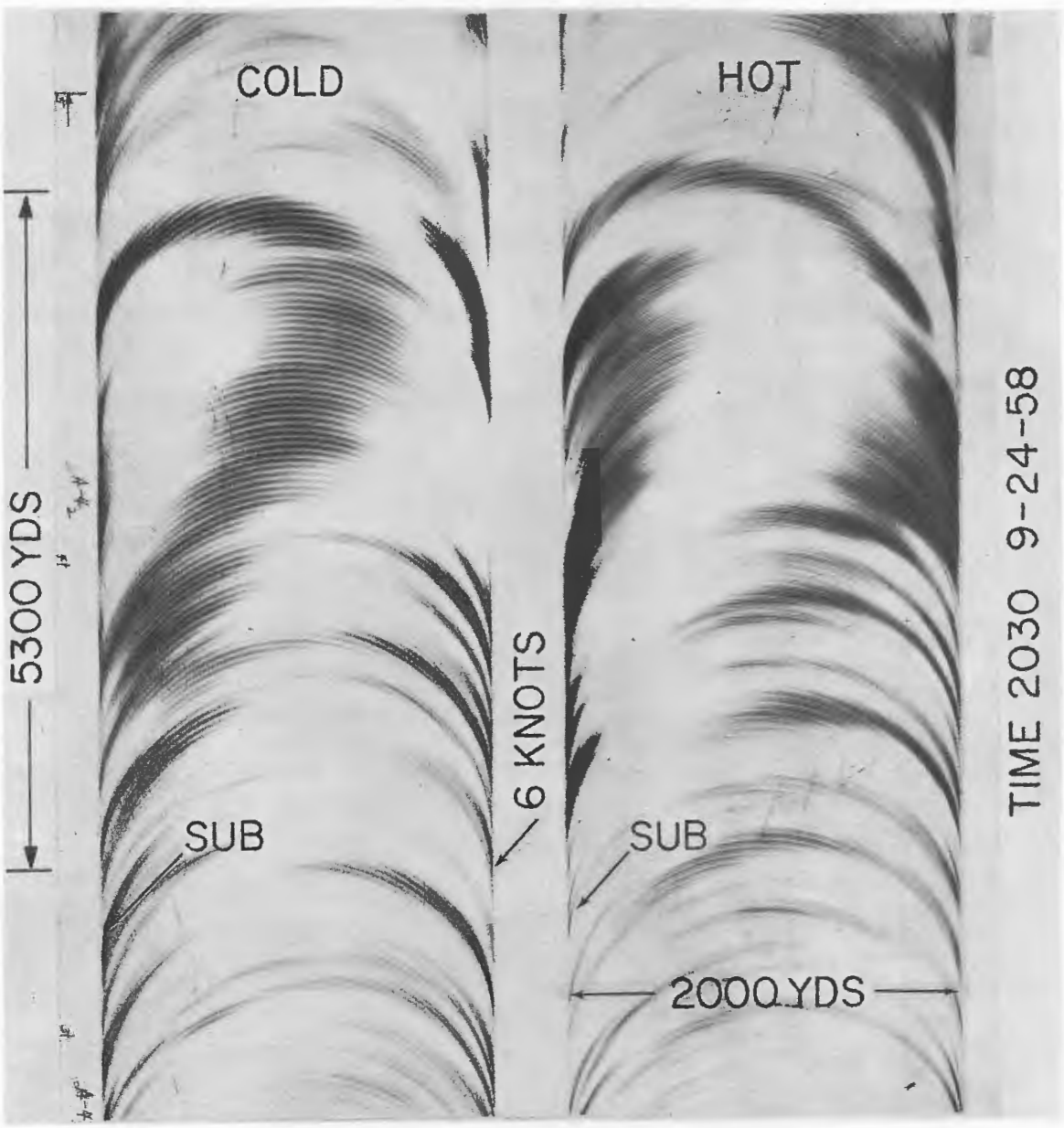

Chart 1 - Section of the scar behind USS GROUPER (5300 yards) as she proceeds at 6 knots at a keel depth of 100 ft. Apparent curvature in scar is due to airship turning off track. ([redacted])

(unclass)

[redacted]

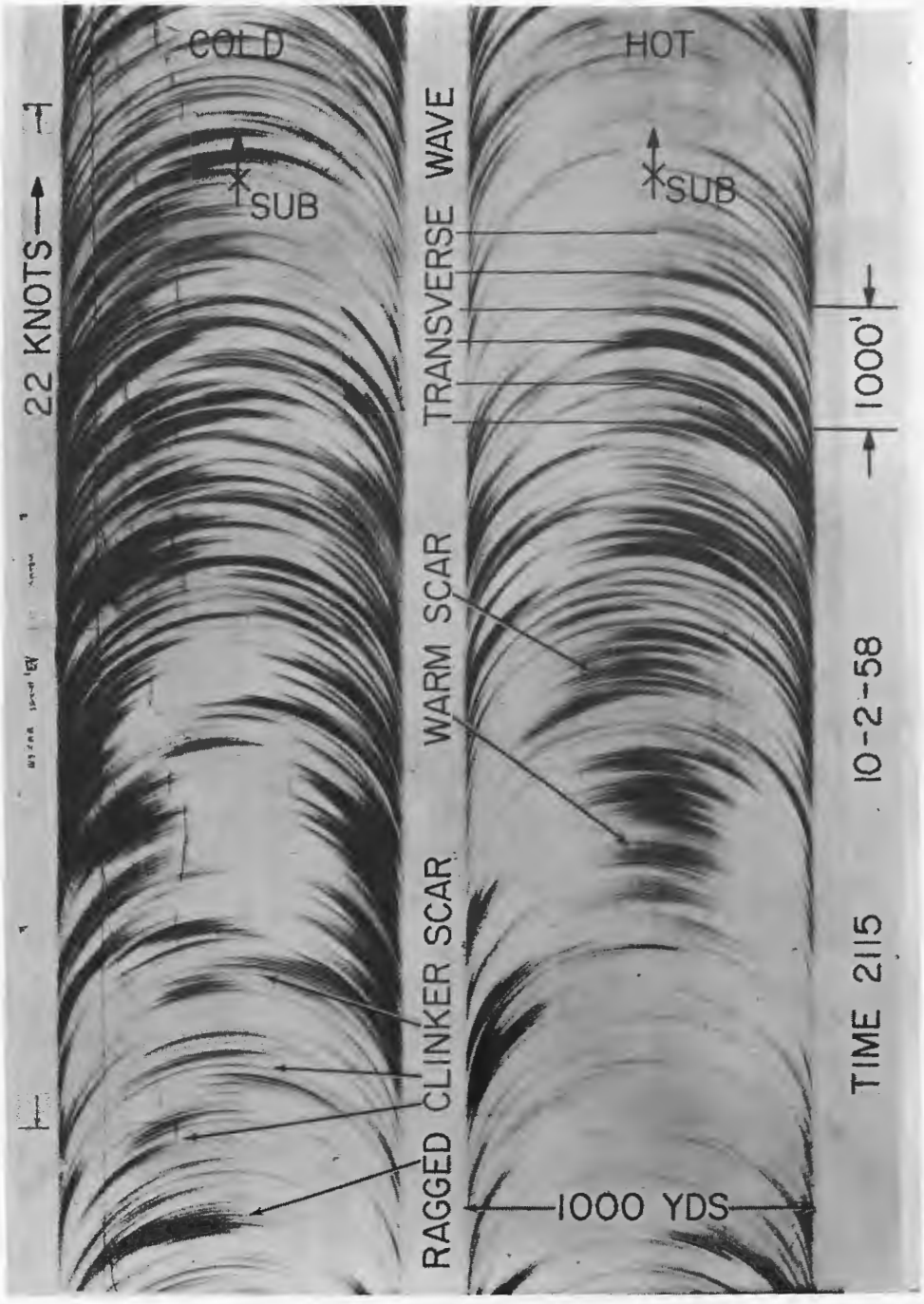

Chart 2 - Scar from USS NAUTILUS proceeding at 22 knots at a keel depth of 60 ft. Radiometric signatures from transverse waves and heat-exchanger water are apparent. ([redacted]) (unclass)

[redacted]

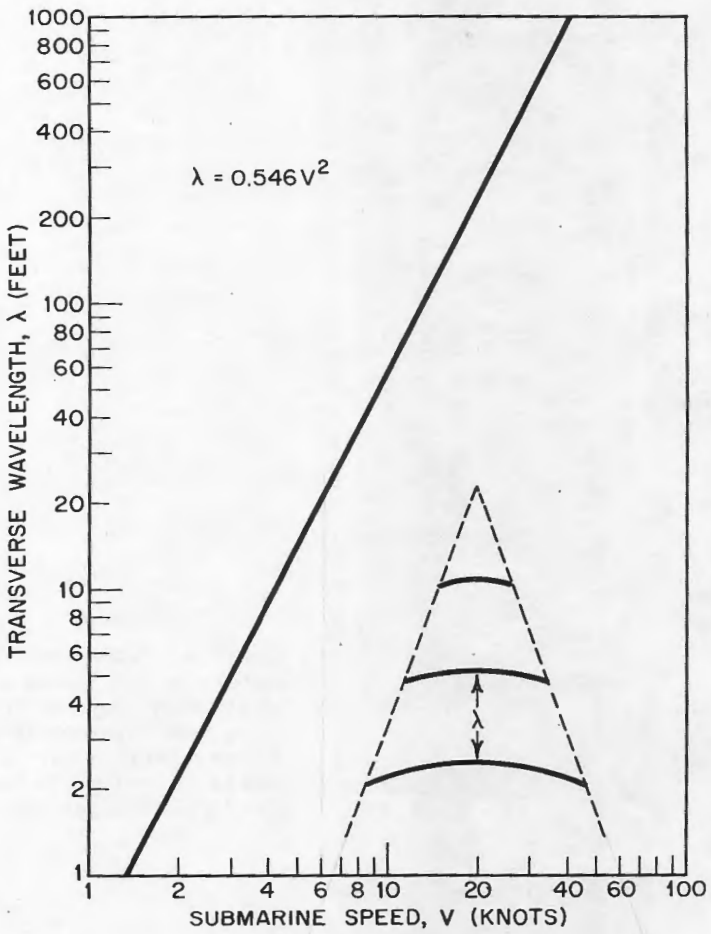

Chart 3 - Theoretical relationship between the speed of a submarine and the wavelength of her surface transverse waves ([redacted])

(unclass)

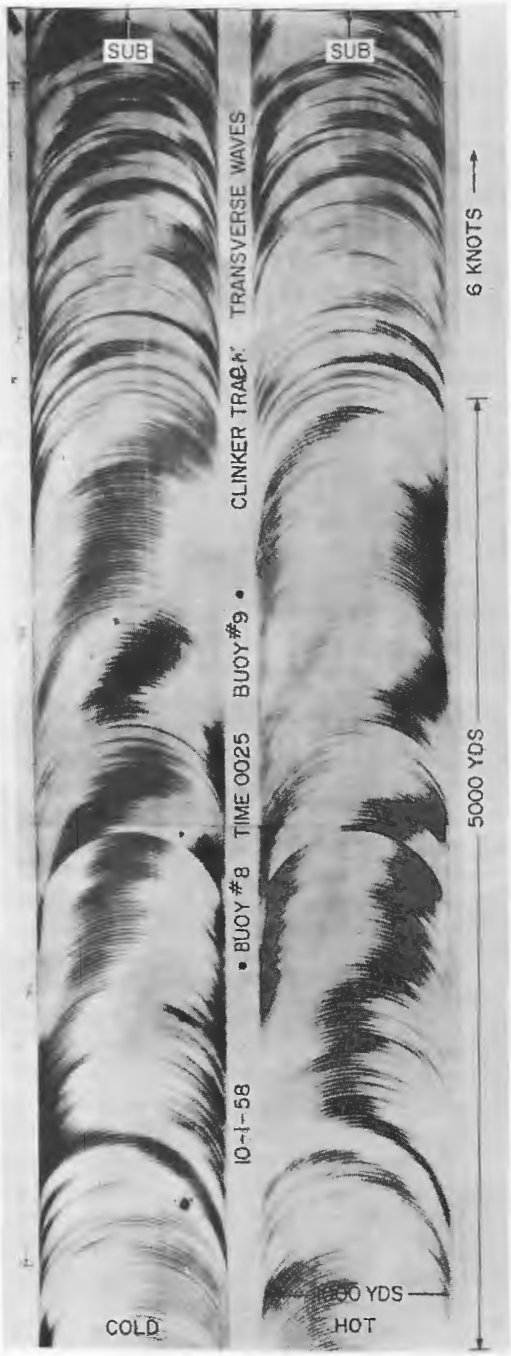

Chart 4 - Scar from USS NAUTILUS underway at 6 knots at a keel depth of 200 ft on edge of hurricane Helene. Apparent jaggedness in the scar is due to motion of airship. Transverse waves at the top are bunched together due to airship pitching. [redacted] (unclass)

[redacted]

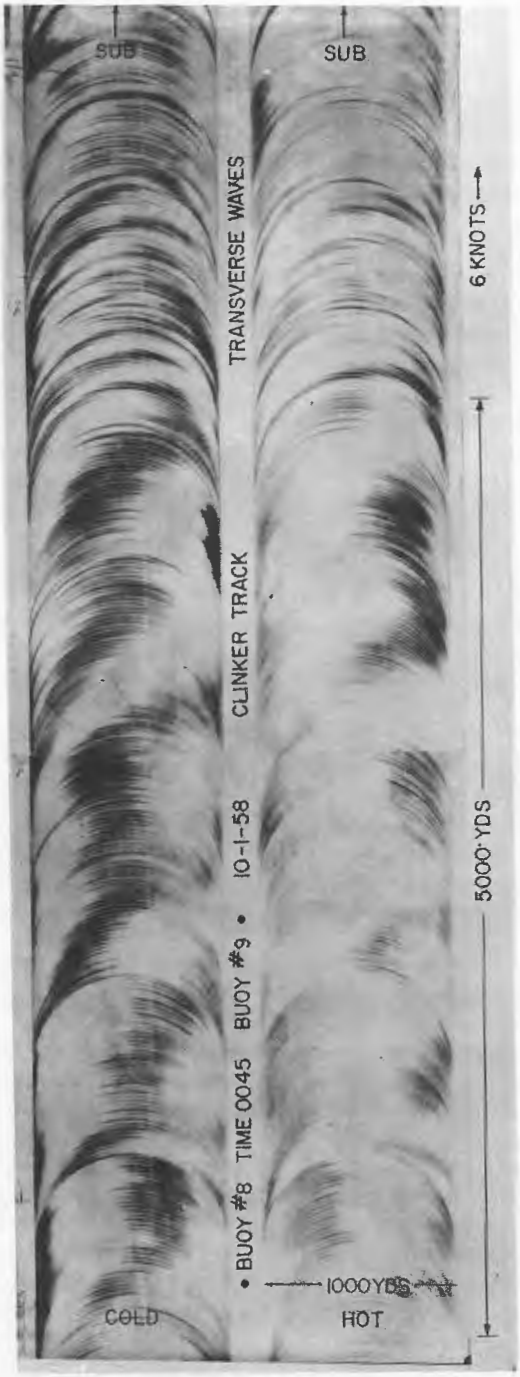

Chart 5 - Second recording made 20 min after that of Chart 3, showing scars behind USS NAUTILUS while underway at 6 knots and a keel depth of 200 ft (unclass)

the area. There was broken cloud cover with a full moon above. The sensitivity of the system was set at 20 percent of maximum to minimize the interference from the slicks. With this setting, the GROUPER's scar appeared strong, with an intensity of approximately 30 times the equivalent noise level of the equipment.

Chart 2 shows the details of the surface scar above and behind the NAUTILUS proceeding at 22 knots at a keel depth of 60 ft. The position of the submarine was determined with the aid of an intense light which she carried topside, indicated in the chart by X. Immediately above and behind her is the radiometric signature from the transverse structure in her gravity wave. From the geometry of the situation – airship altitude, diameter of scan circle, and recorder paper speed – it was determined that the distance between transverse waves was approximately 330 ft. The theoretical curve (17) of Chart 3 predicts that the submarine was proceeding at approximately 23 knots, which is in good agreement with her reported speed of 22 knots. Following the transverse-wave signature is a warm scar which begins 1300 yd astern the submarine and extends aft for another 1000 yd. It appears reasonable to assume that this is the submarine's heat-exchanger water, which is pumped out at the rate of 10,000 gallons per minute at a temperature 12^{0}F above ambient. The rise time for this water appears to be approximately 1.8 minutes for this particular keel depth (60 ft). This warm water completely obliterated the Clinker scar initially, although ragged pieces of it appeared farther astern. Eventually, a normal Clinker scar was observed approximately 2000 yd behind the warm scar.

Charts 4, 5, and 6 are recordings made during successive passes by the airship over the NAUTILUS' track while the latter was proceeding in a straight line at a keel depth of 200 ft and speed of 6 knots. The operating area was the same as that for Chart 2, as were the water conditions. In each case the airship flew up the track toward the submarine from points near marker buoy 8 or 9.

Chart 4 shows the airship turning on to the track from port approximately 7500 yd astern the submarine. The Clinker track appears cold and is actually straight, the apparent jaggedness in the recording being the result of the motion of the blimp in the turbulent air. Within 2000 yd of the submarine, the radiometric pattern from the transverse structure in the submarine's surface gravity wave is evident. However, the pitching of the airship caused the individual signatures to bunch and become unresolvable. Had the system's scanner been gyrostabilized against roll and pitch, this situation would not have existed.

Chart 5 is a second recording made 20 minutes after that shown in Chart 4. The repetitiveness of the Clinker pattern is quite evident.

Chart 6 is a third recording, made 65 minutes after the first (Chart 4). The recording starts more than 12,000 yd astern the submarine, where the Clinker scar is more than one hour old (at bottom of recording) and still strong. The airship flew up the track along the line of marker buoys, which places them on the center lines of the recorded strip maps. Immediately apparent is the relative drift of the Clinker scar to the left. The drift is downwind and results in a skewing of the scar of 500 yd laterally per 2500 yd of scar length, or a drift of approximately 1 knot relative to the marker buoys. This drift rate is approximately 3 percent of the 35-to-40-knot wind blowing at the time. Near the top of the recording is shown the radiometric signature from a knuckle which the submarine produced when she accelerated to a speed of 22 knots for the remainder of the run. The knuckle appears cold and sits atop the Clinker scar. Near the top of the strip maps can be seen the radiometric signals from the submarine's gravity wave. The spacing of these signatures is similar to that of Chart 2 and corresponds to a speed of 23 knots. The radiometric amplitude is less than that of Chart 2, presumably because the amplitude of the wave itself has decreased exponentially with increased depth by a factor of more than ten.

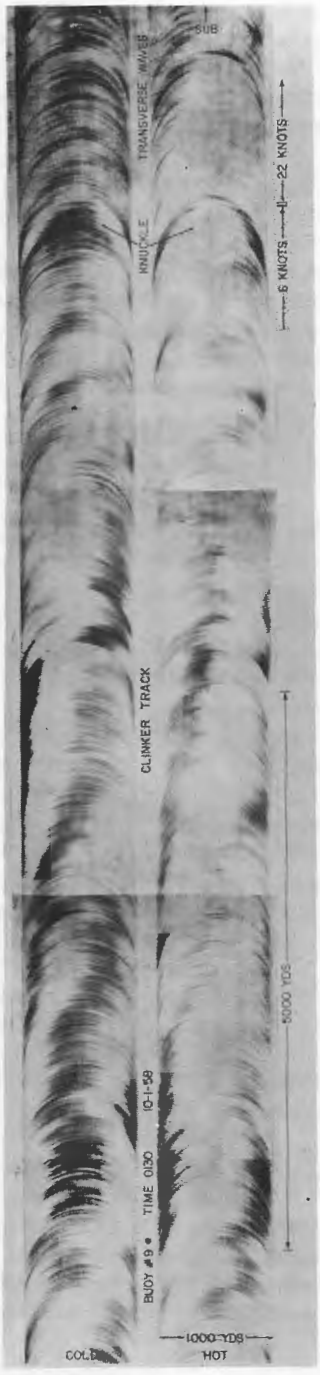

Chart 6 - Approximately 10,000 yards of scar behind USS NAUTILUS obtained under the same conditions of Charts 3 and 4 while running at 6 knots. At top of chart is the radiometric signature from the knuckle which was generated when submarine accelerated from 6 knots to 22 knots to complete her run. ([redacted])

(unclass)

All of the recordings shown from the NAUTILUS in Charts 2, 4, 5, and 6 were obtained on the edge of hurricane Helene. Wind velocities of 35 to 40 knots were encountered, and the sea state was 5 to 6. A solid overcast existed, and the airship was forced to fly below it at an altitude of 500 ft and with crab angles up to 45 degrees. The water was isothermal to 260 ft, 4°F negative to 280 ft, and 11°F negative to 400 ft. In spite of these conditions, the radiometric signals were large, and it was necessary to operate the system at 12 to 15 percent of maximum sensitivity in order to accommodate them.

The conclusions reached from these tests were that the system had adequate sensitivity to detect radiometric scars under a wide variety of weather conditions but that the noise level could become excessively high due to the poor aerodynamics of the enclosure around the equipment's scanner. Air scooping and turbulence in the scanner area were to blame and were eliminated by adding the fairing shown in Fig. 71. This necessitated a complete redesign of the scanner and resulted in changing the angle of incidence with which the optical units viewed the water from 70 to 60 degrees. The final version of the system was completed during Oct. 1959.

TEST FLIGHTS WITH FINAL MODEL

The final version of the system was tested in eleven different exercises against submerged submarines by NRL before being transferred to the Operational Test and Evaluation Force for the Fleet Operational Investigation (6,7). The conditions under which the tests were run are summarized in Table 2. Weather conditions varied from moderate with 1-to-3-ft waves to gales with 8-to-12-ft waves. The target submarines proceeded on straight-line courses* at or near right angles to the prevailing winds at keel depths from 60 to 400 ft. Special marker buoys (36) were released at prescribed intervals by the submarine to mark her track. All tests were run in deep water of 5000 ft or more. All target submarines were Guppies snorkelling or operating with battery power at a speed of 6 knots. Three of these tests were run 150 miles off the New Jersey coast, three in the Havana, Cuba area, and four were run in an operational area known as "Julie's Hole," which is approximately 180 miles west of Key West, Florida. Detections were made in all eleven exercises. Signal levels varied from 1 to 8 times the equivalent noise input of the system. In general, the signal level in the Key West area was two to three times smaller than that observed off the New Jersey coast.

Chart 7 shows a recording of the scar produced by the USS ANGLER snorkelling at 6 knots at a keel depth of 60 ft. Her periscope and snorkel tube were extended above the water. The early portion of the scar is 2 hours and 11 minutes old, at which point the airship turned onto the track and flew up it. The signal magnitudes on all strip maps are approximately equal.†

Chart 8 shows the scar behind the ANGLER while she was proceeding at a keel depth of 100 ft at a speed of 6 knots. In this case, the airship flew down the track away from the submarine. The early part of the scar is 1 hour and 50 minutes old and shows some downwind drift relative to the marker buoys. Lying across the track is a scar produced by a freighter which crossed the area before the submarine got there. Its radiometric magnitude is greater than that produced by the submarine.

*All NRL tests on the system were made with the submarine course perpendicular to the wind, so that the wind rows would be normal to the Clinker scar and would not be confused with it.

†Some fading took place before the maps could be photographed.

Table 2

Environmental Conditions Experienced During Testing of Final Version of Equipment

Date	Start Time	Area	Coordinates	Sub	Sub's Speed (knots)	Keel Depth (ft)	Sub's Rig	Sub's Course (°T)	Wind Direction (°T)	Wind Force (knots)	Swell Height (ft)	White Caps	Sea State	Water Temp (°F)	Bathythermograph Reading	Wet/Dry Bulb (°F)	Water Depth (ft)	Visibility	Moon	Cloud Cover	Ceiling (ft)	Airship Altitude (ft)	Airship Crab (deg)	Comments
10-26-59	2052	N. J. Coast	39° 10'N 71° 03'W	ANGLER	6	60	Schnorkel	150	240	25	8-13	Many	4	66	Isothermal to 60 ft	52/55	8500	Fair	None	Broken	2000	1500	35	Very dark *
10-29-59	1810	N. J. Coast	39° 00'N 71° 38W	ANGLER	6	100	Submerged	250	030	5-7	1-3	None	2-3	66	Isothermal to 100 ft	50/51	8500	Excellent	None	None	–	1500	8	First of two successive runs made this night *
10-29-59	2218	N. J. Coast	39° 00'N 72° 06W	ANGLER	6	200	Submerged	070	160	5-7	1-3	None	2-3	66	1° Neg to 200 ft	50/54	8500	Excellent	None	Few	5000	1500	8	10 miles westward of first run *
11-23-59	2035	Havana	23° 47'N 83° 09W	SEA POACHER	6	60	Schnorkel	210	140	10-15	5-8	Frequent	3-4	76	Isothermal to 60 ft	76/80	5000	Good	None	Complete	1000	700-1000	15	First of two successive runs made this night **
11-24-59	0147	Havana	23° 25'N 82° 56'W	SEA POACHER	6	200	Submerged	060	195	8	3-5	Scattered	3	76	Isothermal to 120 ft, 6° Neg to 200 ft	74/80	5000	Good	Occasional	Broken	1500	1000	10	10 miles south of first run **
11-24-59	1905	Havana	23° 42'N 82° 58'W	SEA POACHER	6	100	Submerged	170	240	8	3-5	Scattered	3	76	Isothermal to 100 ft	75/81	5000	Good	None	Broken	1500	1300	10	Rain squalls terminated test **
11-30-59	1840	Julie's Hole	24° 00'N 84° 30'W	SEA POACHER	6	100	Submerged	150	060	15-20	5-8	Many	4	74	Isothermal to 350 ft	58/67	6000	Good	None	Complete	2500	1500	20	First of two successive runs made this night **
11-30-59	2215	Julie's Hole	24° 00'N 84° 20'W	SEA POACHER	6	200	Submerged	330	060	15-20	5-8	Many	4	74	Isothermal to 350 ft	61/70	6000	Good	None	Complete	2500	1500	20	5 miles upwind from first run **
12-10-59	2010	Julie's Hole	23° 49N 84° 35W	PICUDA	6	100	Submerged	000	080	28	8-12	Foam (Gale)	5	72	Isothermal to 300 ft, 4° Neg to 400 ft	69/75	6000	Excellent	3/4 Zenith	Few	2300	1500	40	First of three successive runs made this night **
12-10-59	2357	Julie's Hole	24° 08'N 84° 25W	PICUDA	6	400	Submerged	180	080	28	8-12	Foam (Gale)	5	72	Isothermal to 300 ft, 4° Neg to 400 ft	68/74	6000	Excellent	3/4 Setting	Few	2300	1500	40	10 miles upwind from first run **
12-11-59	0412	Julie's Hole	23° 49'N 84° 15'W	PICUDA	6	200	Submerged	000	080	15	5-8	Many	4	72	Isothermal to 300 ft, 4° Neg to 400 ft	69/75	6000	Excellent	3/4 Setting	Few	2300	1500	20	20 miles upwind from first run **

*Environmental data from USS Brattleboro

**Environmental data from USS Rockville

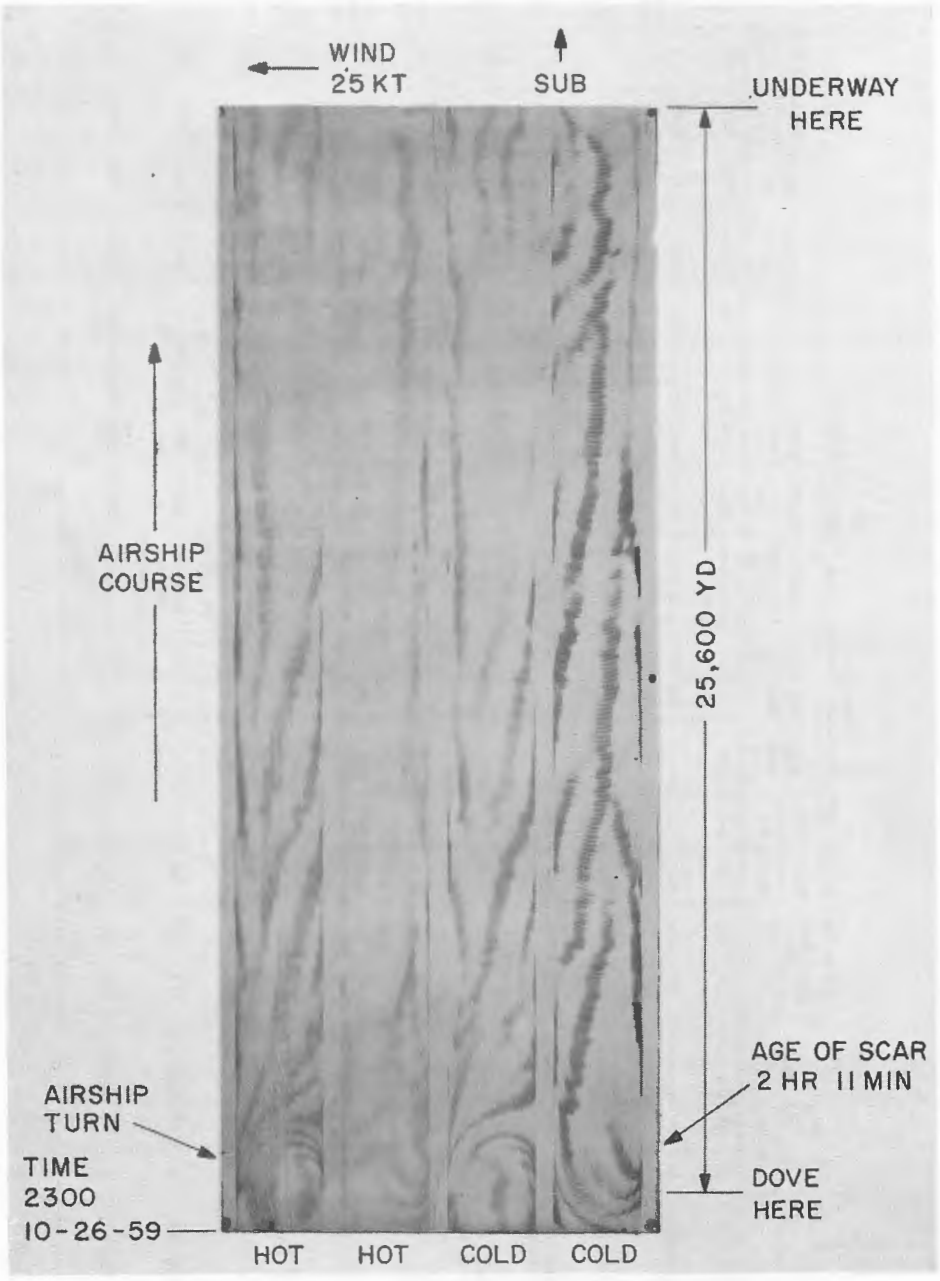

Chart 7 - USS ANGLER snorkelling at 6 knots at a keel depth of 60 ft ([redacted])
(unclass)

[redacted]

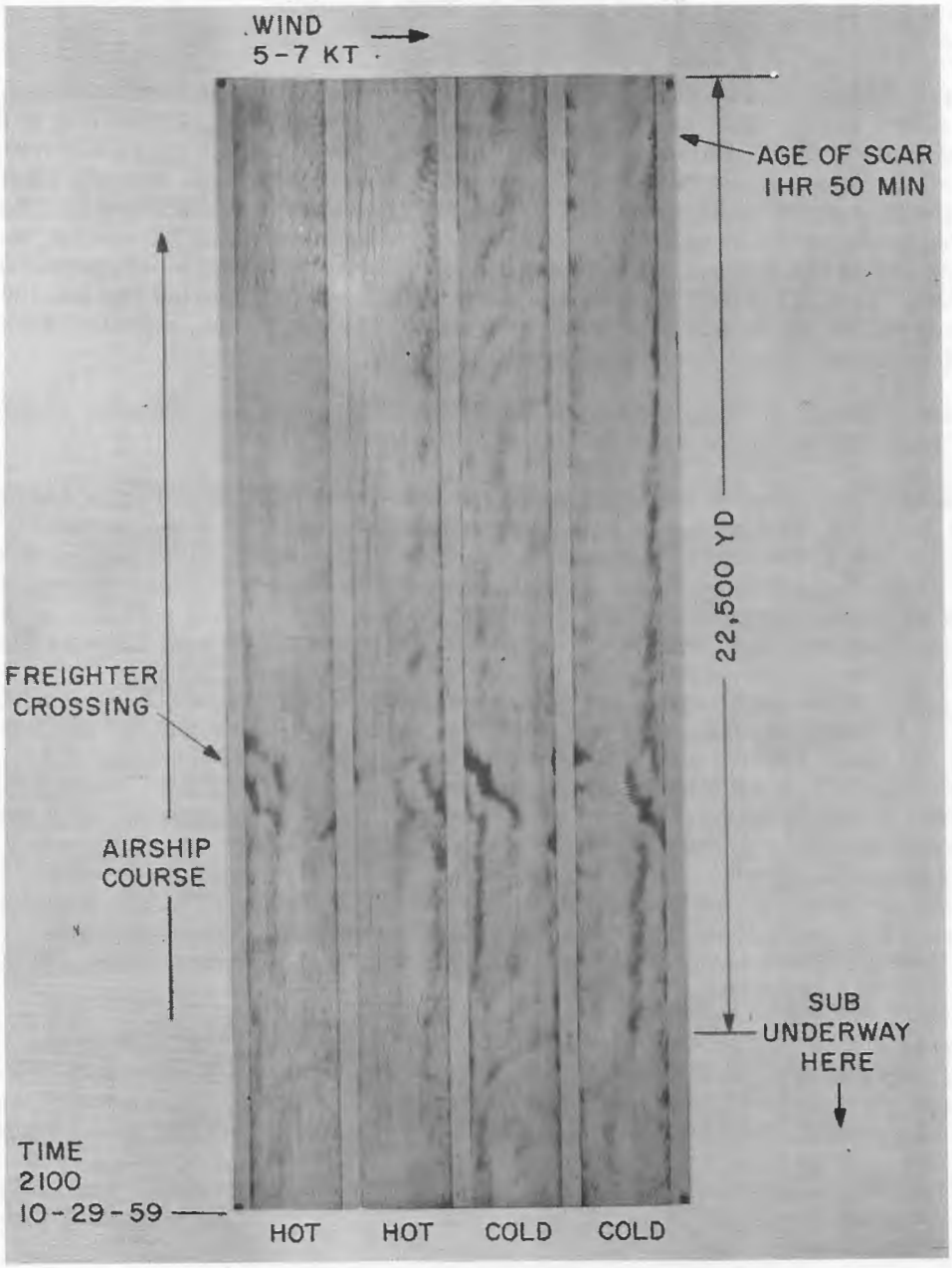

Chart 8 - USS ANGLER proceeding at 6 knots
at a keel depth of 100 ft ([redacted])

(unclass)

Chart 9 shows the scar produced by the ANGLER at a keel depth of 200 ft while proceeding at 6 knots. In this case, the airship flew toward the submarine beginning at a point on the scar which was 2-1/2 hours old. Some downwind drift is noticeable at this point.

Charts 10 and 11 are samples of the results obtained from the first exercise in the Havana area. In this case the submarine was the SEA POACHER, snorkelling at 6 knots at a keel depth of 60 ft. During her run the submarine passed under a rain storm, the effects of which are shown in Charts 10 and 11. Chart 10 was made with the airship flying toward the submarine at an altitude of 700 ft, and the effects of clouds and rain both above and below the airship are shown. Outside the storm area, near the submarine, the scar is strong; inside the storm it has become weaker. Eventually, the storm obliterated the scar. Chart 11 is a return trip down the scar. By now the submarine has left the storm far astern and is proceeding through clear weather. In this figure, also, the weakening effect of the storm on the scar is apparent.

Chart 12 shows the scar behind the SEA POACHER which she produced while proceeding at 6 knots and a keel depth of 200 ft.

Charts 13 and 14 show the scar behind the SEA POACHER as she proceeded at a keel depth of 100 ft and at 6 knots. In both cases, the airship started at the submarine's point of dive and flew up the track toward the submarine. The second flight was made approximately 40 minutes after the first. The improvement in the scar with age is apparent, that of Chart 14 being stronger than that of Chart 13. Both charts show a 45-degree crossing by a Cuban gunboat. The radiometric magnitude of this vessel's scar appears to be decreasing with age, while that of the submarine is increasing. In Chart 13, the radiometric noise on the water due to heavy broken clouds is quite apparent. The submarine's scar can be traced into the cloud noise, but separation becomes difficult. In Chart 14, some of the fine structure of the Clinker scar is apparent. Near the point of dive, where the airship turned onto the track, seven ribbons can be counted in the Clinker scar. These are spread over a distance of more than two miles. Thus, it can be concluded that the diameter of the equipment's scar circle is inadequate. However, there appears to be no way to increase it except to increase altitude, cloud cover permitting. Another feature of the scar is the small dot at the submarine's position. This appears to be the radiometric signature from the Bernoulli depression. This effect is not always observable. It appeared in later exercises and was subsequently observed by Fleet personnel during their investigations with this equipment.*

Charts 15 and 16 show the scar above and behind the SEA POACHER as she ran in the deep water of Julie's Hole at a keel depth of 200 ft and a speed of 6 knots.† The ruggedness of the equipment was demonstrated during this exercise when three of the six tires on the scanner rolled off and were lost. The resulting vibration shook the entire airship and produced a low level of vibration noise in the system which appears as dots on the recordings. Nonetheless, the equipment continued to function normally, and the detections shown in Charts 15 and 16 were made. Finally the pilot concluded that the gear should be shut down.

Chart 17 is a recording obtained during a 28-knot gale while operating with the PICUDA at a keel depth of 100 ft and speed of 6 knots. This scar is badly broken up and is characterized by washed-out sections. The buoys themselves underwent considerable lateral displacement in these areas, indicating the presence of crosscurrent.

*See Figs. 6 and 7 of Ref. 37.
†Records from the SEA POACHER's 100-ft run faded so badly that they could not be photographed.

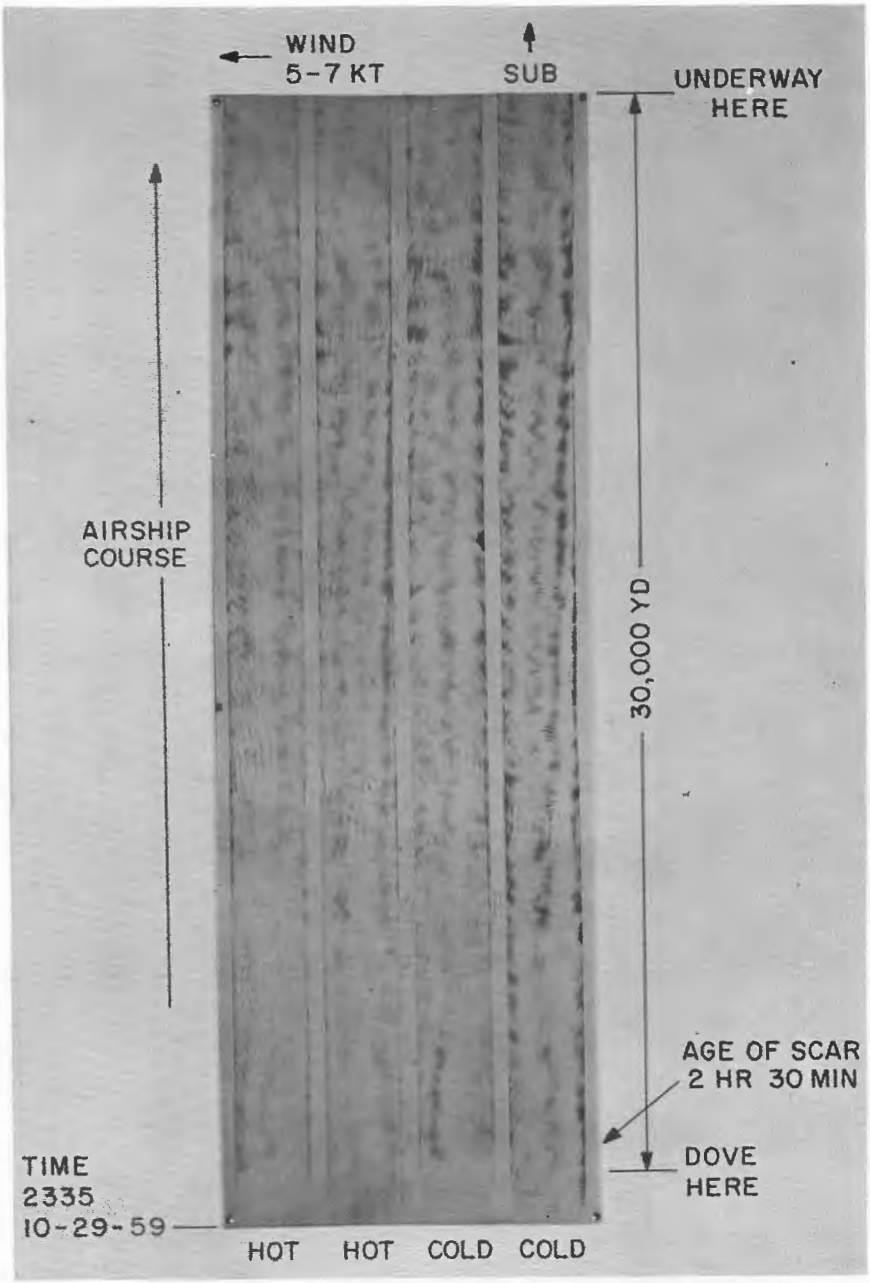

Chart 9 - USS ANGLER proceeding at 6 knots
at a keel depth of 200 ft [redacted]
(unclass)

[redacted]

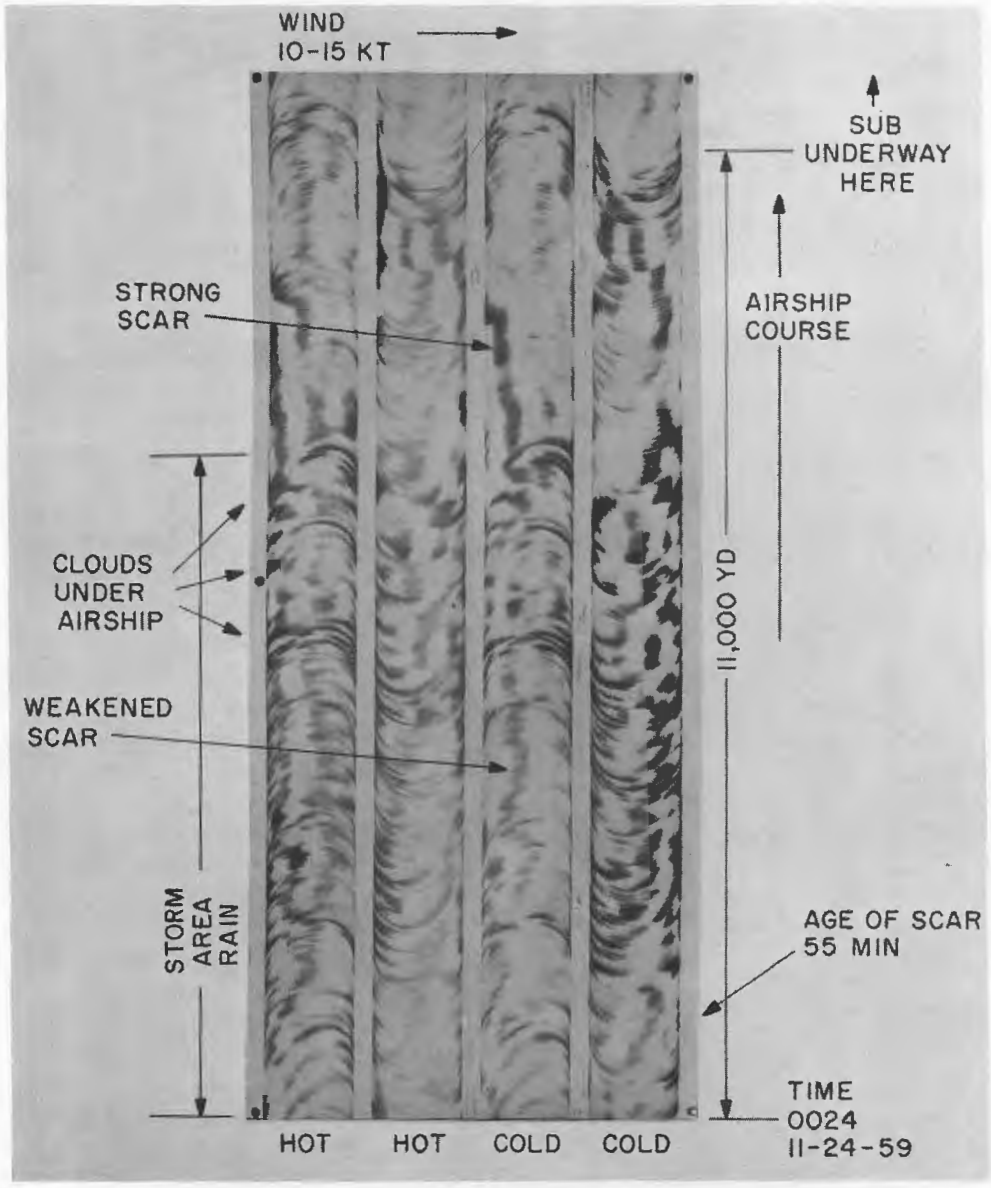

Chart 10 - USS SEA POACHER leaving rain storm while snorkelling at 6 knots at a keel depth of 60 ft ([redacted])

(unclass)

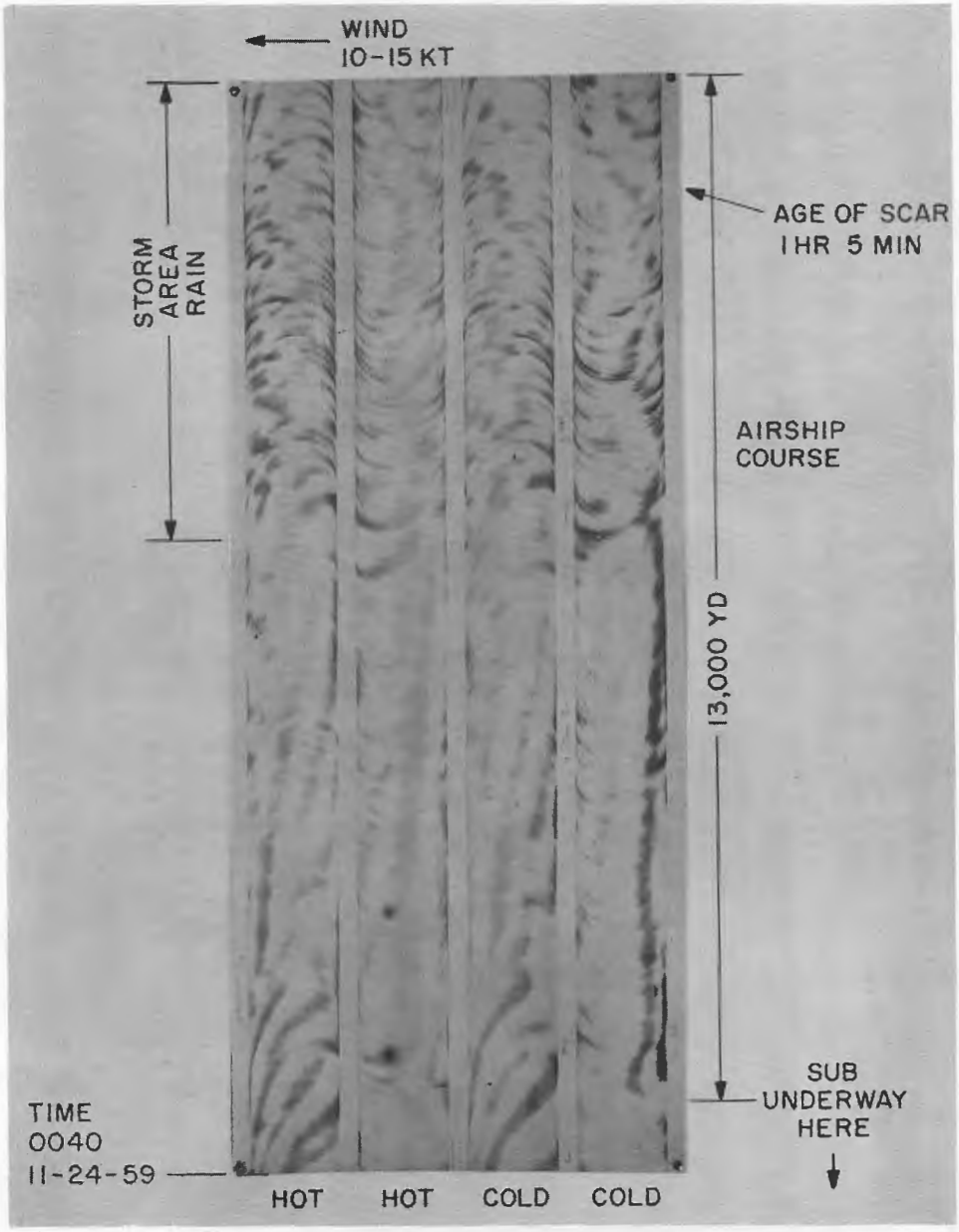

Chart 11 - USS SEA POACHER leaving storm far behind at 6 knots and keel depth of 60 ft ([redacted])

(unclass)

SECRET

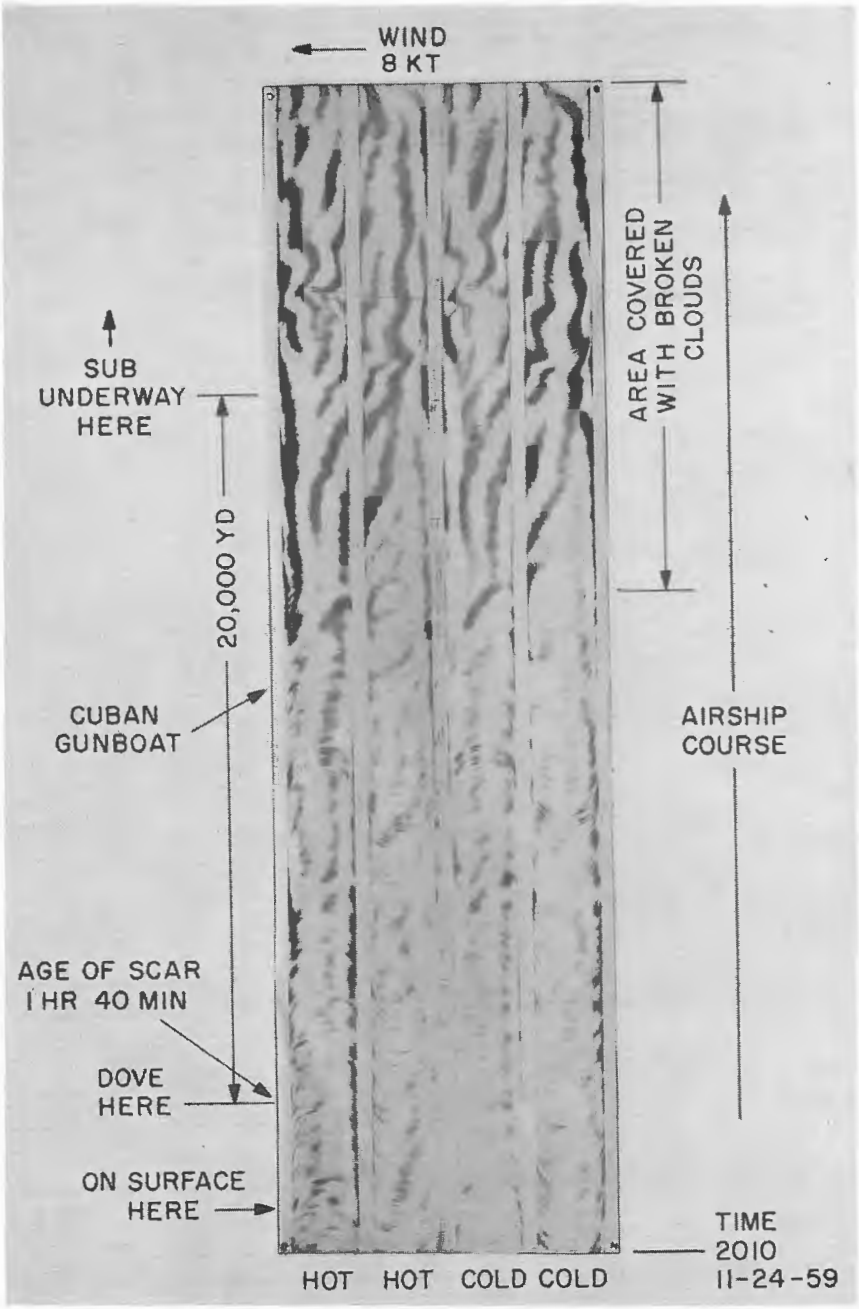

Chart 13 - USS SEA POACHER proceeding at 6 knots at a keel depth of 100 ft. Early portion of the track was under a clear sky; the latter under broken clouds. [redacted] (unclass)

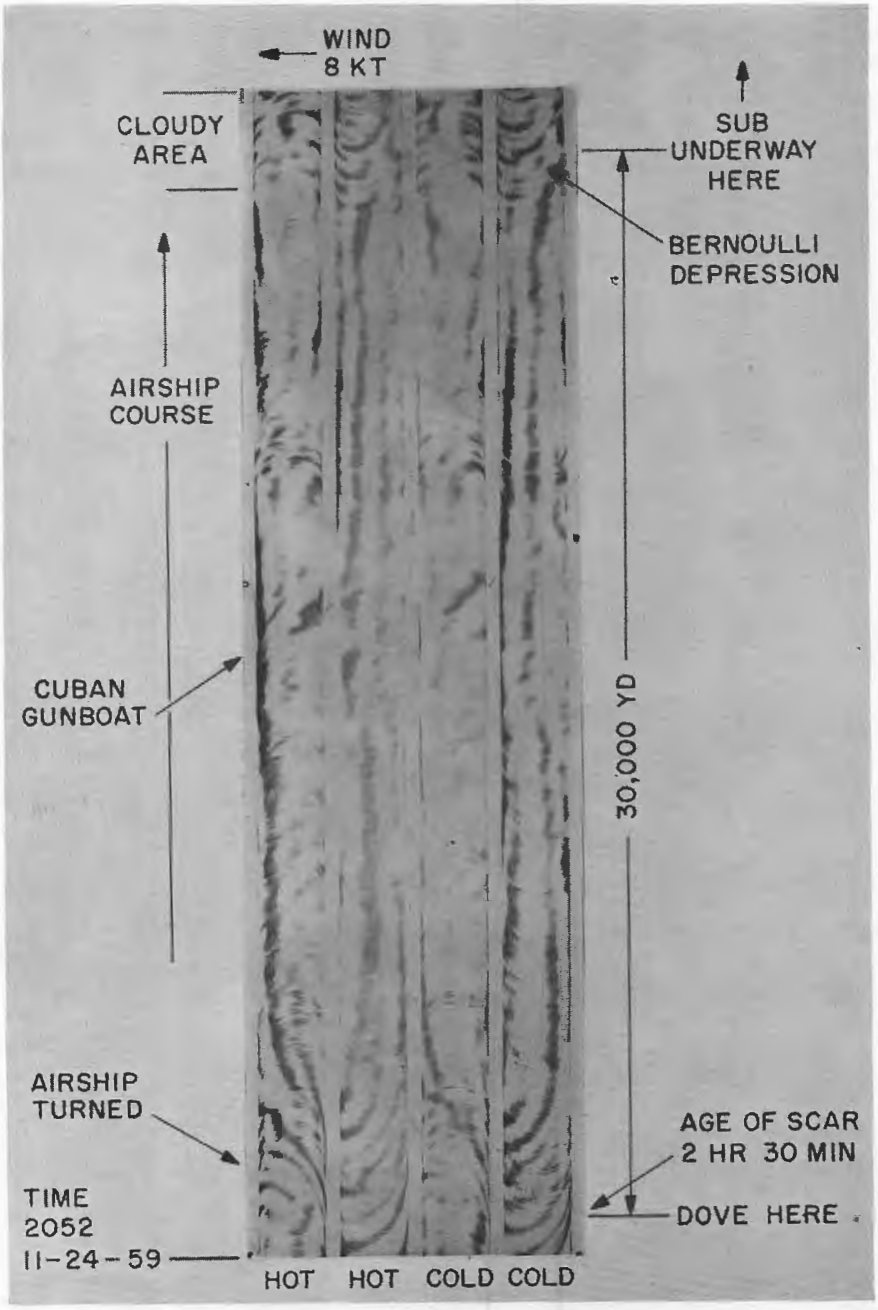

Chart 14 - USS SEA POACHER proceeding at 6 knots at a keel depth of 100 ft. The clouds of Chart 13 have passed ahead of submarine. [redacted] (unclass)

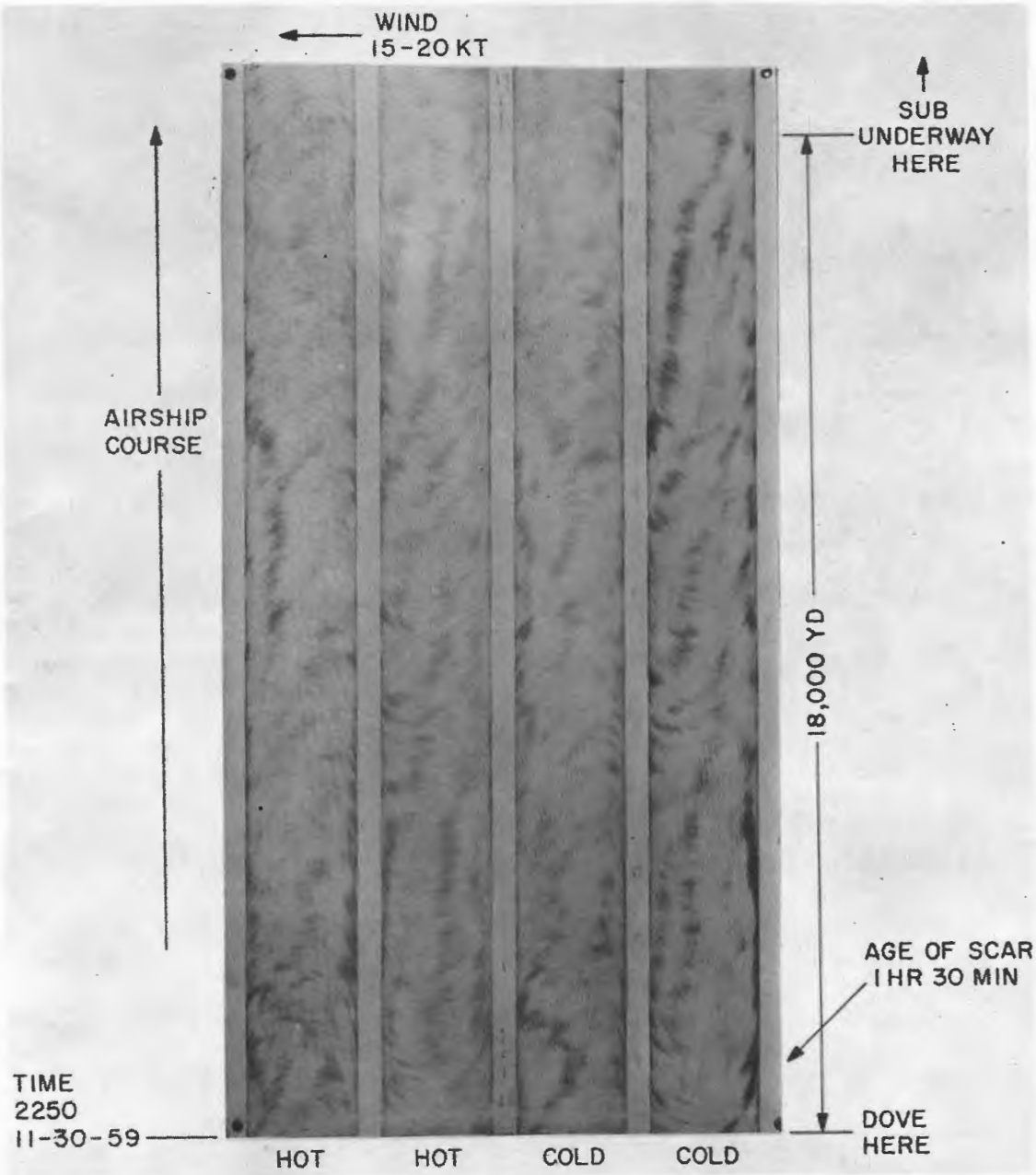

Chart 15 - USS SEA POACHER underway at 6 knots at a keel depth of 200 ft [redacted]

(unclass)

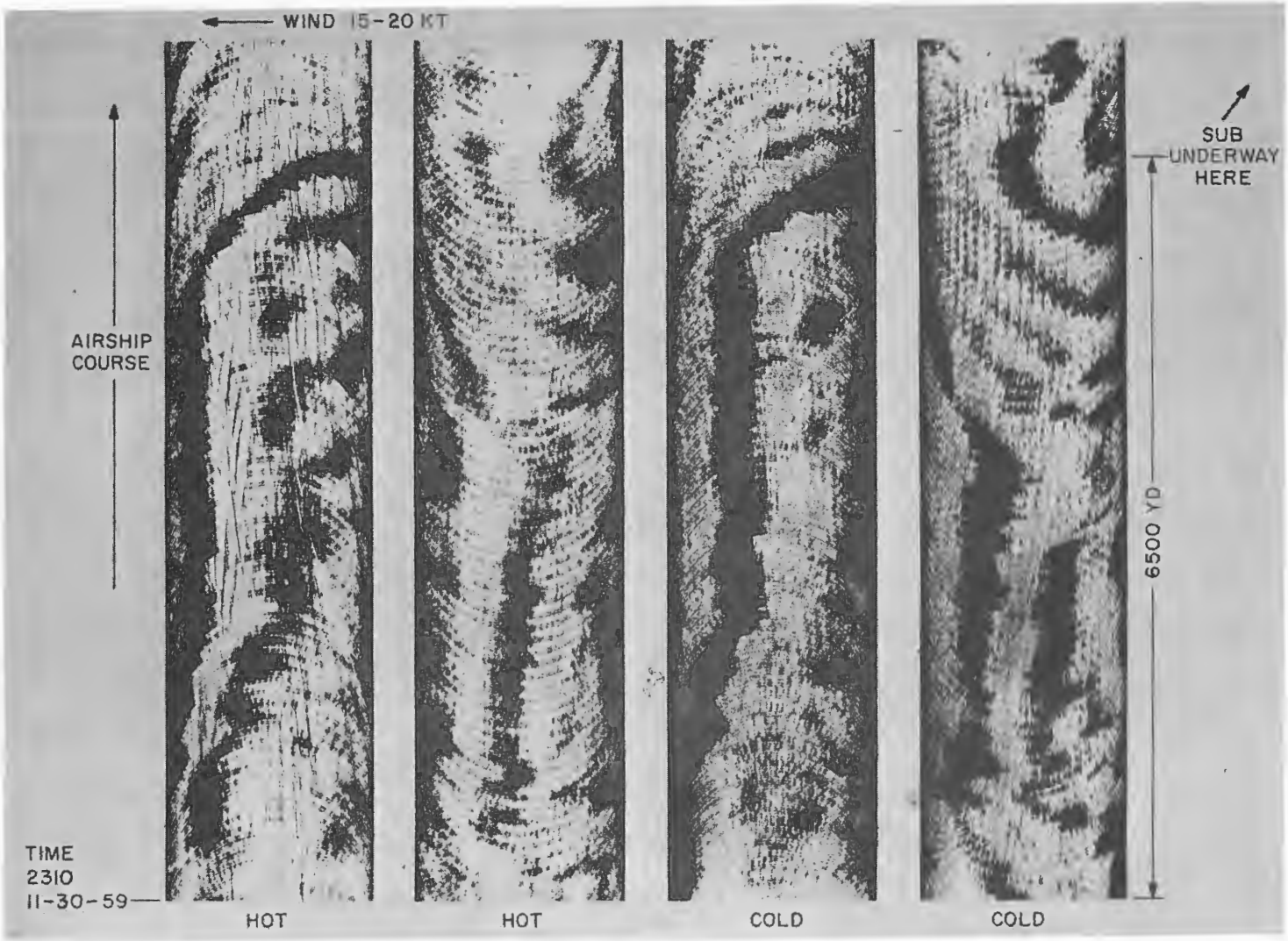

Chart 16 - Area immediately astern USS SEA POACHER. Airship passed over [redacted] minutes after recording of Chart 15 was made.

(unclass)

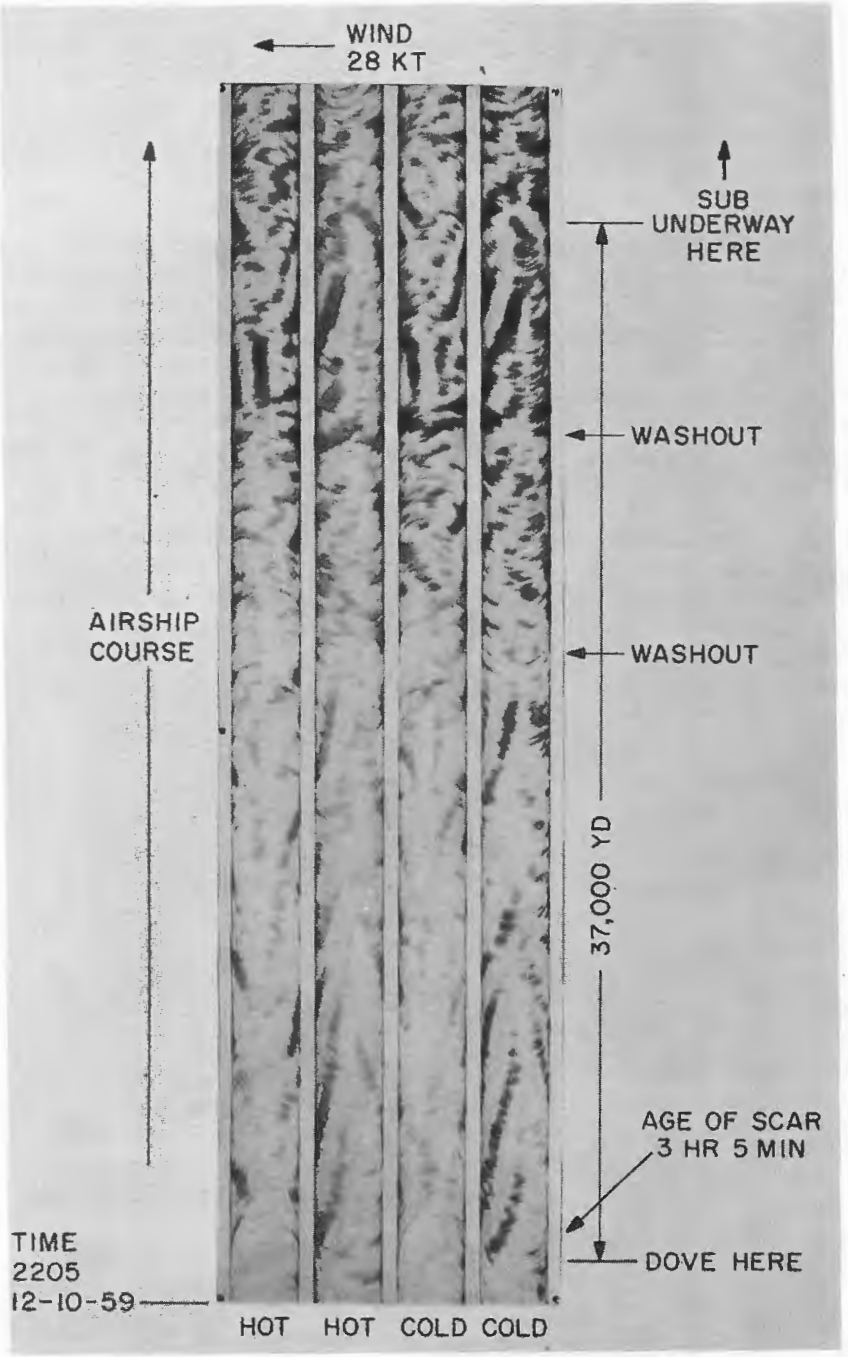

Chart 17 - USS PICUDA underway at 6 knots and a keel depth of 100 ft in a 28-knot gale ([redacted]) (unclass)

Charts 18 and 19 are recordings obtained in the same gale, but with the PICUDA at a keel depth of 400 ft. In the 28-knot wind, the airship had difficulty staying on course. Chart 19 shows the result of being blown across the track twice. The downwind drift of the scar is apparent in Chart 18. Signal levels were approximately three to five times the equivalent noise input of the system. The noise background provided by the sea was very low, as can be seen ahead of the submarine (Chart 19). It was the opinion of the equipment operators that, under these conditions, the PICUDA could be detected easily during any blind search.

Charts 20 and 21 show the PICUDA operating at a keel depth of 200 ft in the same gale, but after it had abated somewhat. The drift of the scar to the right, or downwind, is noticeable. Chart 20, the radiometric signal from the Bernoulli depression over the submarine is apparent. In Chart 21, a peculiar signature appears ahead of the submarine. It has many of the characteristics of the scar behind the submarine and could be due to surface vessels, although none except the freighter, which crossed behind the submarine, were noted. On the other hand, it could be a short-lived precursor of the type subsequently reported by Fleet personnel. Because of the skew and fragmentation of both this signature and the submarine's scar, it is difficult to draw any conclusions with respect to it.

The testing of the AN/AAR-23(XB-1) was concluded by NRL on Dec. 11, 1959, and it was transferred to Squadron VX-1, OPTEVFOR, on Dec. 14, 1959 for the Fleet Operational Investigation under Project F/018 FY 60. This investigation was completed during October 1960 and has been reported (6,7). A subsequent decision by the Chief of Naval Operations to decommission all Fleet airships automatically placed the AN/AAR-28(XB-1) in a research status. As such, it has been operated by the Naval Air Development Unit along both the Atlantic and Pacific Coasts (38).

CONCLUSIONS

As a result of this work, it is concluded that an extremely reliable 8-to-13-micron passive-detection equipment for use in airships is practical and that this equipment, although at present limited to operation at night, can detect the surface scars from submarines operating at keel depths down to 400 ft in sea states up to 5 or 6 for periods as long as three hours after the passage of the submarine.* The present availability of photoconductive detector elements which are considerably better than the thermopile detectors employed in the NRL equipment should permit this same performance to be realized from high-speed, fixed-wing aircraft.

ACKNOWLEDGMENTS

The success of this work is due in large measure to the assistance given by the following groups and individuals:

CDR W. Ashe and staff of the Airship Test and Development Department, U. S. Naval Air Station, Lakehurst, New Jersey, and in particular Mr. W. A. Hiering who contributed to the solution of the aerodynamic problem.

*OPTEVFOR realized even better performance as the result of equipment modifications made by NRL during the Fleet Operational Investigation.

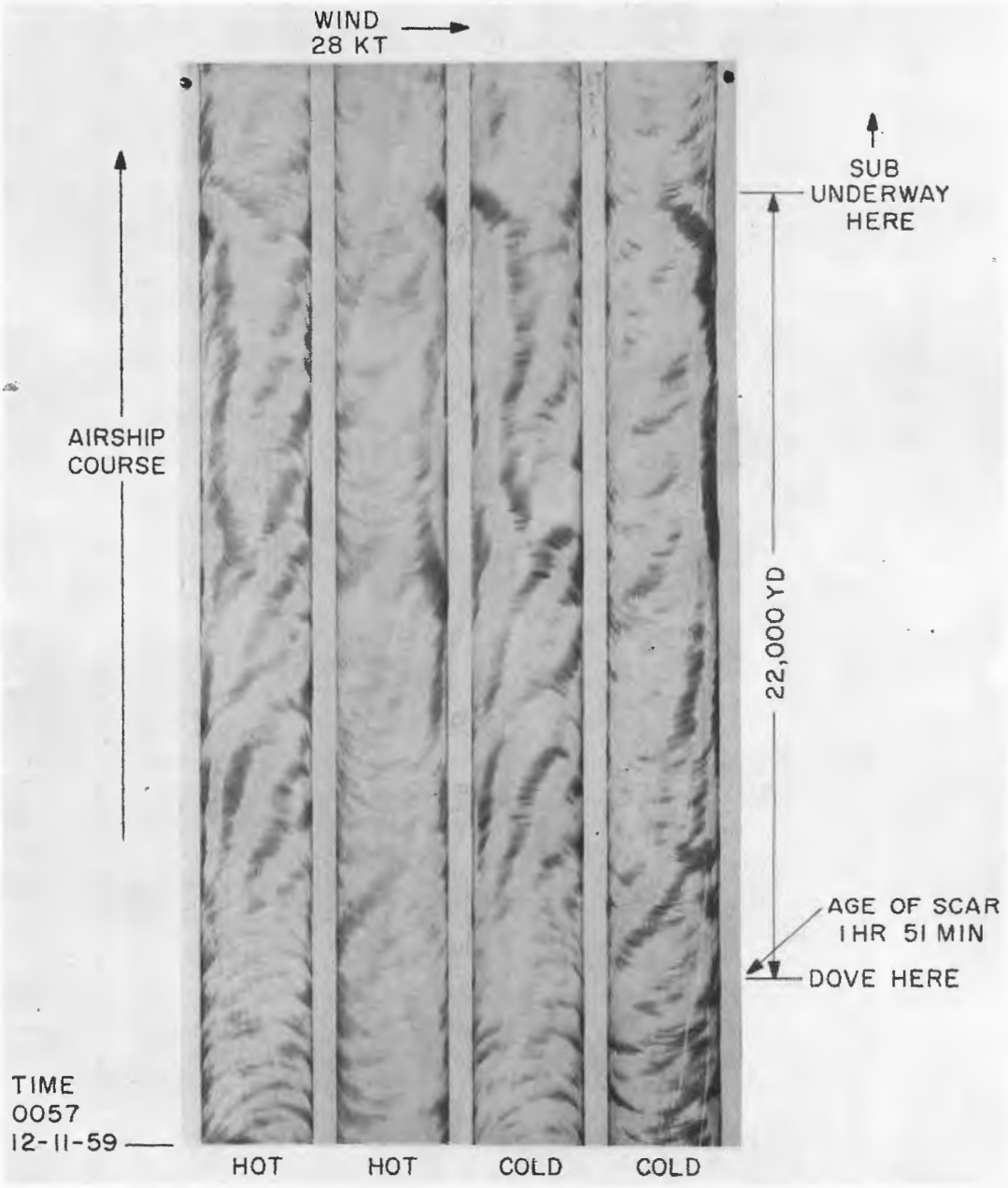

Chart 18 - USS PICUDA underway at 6 knots and a keel depth of 400 ft in a 28-knot gale ([redacted]) (unclass)

[redacted]

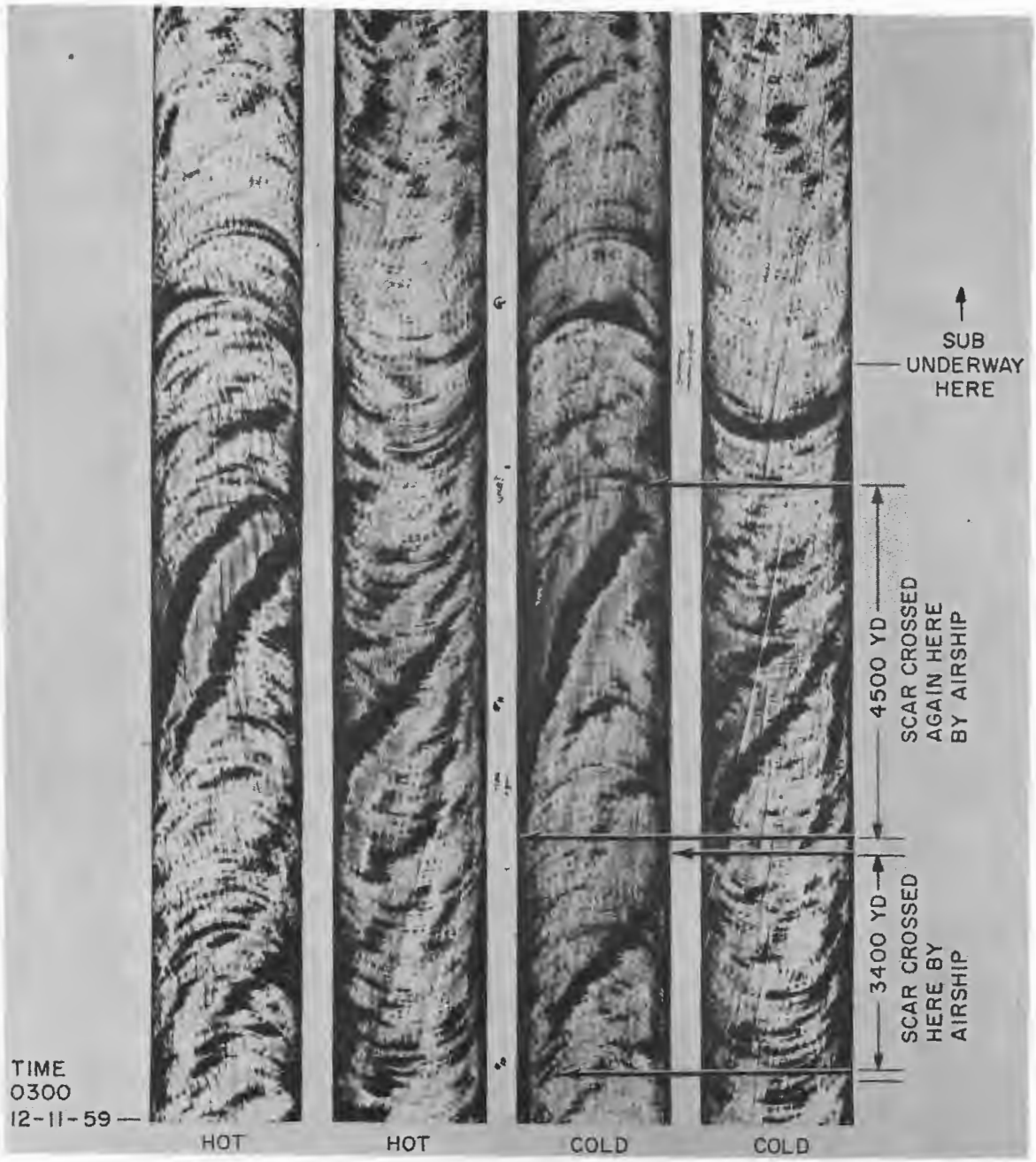

Chart 19 - Results from airship being blown across PICUDA's track during the run shown in Chart 18, with submarine proceeding at a keel depth of 400 ft and 6 knots ([redacted])
(unclass)

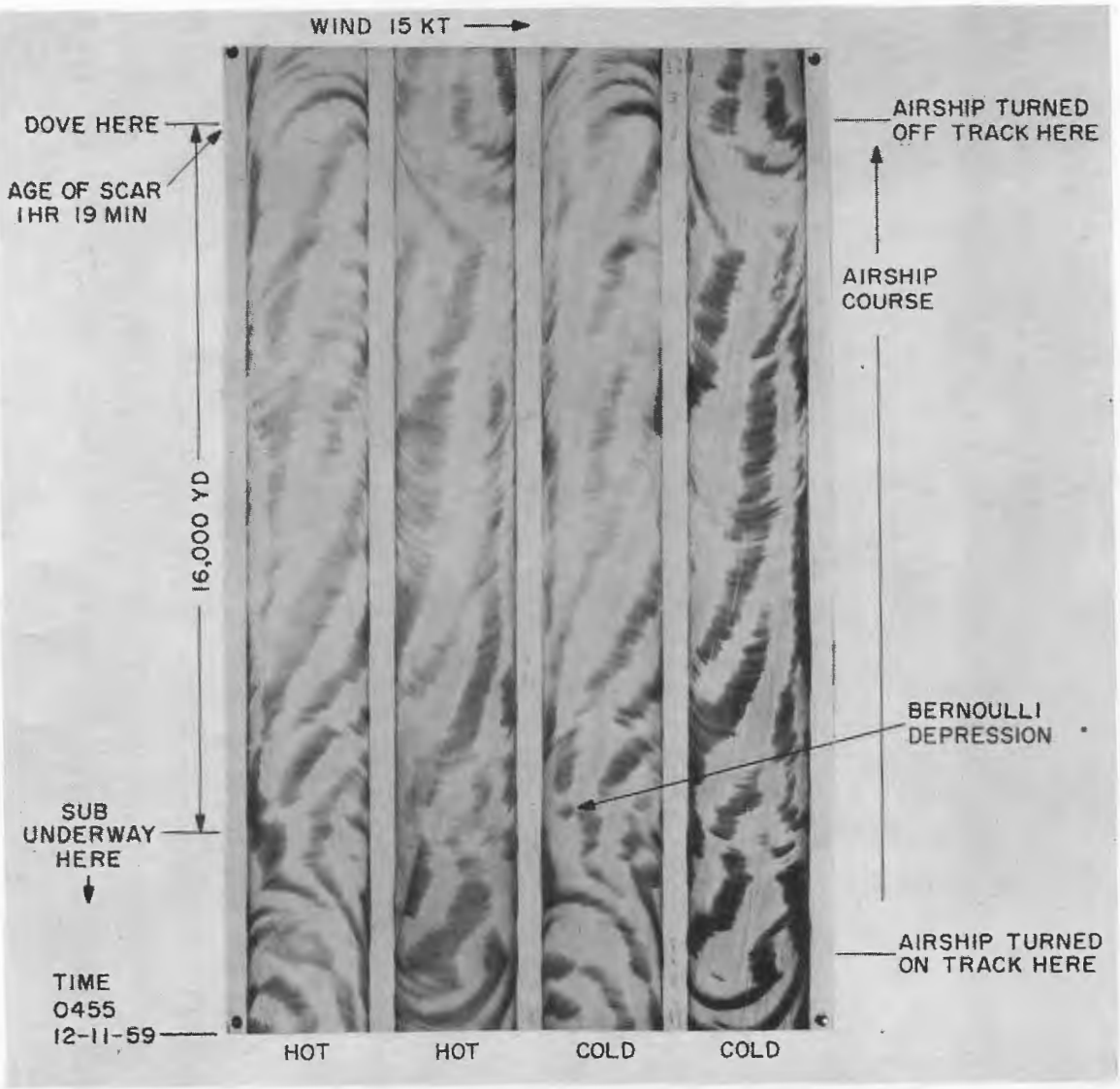

Chart 20 - USS PICUDA underway at 6 knots at a keel depth of 200 ft ([redacted]) (unclass)

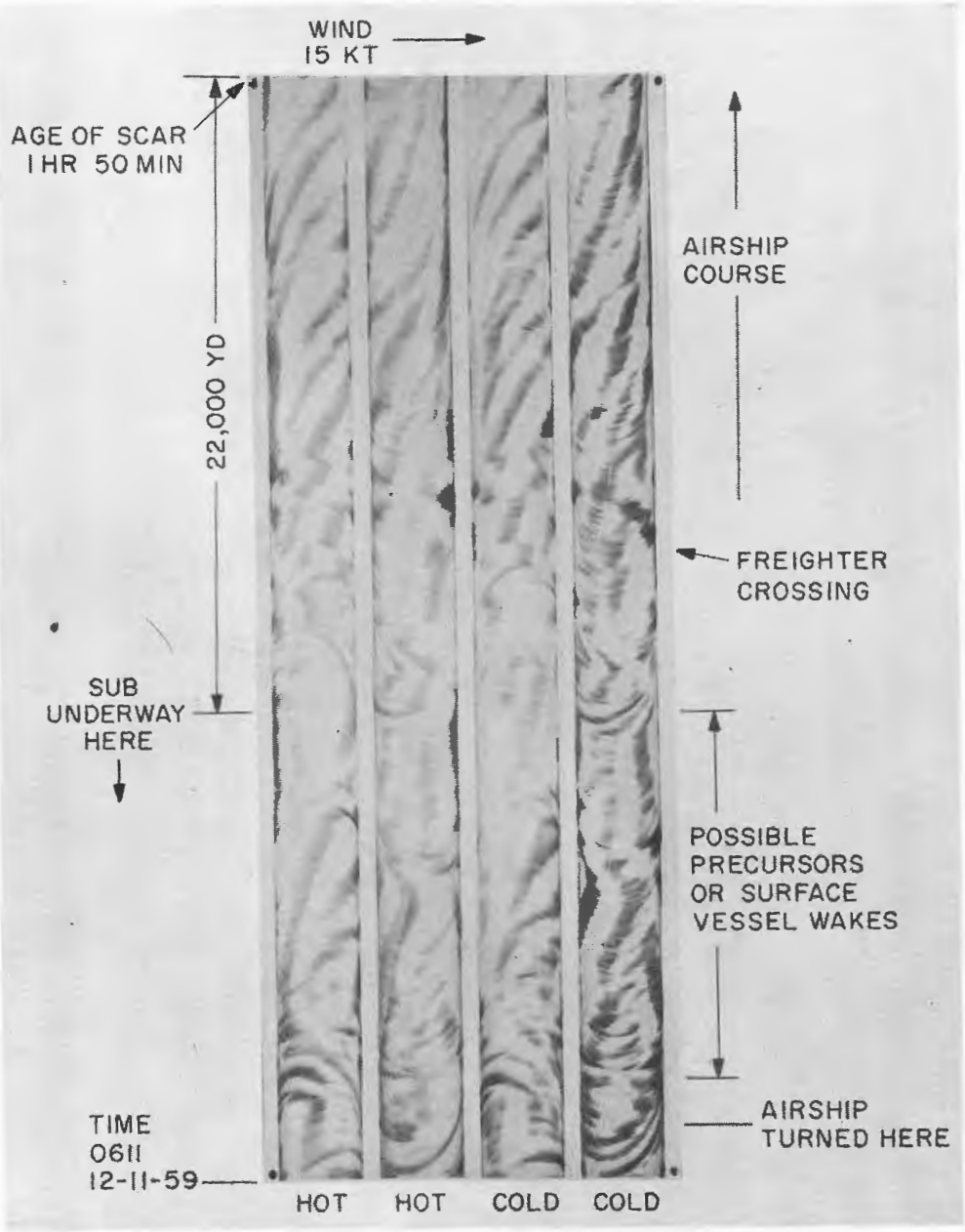

Chart 21 - USS PICUDA underway during the same run as Chart 20, at 6 knots and 200-ft keel depth but 75 minutes later ([redacted])

(unclass)

[redacted]

CAPT E. Rogers and staff of the U. S. Naval Air Development Unit, South Weymouth, Massachusetts, and in particular LCDR C. Manship and crew of the ZPG-2 (141561) airship, who put in long hours of flying.

CDR J. R. Grieve, ASW Liaison Officer at the U. S. Naval Research Laboratory, whose drive and initiative were invaluable in supporting the field work.

Mr. J. P. Manning and personnel of the Engineering Services Division, whose fine workmanship contributed so heavily to the reliability and performance of the equipment.

Lastly the scientific personnel and authors' coworkers, who contributed so heavily to the development: Mr. C. F. Bieber, Mr. F. J. Bury, Mr. E. J. Butcher, Mr. W. H. Hawley, Mr. L. Hillegass, Mr. J. D. Mahloy, and Mr. J. B. Slaughter.

REFERENCES

1. Clark, H.L., "Airborne Measurements of the Thermal Radiation from the Schnorkel and Wake of the USS DOGFISH," NRL Report 3386 (Confidential Report, Unclassified Title), Nov. 22, 1948

2. Clark, H.L., "Airborne Measurements of the Thermal Radiation from Submarine Wakes in the Key West Area," NRL Report 3606 (Secret Report, Confidential Title), Jan. 4, 1950

3. Clark, H.L., "Airborne Measurements of the Thermal Radiation from the Wake of the USS IREX," NRL Report 3783 (Secret Report, Unclassified Title), Feb. 16, 1951

4. Clark, H.L., "Airborne Measurements of the Thermal Radiation from Submarine Wakes in the Gulf Stream" NRL Report 3938 (Secret Report, Confidential Title), Feb. 6, 1952

5. Bieber, C.F., Bradford, J.N., and Clark, H.L., "Project Clinker Report No. 2, Airborne Measurements of the Widths of Submarine Wakes in the Oriente Deep," NRL Report 4805 (Secret Report, Confidential Title), July 1956

6. OPTEVFOR First Partial Report on Project F/018 FY 60, "Conduct Fleet Operational Investigation of Detecting Set, Infrared, AN/AAR-23(XB-1)" (Secret Report, Unclassified Title), Oct. 13, 1960

7. OPTEVFOR Final Report on Project F/018 FY 60, "Infrared Detection of Submerged Submarines" (Secret Report, Confidential Title), Feb. 10, 1961

8. Holter, N.J., Lyon, W.K., Moe, C.R., and Delsasso, L.P., "The Geometry of Surface Wakes and Experiments on Artificial Wakes," USNR and S/NEL Report S-10 (Confidential), May 24, 1943

9. Gaylord, H.E., "Evaluation of the AN/UQQ-1 Detecting Set," NEL Report 275 (Secret), Feb. 13, 1952

10. Jones, J.L., "Thermal Gradients in Submerged Submarine Wakes," NOTS Report PA-02067 (Secret), Sept. 25, 1954

11. Beck, L., Igarashi, Y., and Thompson, B.L., "Submarine Echoes and Wakes, A Summary and Evaluation of the Literature," NOTS Report 2033, NAVORD Report 5891 (Confidential), May 20, 1958

12. Rapp, R.A., "An Exploratory Model Study of Submarine Wake Dispersion," DTMB Report C-629 (Confidential), Apr. 1955

13. Mahloy, J.D., "Project Clinker Report No. 7, An Observation of the Joule Heating of the Ocean by a Submerged Submarine," NRL Report 5376 (Secret Report, Confidential Title), Aug. 31, 1959

14. Hershey, A.V., "Surface Elevations in Waves Generated by Submarines," U. S. Naval Proving Ground Report 1667 (Confidential), Aug. 14, 1959

15. Unpublished Calculations by the David Taylor Model Basin (unclass)

16. Clark, H.L., "Project Clinker Report No. 8, Visual Observation of the Change in Surface-Wave Structure Produced by a Submerged Submarine," NRL Report 5395 (unclass Report, unclass Title), Sept. 10, 1959

17. Stromberg-Carlson Report, "A Table of Amplitudes of Surface Waves Generated by Submerged Submarines" (unclass), Sept. 17, 1959

18. Keener, E.E., "Detection of Nuclear Powered Submarines by Thermal Effects," NADC Report NADC-WR-5726 (uncl.), Apr. 1958

19. Bieber, C.F., Hawley, W.H., and Mahloy, J.D., "Project Clinker Report No. 9, Airborne Measurements of the Parameters of Wakes Generated by Submarines Operating Down to 400-Foot Depth," NRL Report No. 5438 (unclass Report, unclass Title), Dec. 8, 1959

20. Sanderson, J.A., "The Experimental Background of Clinker," Proceeding of Symposium on Surface Effects of Submerged Submarines, ONR Symposium Report ACR-54, pp. 1-12 (uncl), Oct. 4-5, 1960

21. Plyler, E.K., and Acquista, N., "Infra-red Absorption of Liquid Water from 2 to 42 Microns," JOSA, 54:505 (1954)

22. Mahloy, J.D., "Project Clinker Report No. 6, Surface Measurements of the Width and Temperature of Wakes from Submerged Submarines," NRL Report 5375 (unclass Report, unclass Title), Sept. 1, 1959

23. Holm, W.R., "Thermal Signals Due to the Reflection of Sky Radiation by the Sea," NRL Report 2506 (Unclassified), Apr. 20, 1945

24. Bell, E.E., Eisner, L., Young, J., and Oetjen, R.A., "Spectral Radiance of Sky and Terrain at Wavelengths Between 1 and 20 Microns, II Sky Measurements," JOSA 50:1313-1320 (1960)

25. Taylor, J.H., and Yates, H.W., "Atmospheric Transmission in the Infrared," JOSA 47:223-226 (1957)

26. Bieber, C.F., "Radiation Temperature of Sea and Sky," NRL Memo. Rept. 1163, Apr. 1961

27. McComb, C.T., "Optimum f-Number for Parabolic Mirrors Used in Non-Image-Forming Optical Systems," NRL Report 5396 (Unclassified), Sept. 10, 1959

28. NAS, Lakehurst, New Jersey, letter, Code No. 71, Jan. 21, 1959

29. Cook, M.L., "Wind-Tunnel Tests of 1/8-Scale Aerodynamic Enclosure for the AN/AAR-23(XB-1) Equipment Used on the ZPG-2 Airship," DTMB Aero Report 963 (Unclassified), Jan. 1960

30. Murphy, R.D., and Rosenik, W.F., "Cavity Turbulence Tests Using a 0.0646 Scale Model R50-2 Airplane," Aero Report No. 1017, Sept. 1961

31. "Infrared Detection Set, AN/AAR-23(XB-1)," NRL Instruction Book No. 24 (unclass), March 1960

32. Hall, J.F., and Allen, R.C., "Reflectance of Oxidized Silicon Monoxide Films Deposited onto Aluminum Mirrors Compared with Silicon Monoxide Evaporated in High Vacua," JOSA 51:367-368 (1961)

33. Clark, H.L., "Project Clinker," NRL Memo. Rpt. 463 ([redacted] Report, Unclassified Title), Jan. 1955 unclass

34. Kohn, E.J., Venezky, D.L., Ross, F.J., Asbury, C.F., and Rice, R.G., "The Development of the NRL Electrochemical Recorder Paper," NRL Report 4685 (Unclassified), Mar. 1956

35. Neubauer, W.G., "A Multi-finger Stylus for Use with a Current-Sensitive Chemical Recording Paper," NRL Memo. Rpt. 398 (Unclassified), Nov. 1954

36. Tucker, J.W., "A Submarine-Launched Flashing-Light Buoy," NRL Report 4201 (Unclassified), Sept. 1953

37. Spann, W.L., "Fleet Operational Investigation of Detecting Set Infrared AN/AAR-23 (XB-1)," Proceedings of Symposium on Surface Effects of Submerged Submarines, ONR Symposium Report ACR-54 ([redacted]), pp. 16-31, Oct. 4-5, 1960 unclass

38. "First Partial Report on RTED Project NDSW-ONR-46140," NADU Rpt., May 1961

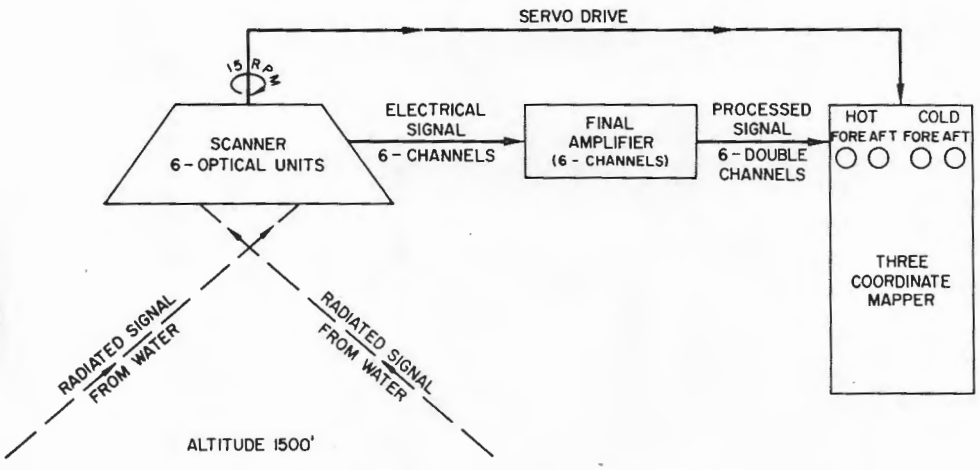

Fig. 12 - Block diagram of AN/AAR-23(XB-1) ([redacted] (unclass)

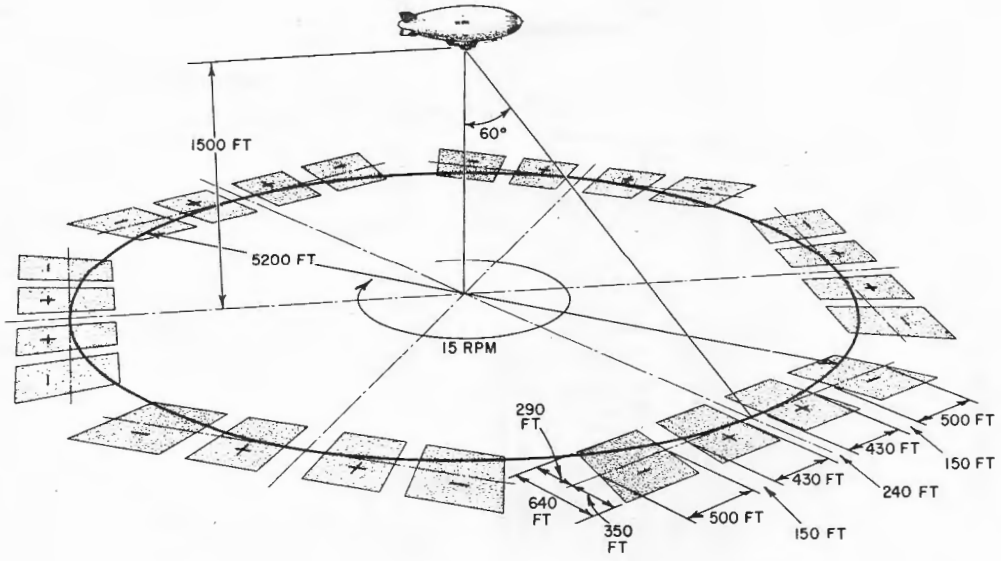

Fig. 13 - Scan parameters of AN/AAR-23(XB-1) ([redacted] (unclass)

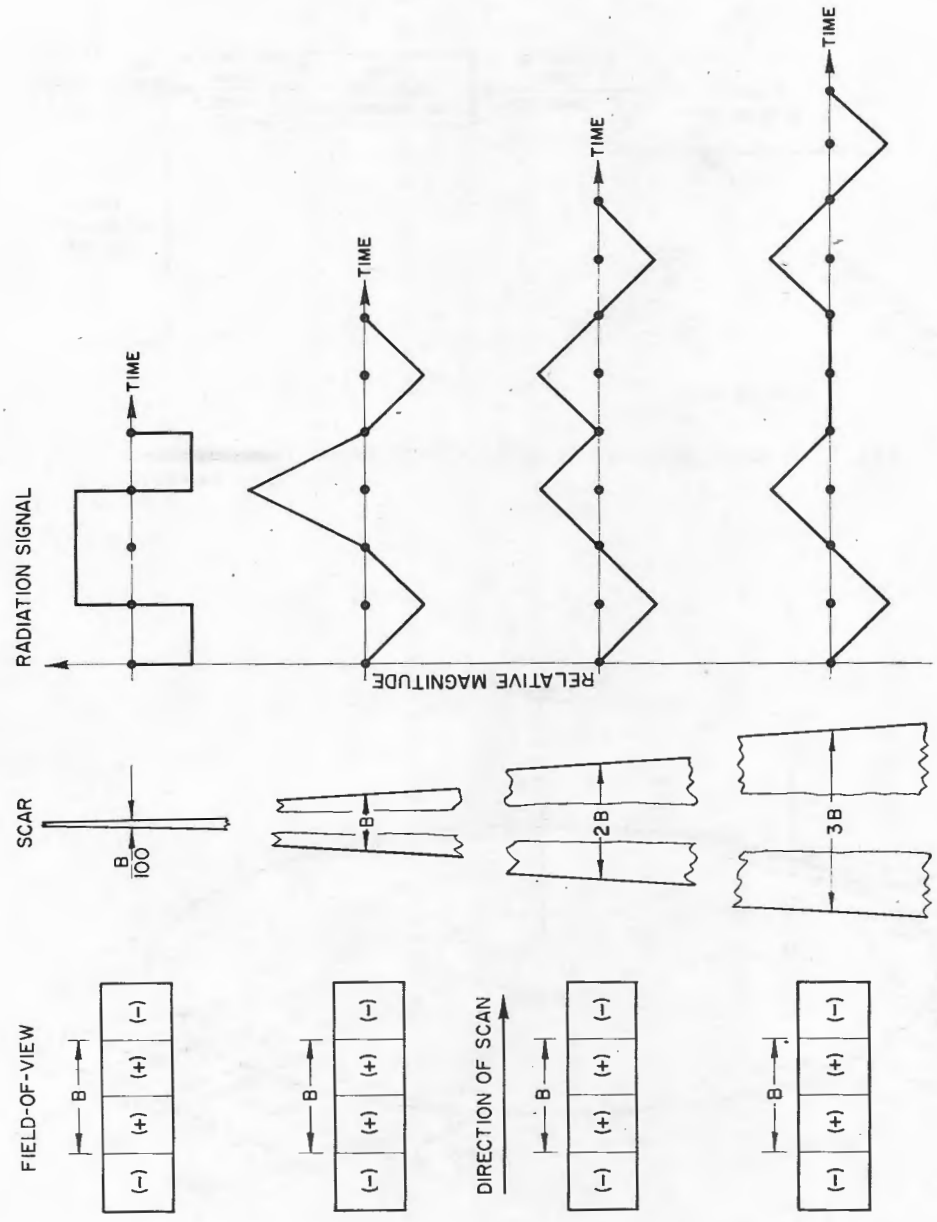

Fig. 14 - Radiation signals generated by scanning across "cold" scars of different widths but equal radiant intensities (idealized) ([redacted] (unclass))

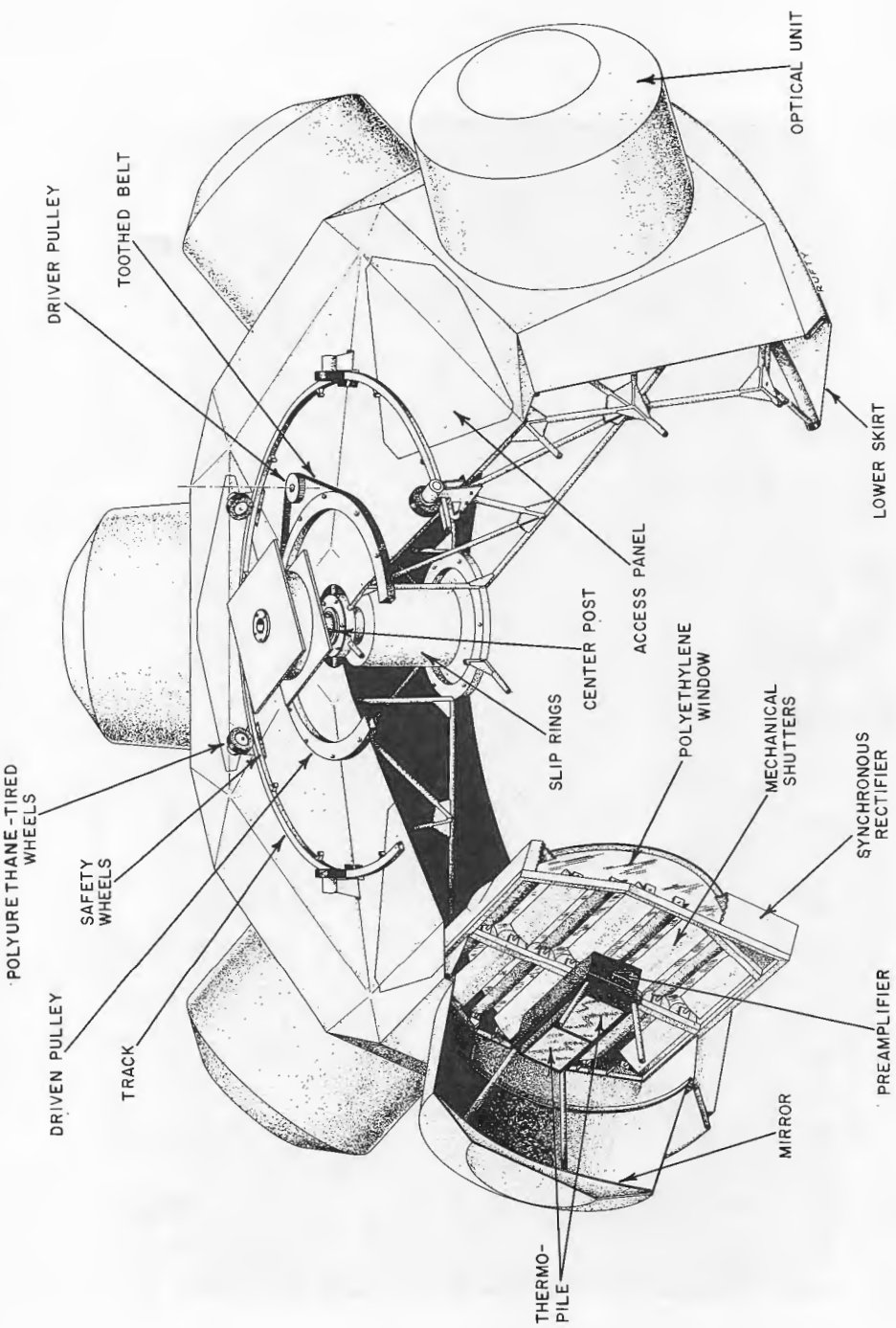

Fig. 15 - Details of scanner assembly ([redacted] (unclass)

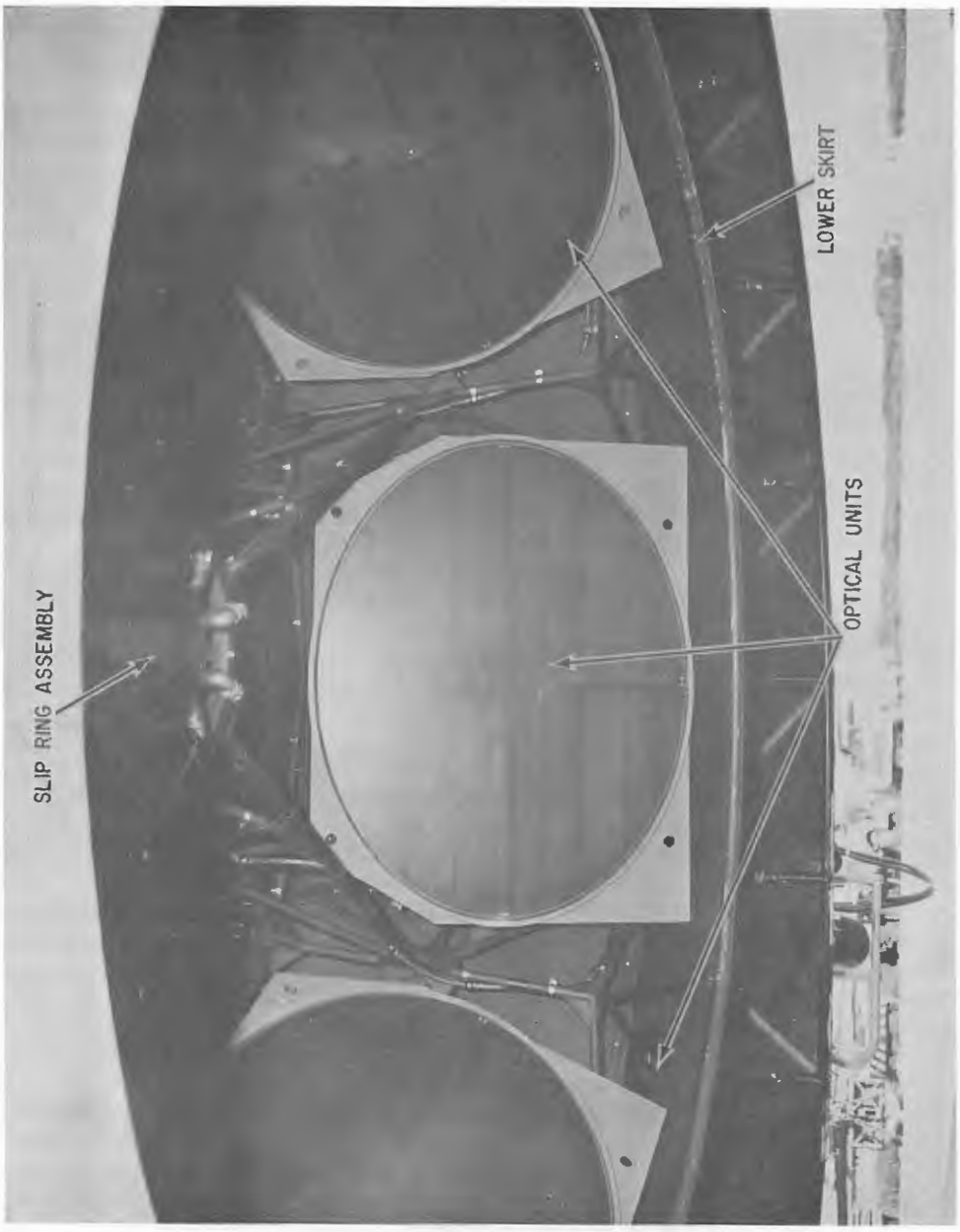

Fig. 16 - Complete scanner, showing rigid tubular frame to which optical units are attached ([redacted] (unclass))

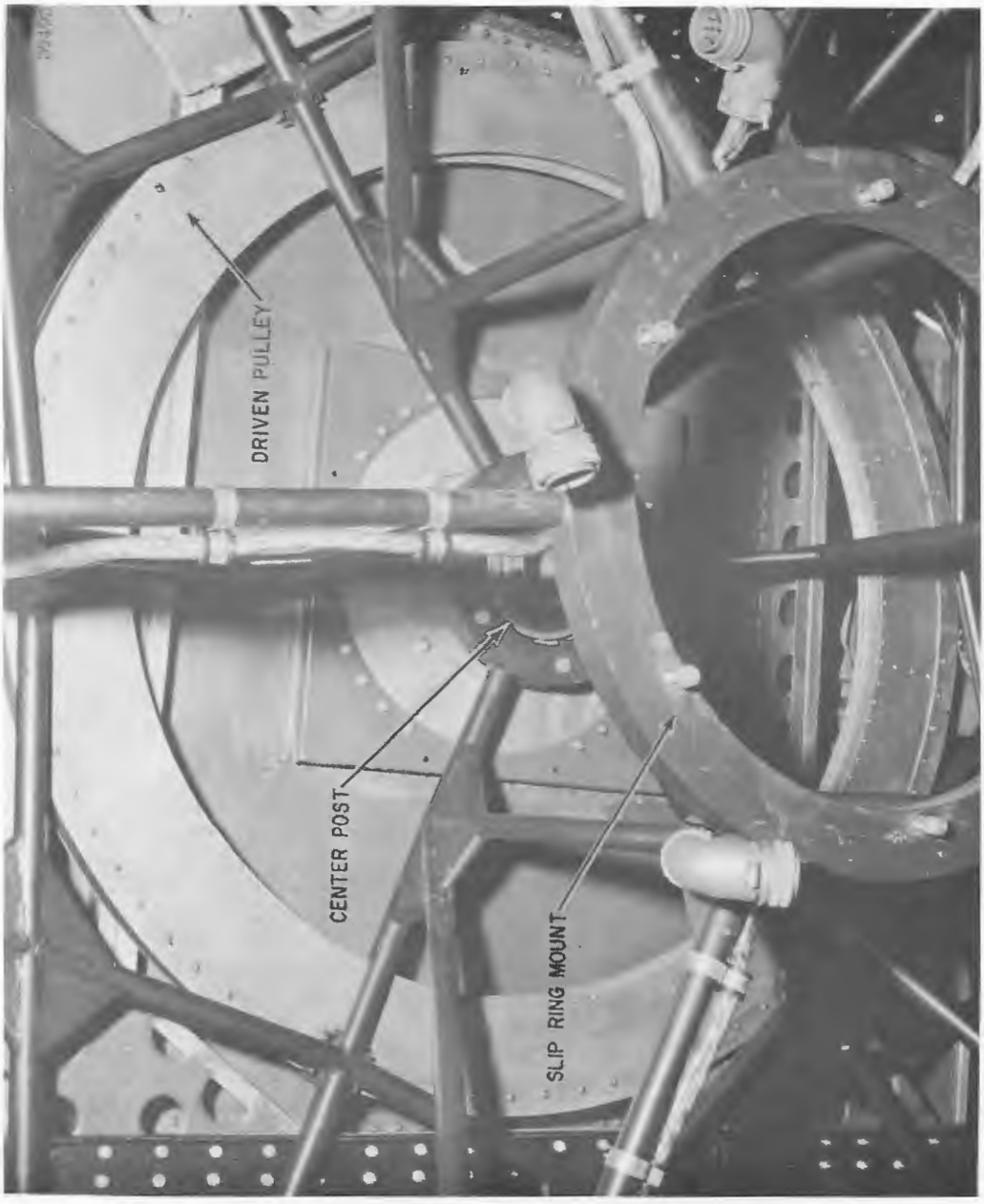

Fig. 17 - Center of scanner, with aerodynamic skin removed to show center post ([redacted]) (unclass)

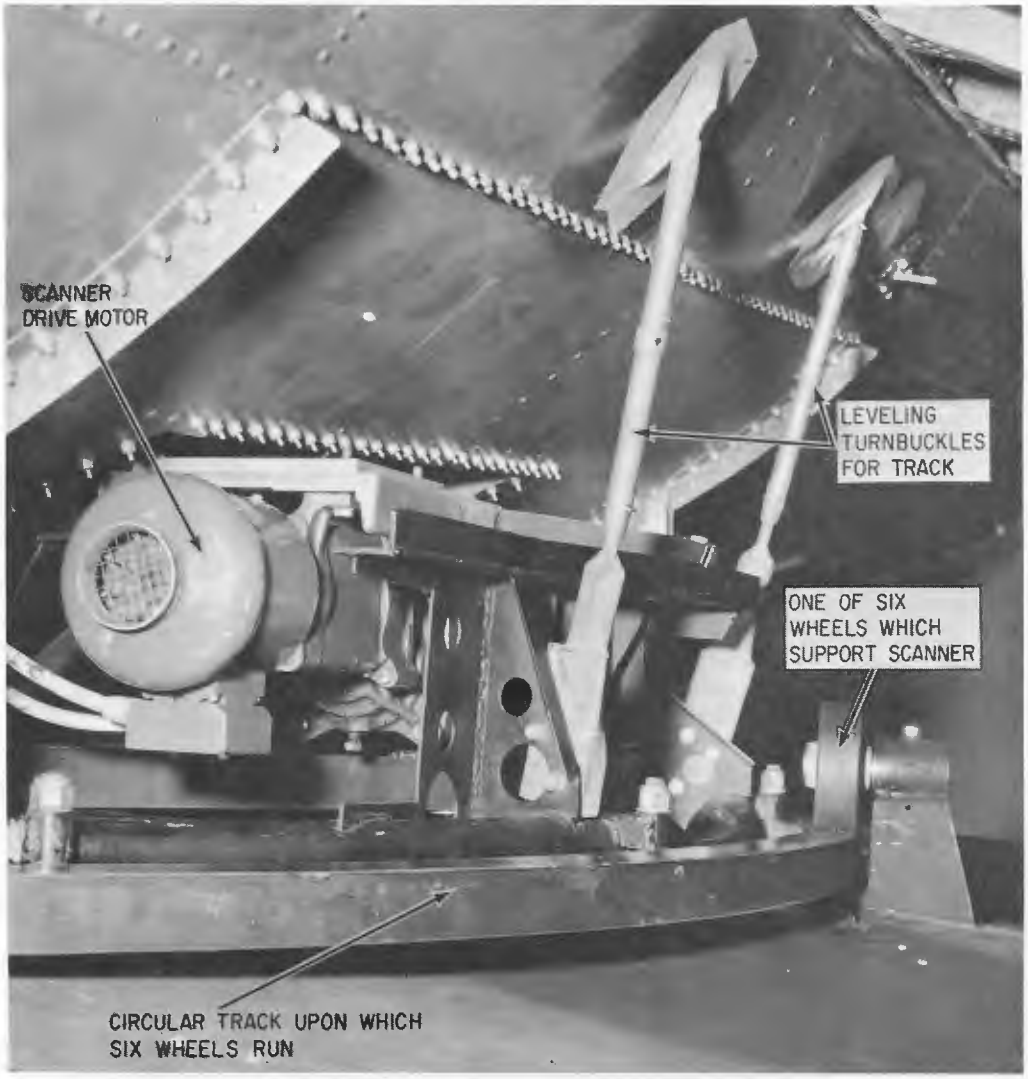

Fig. 18 - Scanner track and one of the six supporting wheels (C[redacted]l)
(unclass)

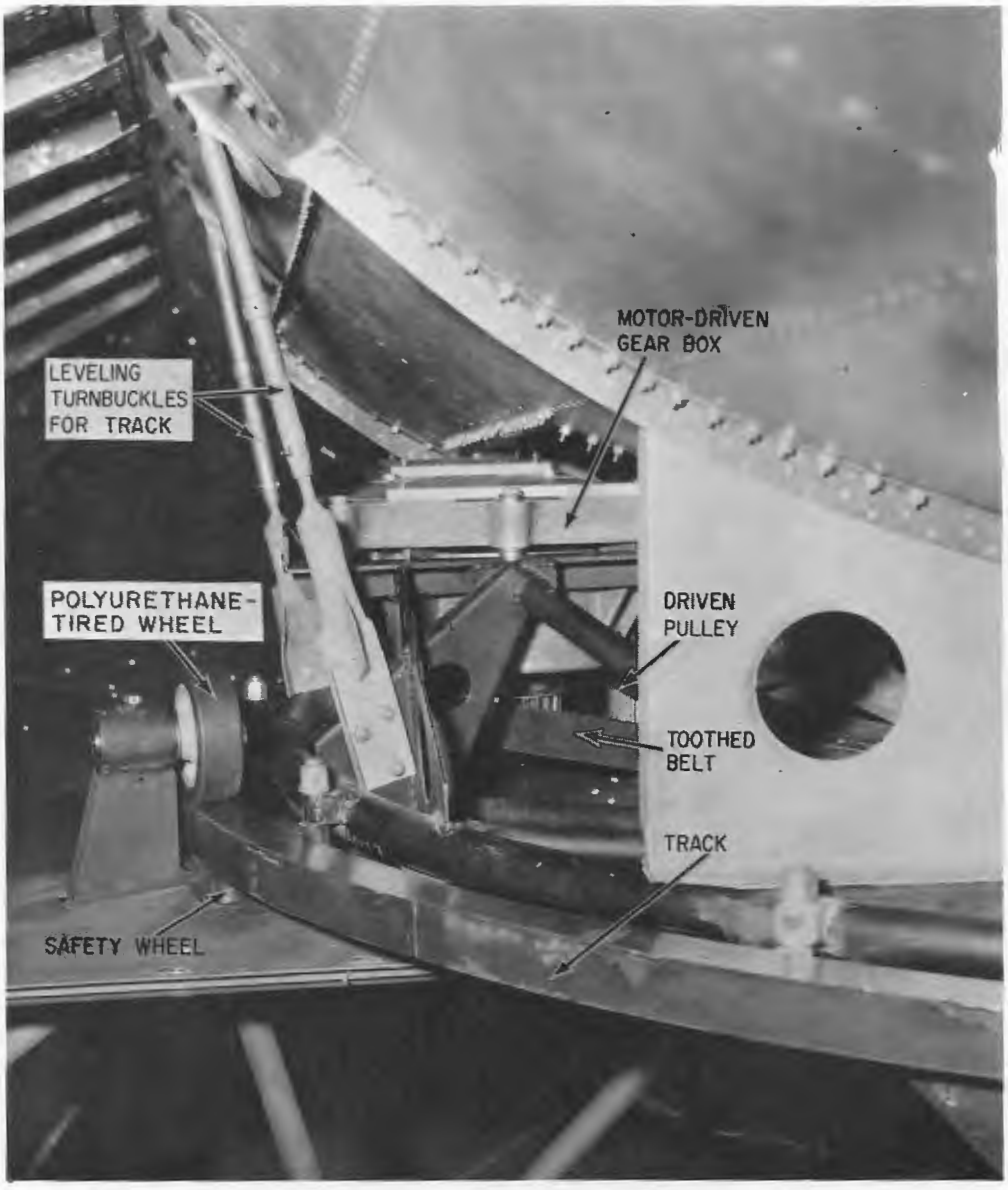

Fig. 19 - Scanner belt drive ([redacted])
(unclass)

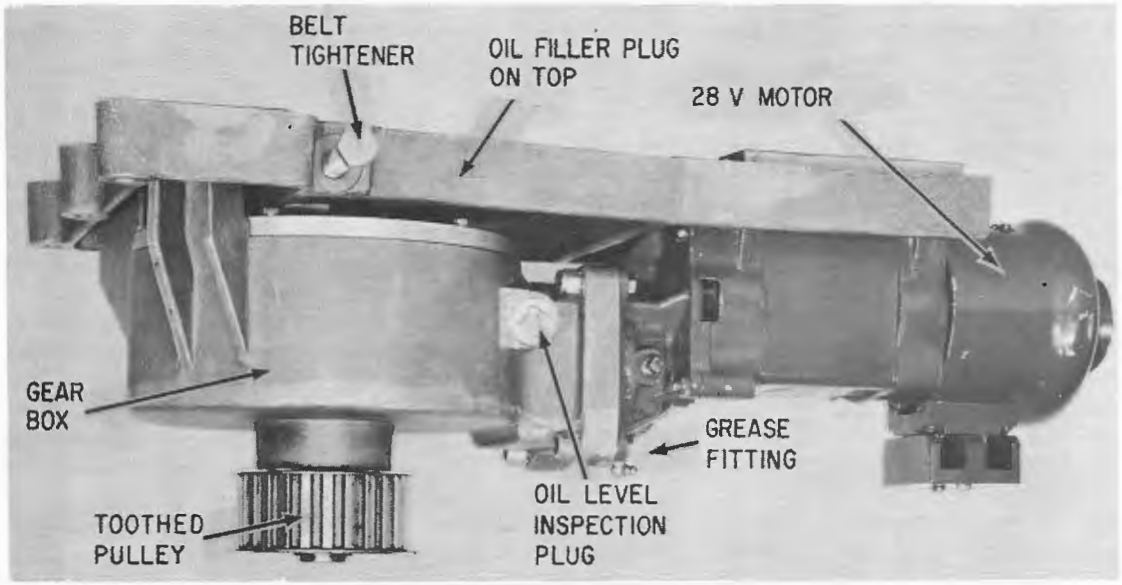

Fig. 20 - Motor drive unit (Unclassified)

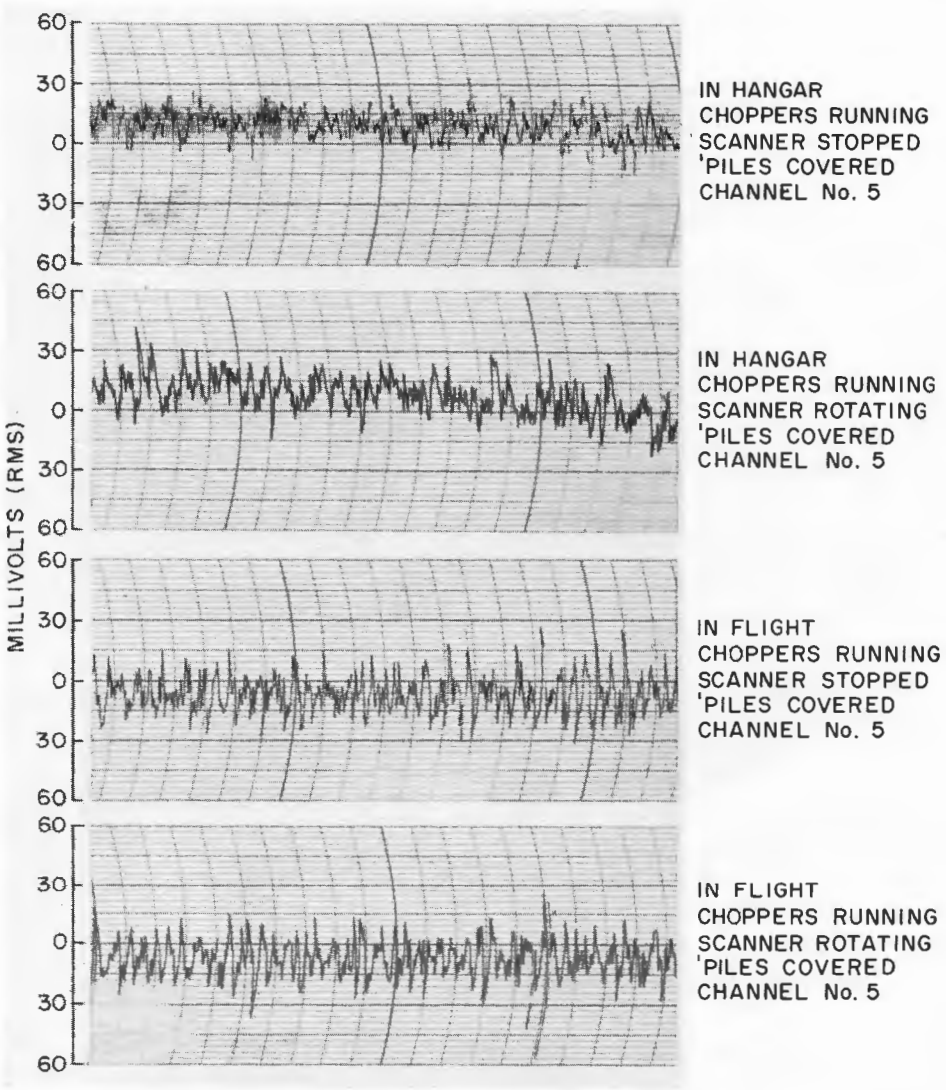

Fig. 21 - Noise level of an optical unit under various conditions of operation. Thermopiles are covered. Noise is vibrational. ([redacted])

(unclass)

[redacted]

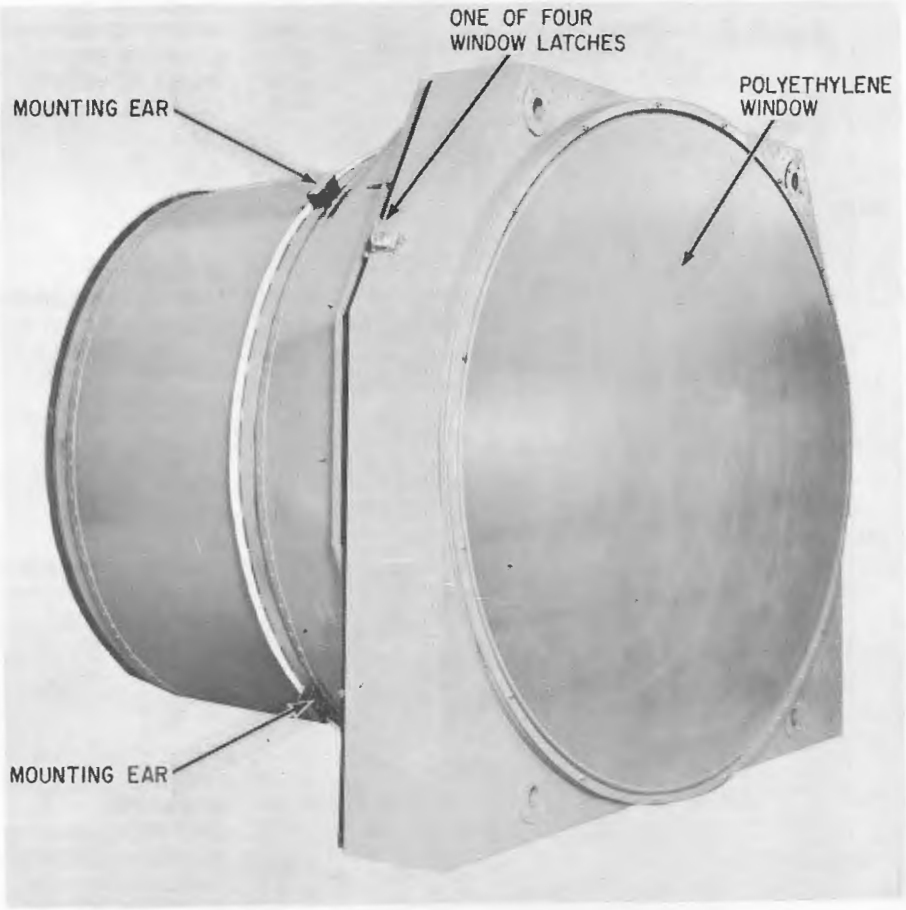

Fig. 22 - Complete optical unit [redacted] (unclass)

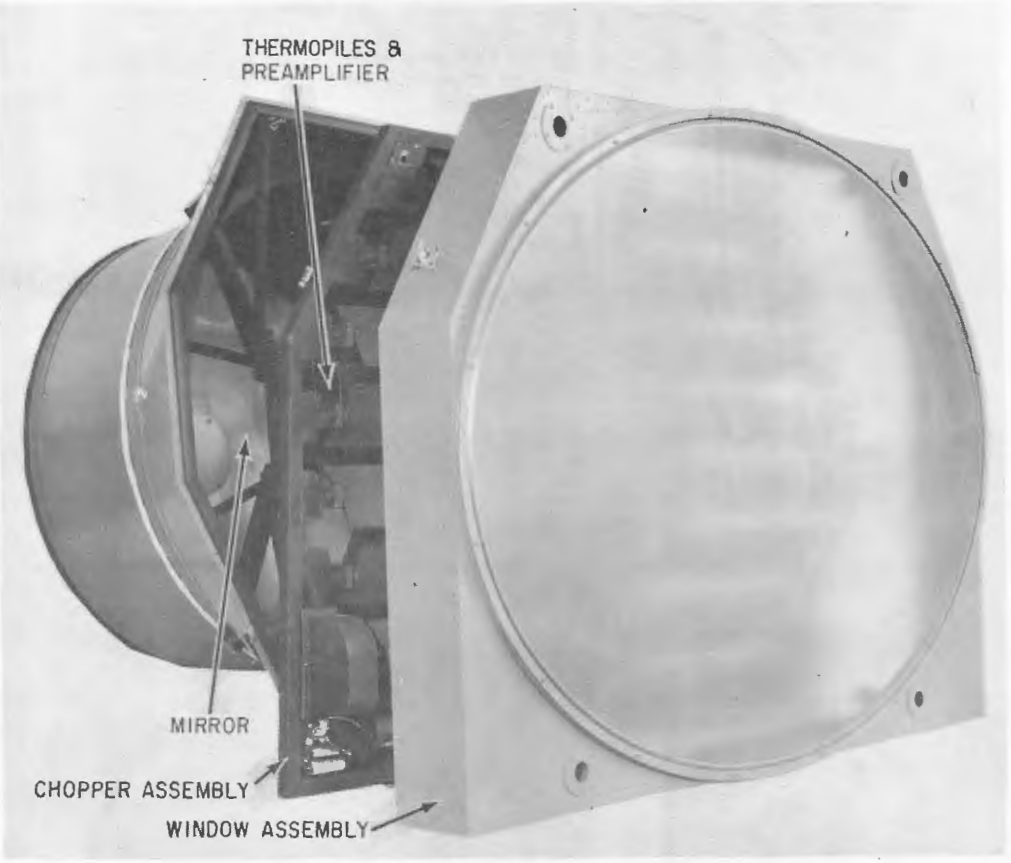

Fig. 23 - Optical unit disassembled ([redacted])
(unclass)

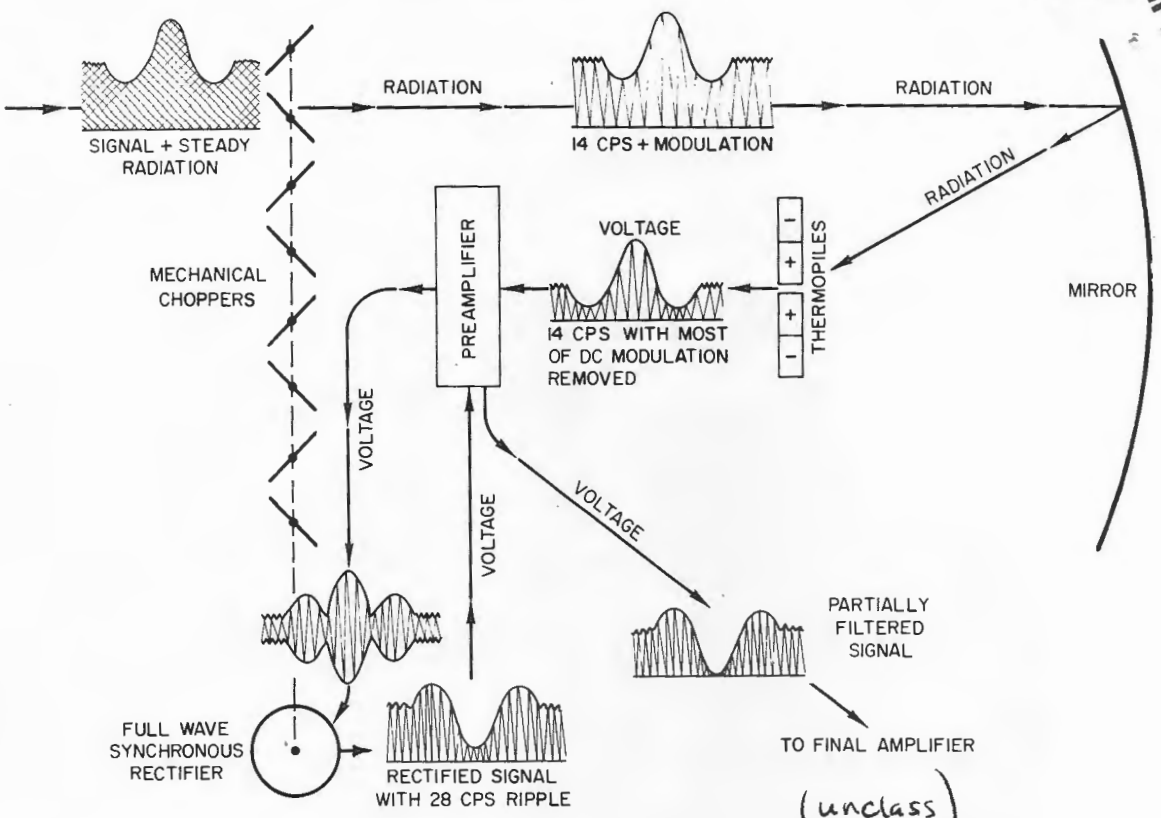

Fig. 24 - Functional diagram of an optical unit ([redacted]) (unclass)

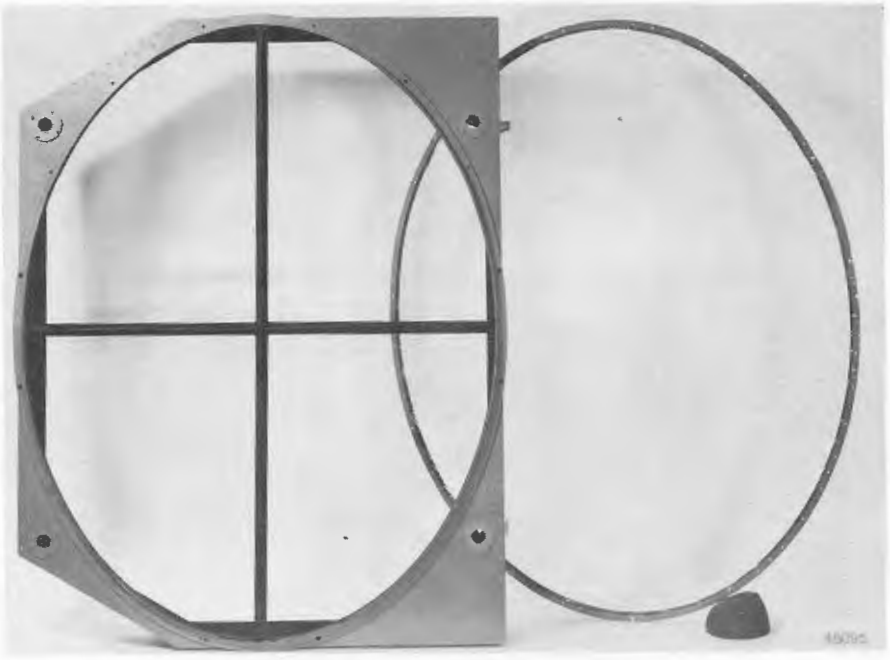

Fig. 25 - Polyethylene window assembly ([redacted]) (unclass)

[redacted]

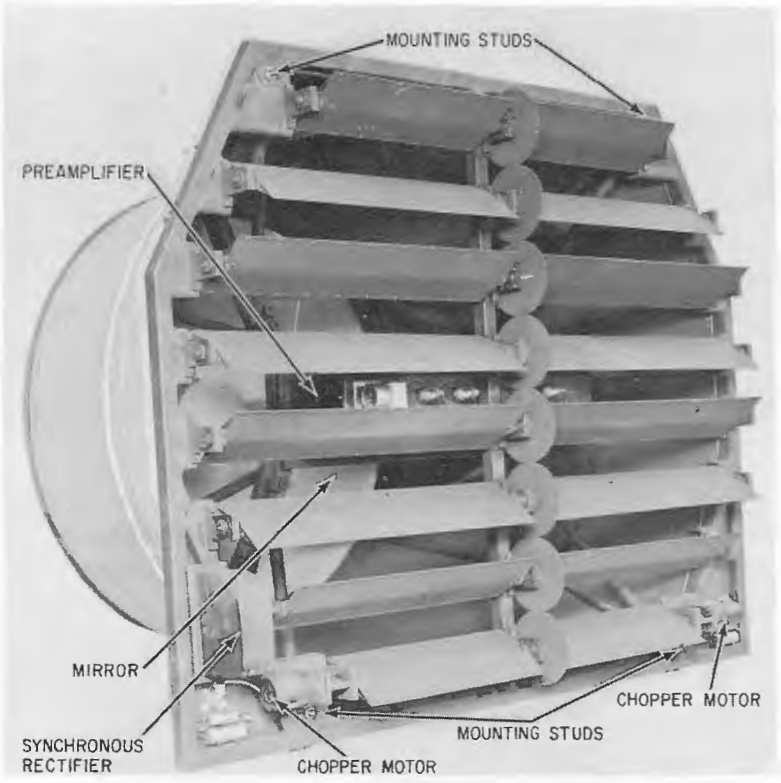

Fig. 26 - Optical unit with window assembly removed (unclass)

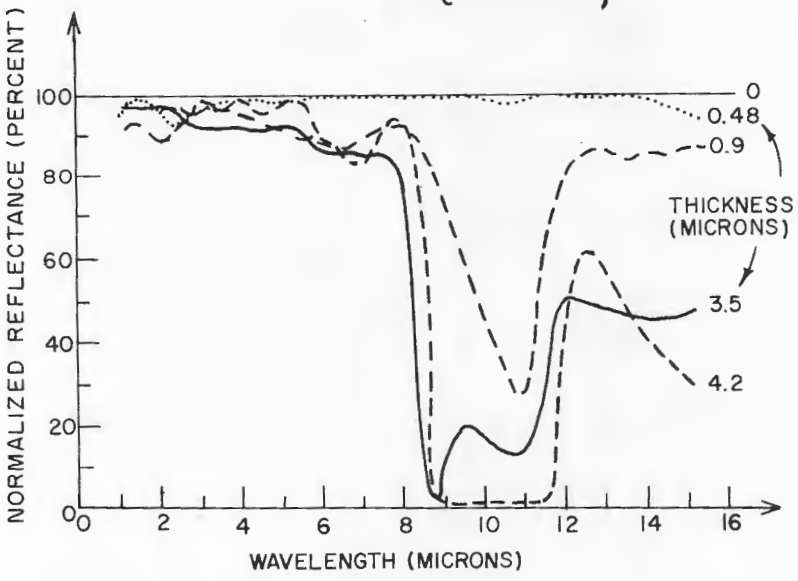

Fig. 27 - The effect on reflectivity of various thicknesses of silicon monoxide vacuum deposited on aluminum (Unclassified)

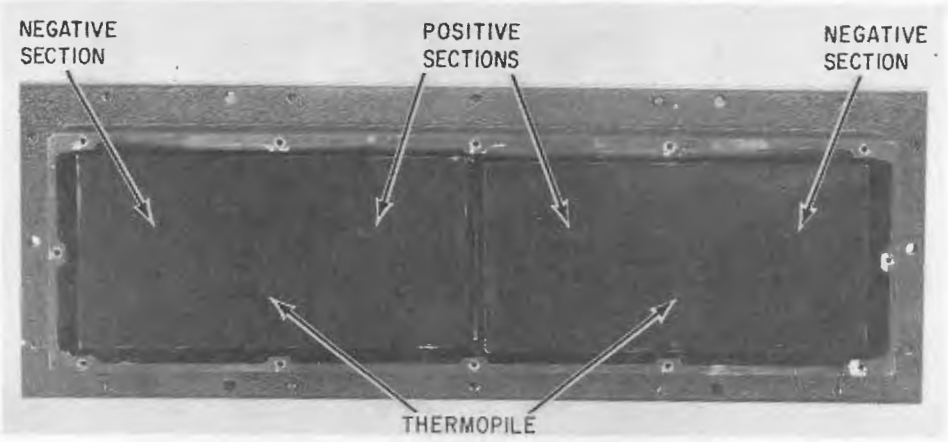

Fig. 28 - Mirror side of preamplifier, showing thermopiles. Only silver chloride windows are visible. ([redacted]) (unclass)

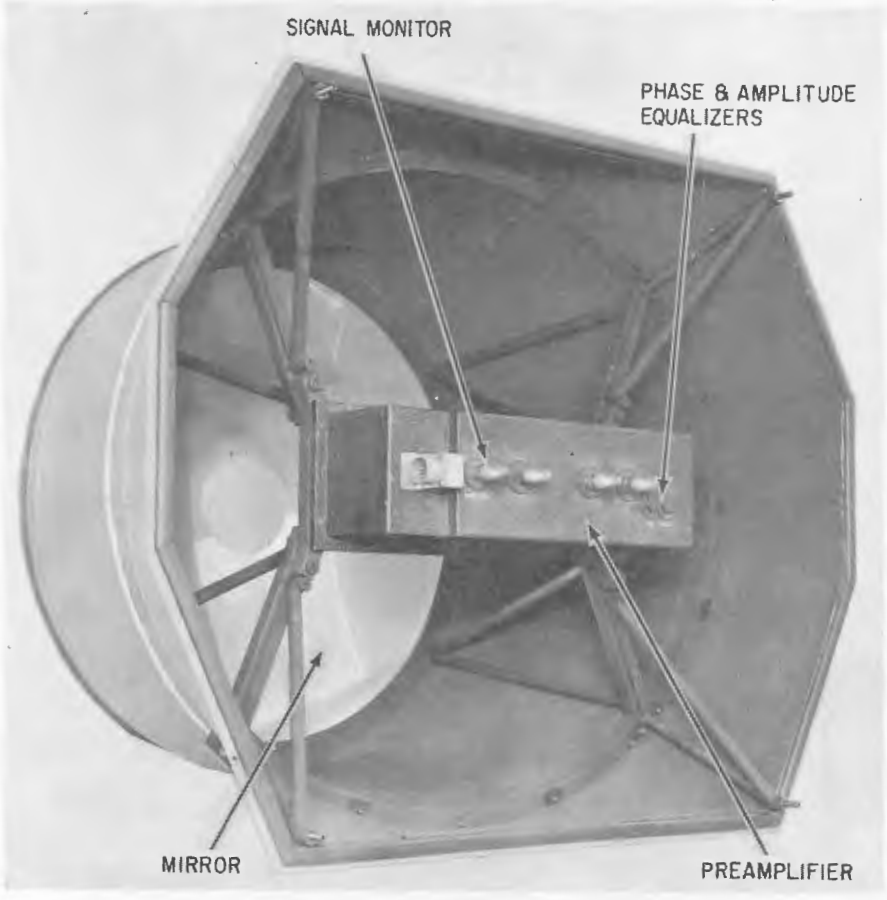

Fig. 29 - Optical unit with chopper assembly removed ([redacted] (unclass)

[redacted]

(PAGE 76 BLANK)

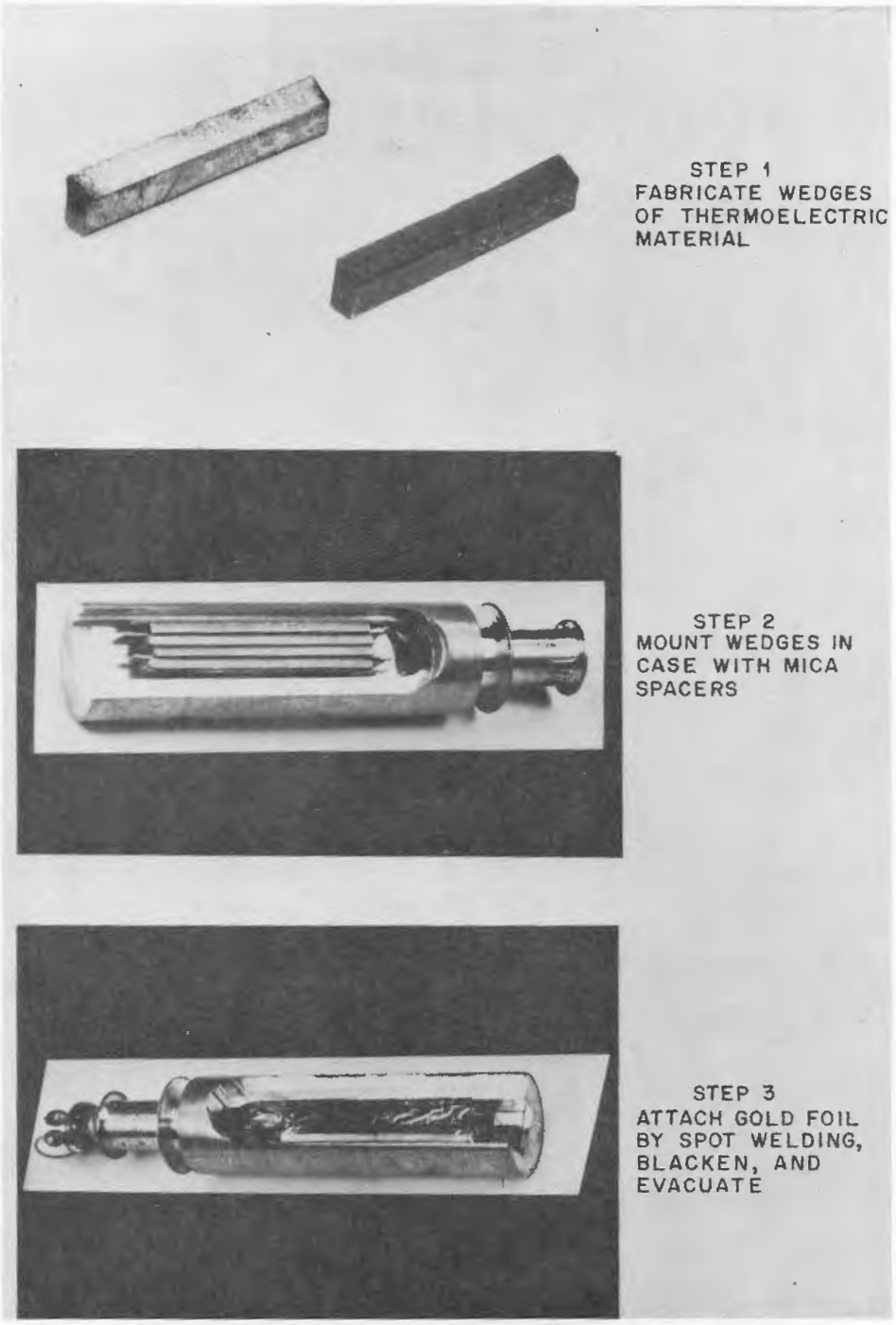

Fig. 30 - Steps in the manufacture of the special thermopiles used in the AN/AAR-23(XB-1). Mounting case shown is for illustrative purposes only. Actual units employ a rectangular 5 × 11 in. case in which these basic units are stacked. (Confidential)

(unclass)

[redacted]

[redacted]

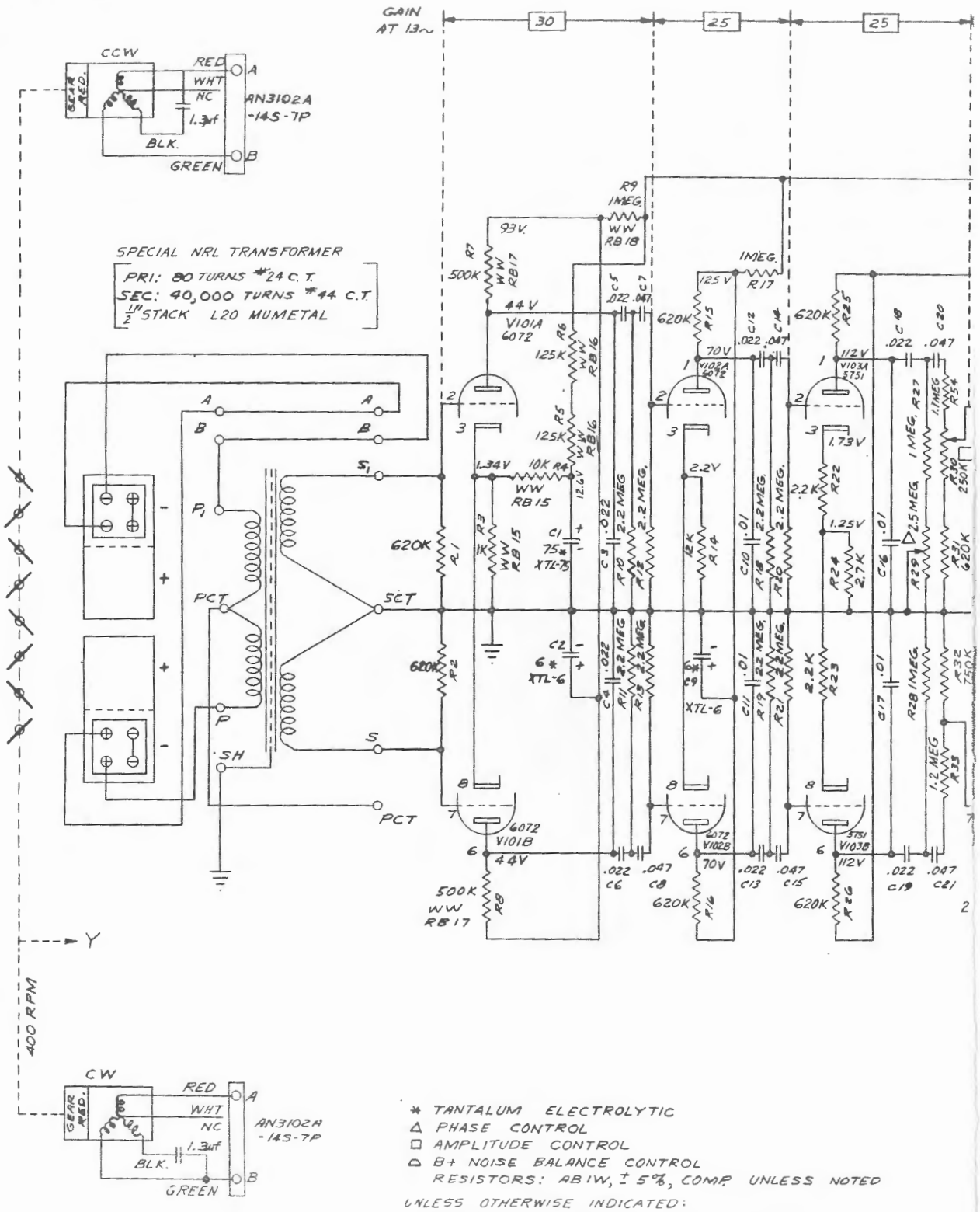

* TANTALUM ELECTROLYTIC
△ PHASE CONTROL
□ AMPLITUDE CONTROL
⏀ B+ NOISE BALANCE CONTROL
RESISTORS: AB 1W, ± 5%, COMP. UNLESS NOTED

UNLESS OTHERWISE INDICATED:
ALL RESISTANCE VALUES ARE IN OHMS.
ALL CAPACITANCE VALUES ARE IN MICROFARADS.

GLOBE IND., INC.
AC-16315
115V, 400~ HYSTERESIS SYNCHRONOUS
(2-REQ'D)

[redacted]

(PAGE 78 BLANK)

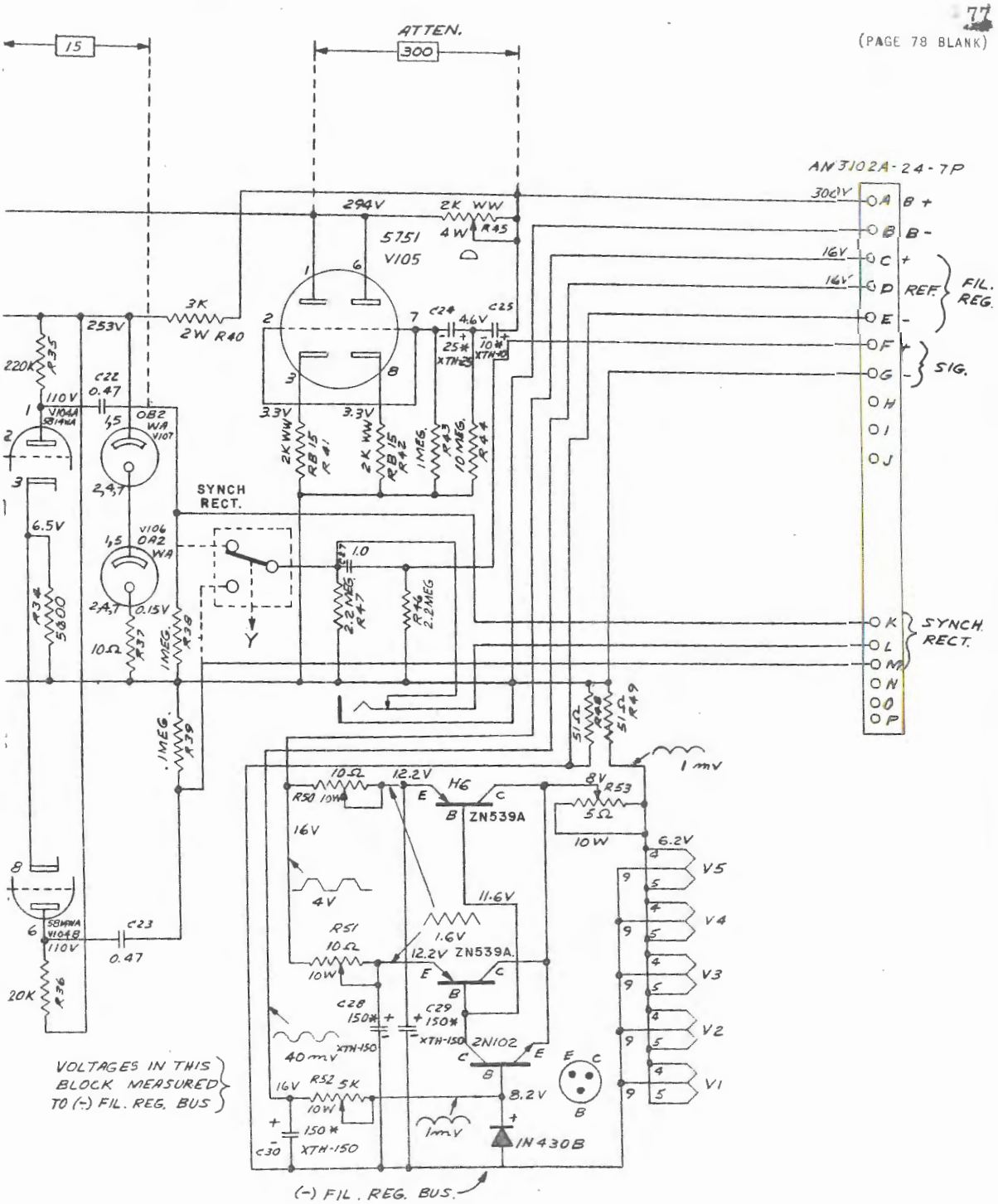

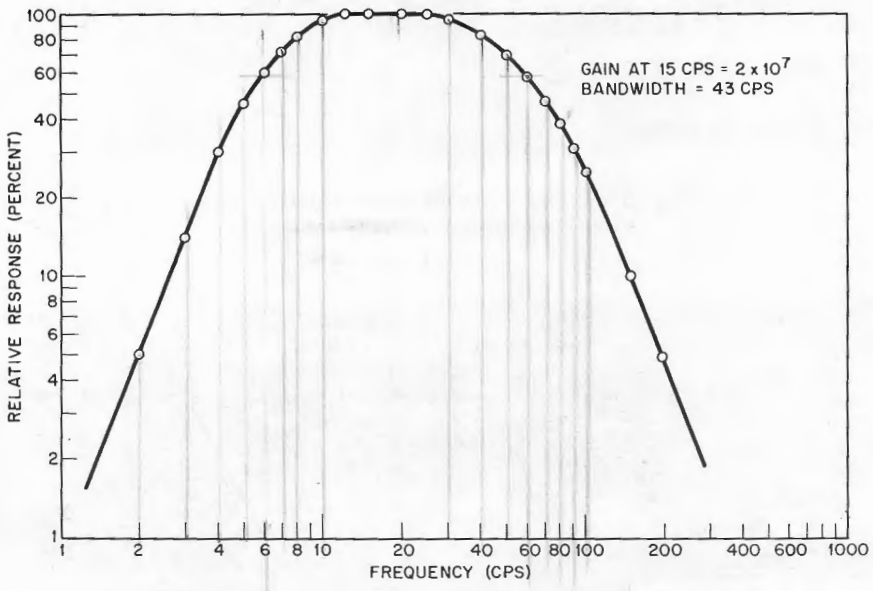

Fig. 32 - Frequency response of preamplfier

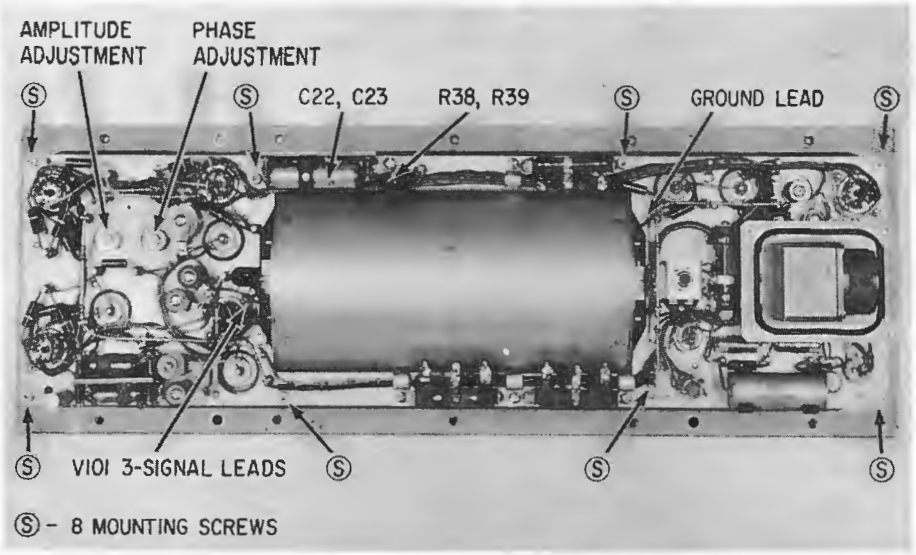

Fig. 33 - Top view of preamplifier with cover removed [redacted] (unclass)

(35)

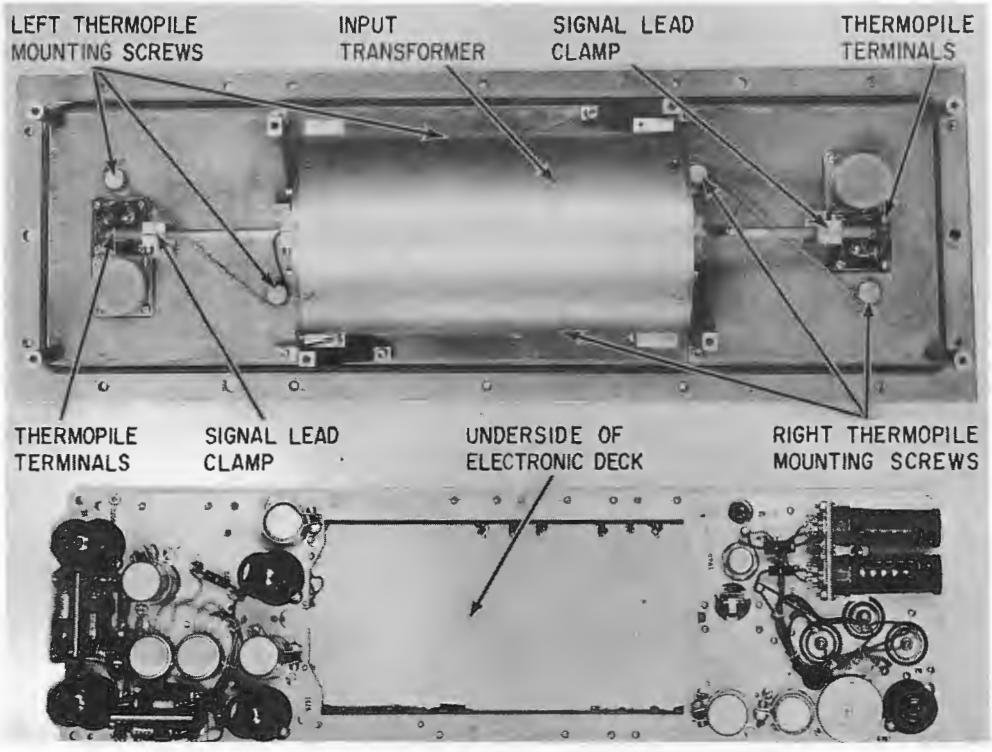

Fig. 34 - Preamplifier with electronic deck removed [redacted] (unclass)

[redacted]

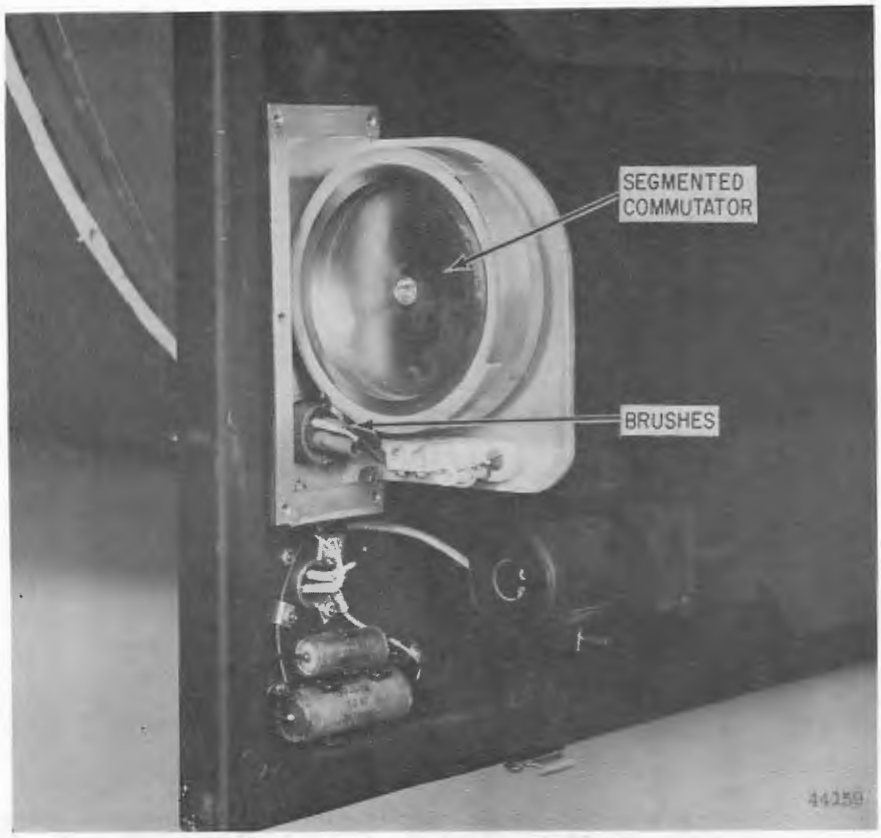

Fig. 35 - Synchronous rectifier [redacted]
(unclass)

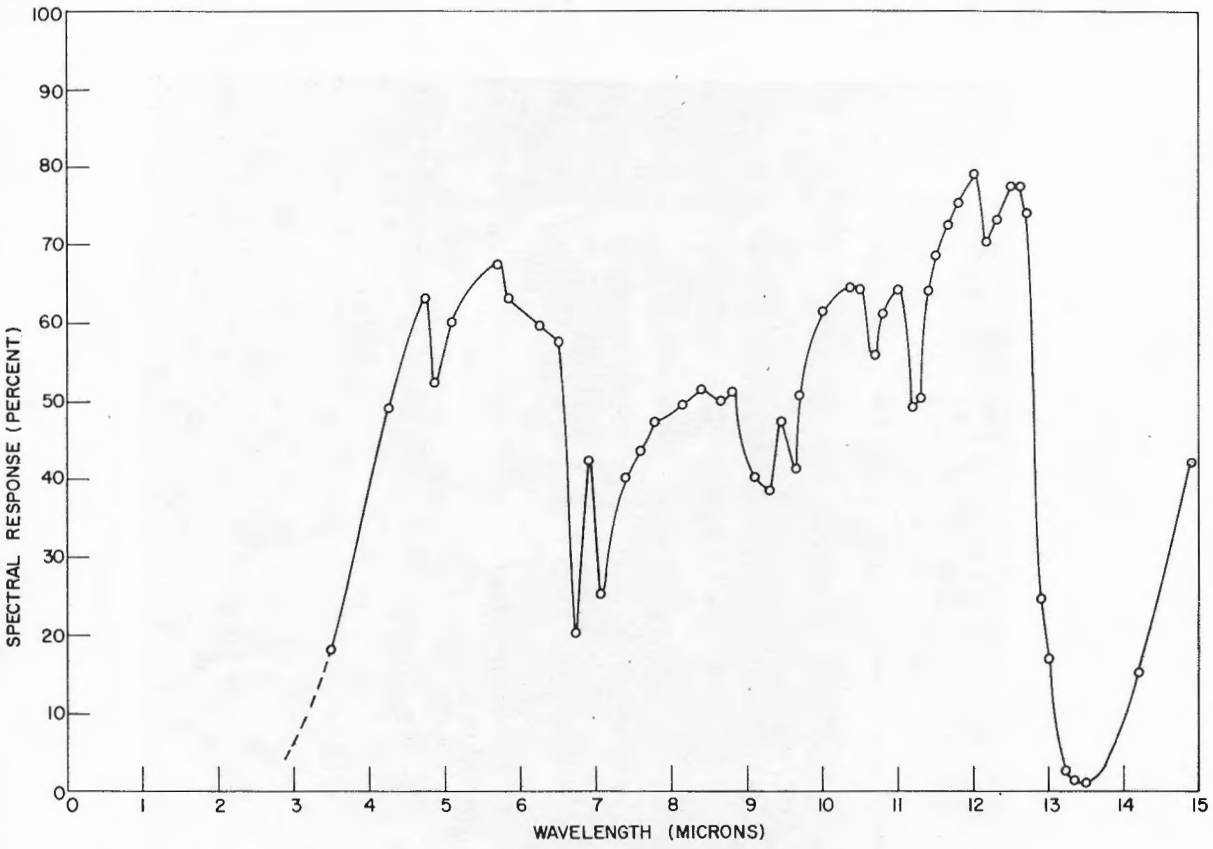

Fig. 36 - Spectral response of thermopile with coated window in place and mounted behind a 0.004-in.-thick sheet of polyethylene [redacted]

(unclass)

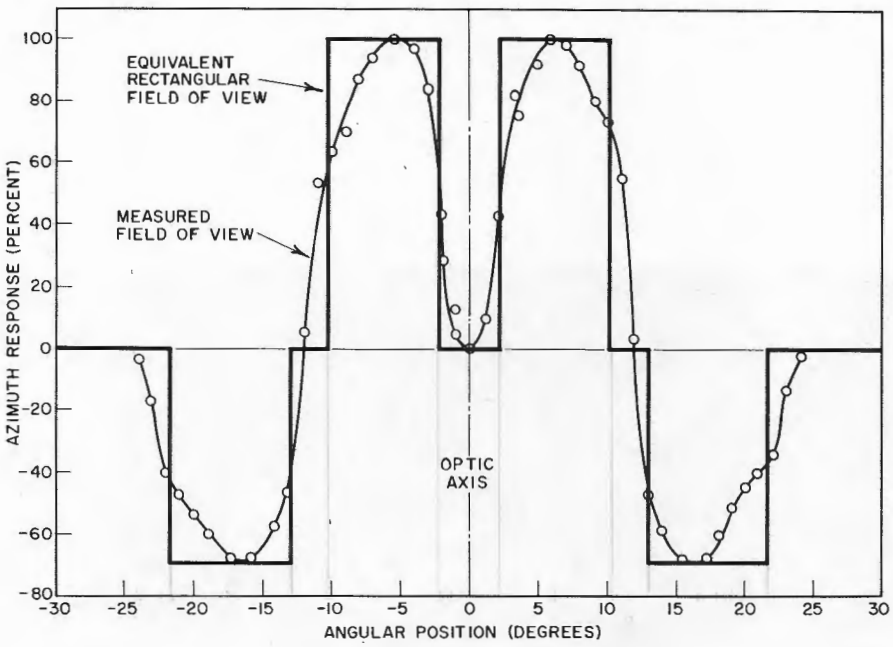

Fig. 37 - Horizontal dimensions of an optical unit's field of view (measured) [redacted] (unclass)

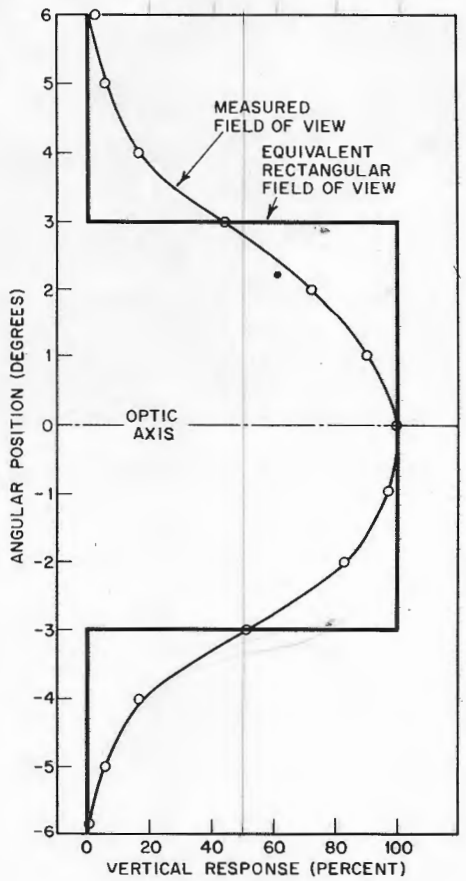

Fig. 38 - Vertical dimensions of an optical unit's field of view (measured) [redacted] (unclass)

[redacted]

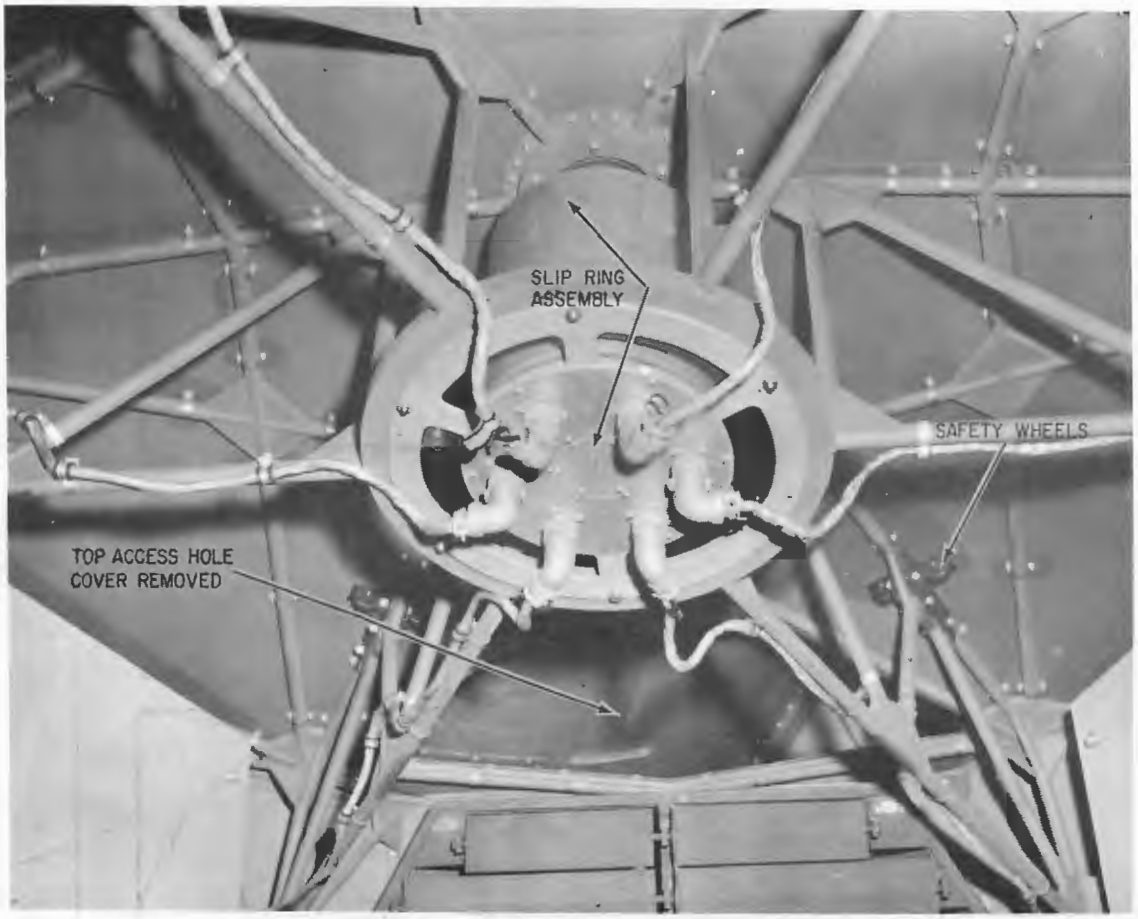

Fig. 39 - Center of scanner, showing slip-ring assembly ([redacted]1)
(unclass)

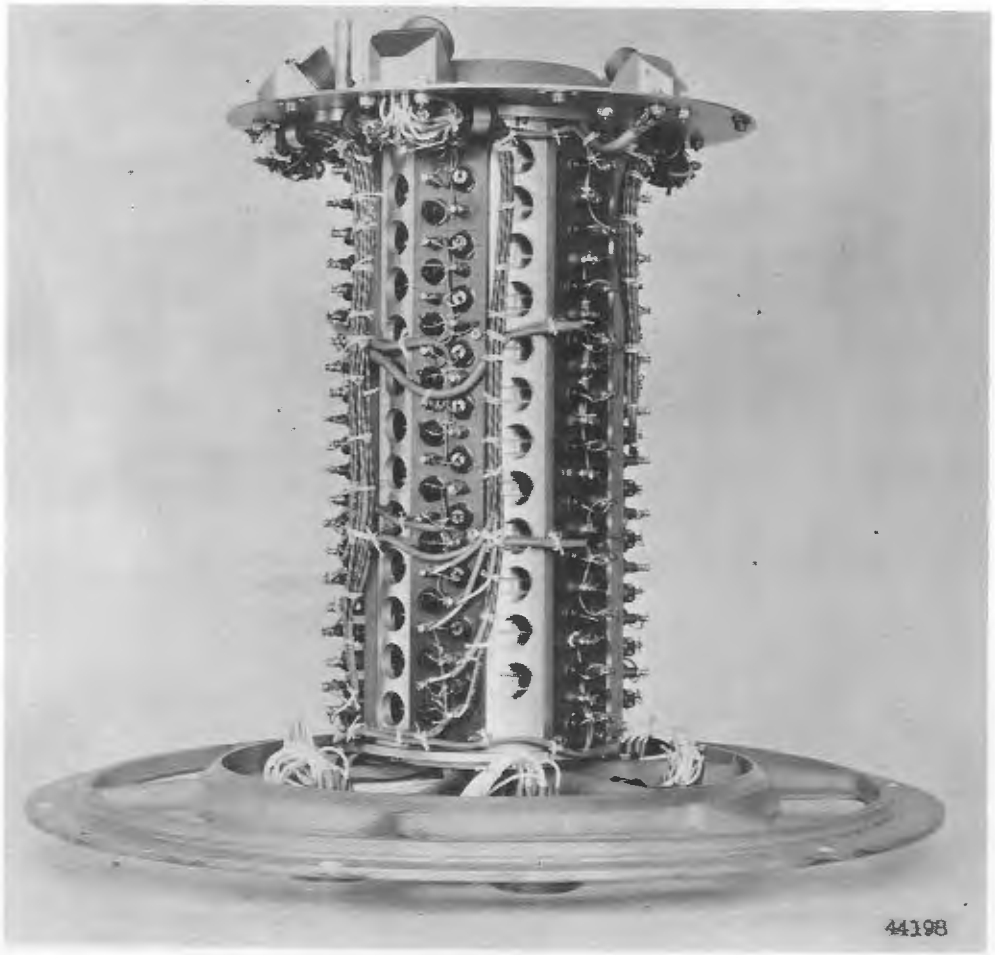

Fig. 40 - Slip-ring assembly with cover removed (Unclassified)

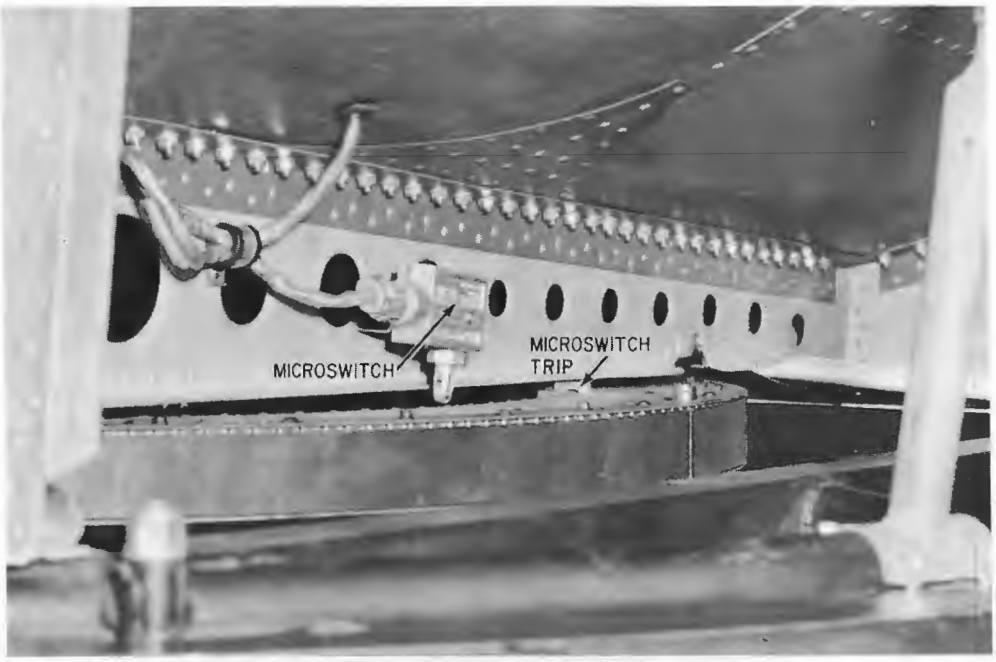

Fig. 41 - Microswitch used to check servo alignment between mapper and scanner ~~(Confidential)~~ (unclass)

Fig. 42 - Final amplifier ~~(Confidential)~~ (unclass)

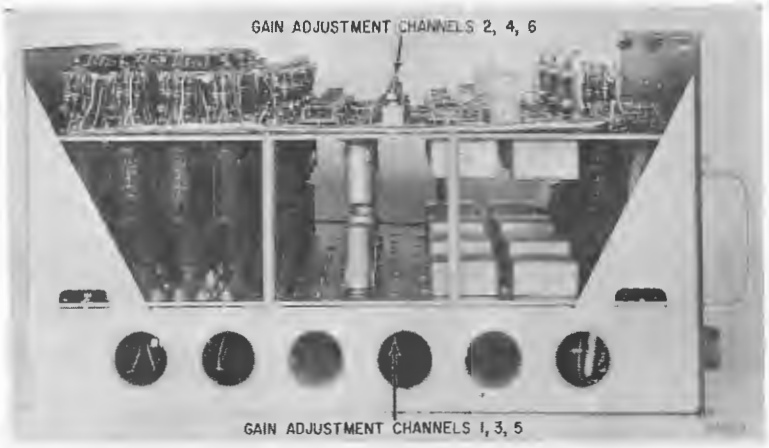

Fig. 43 - Side view of final amplifier, showing two-deck construction [redacted] (unclass)

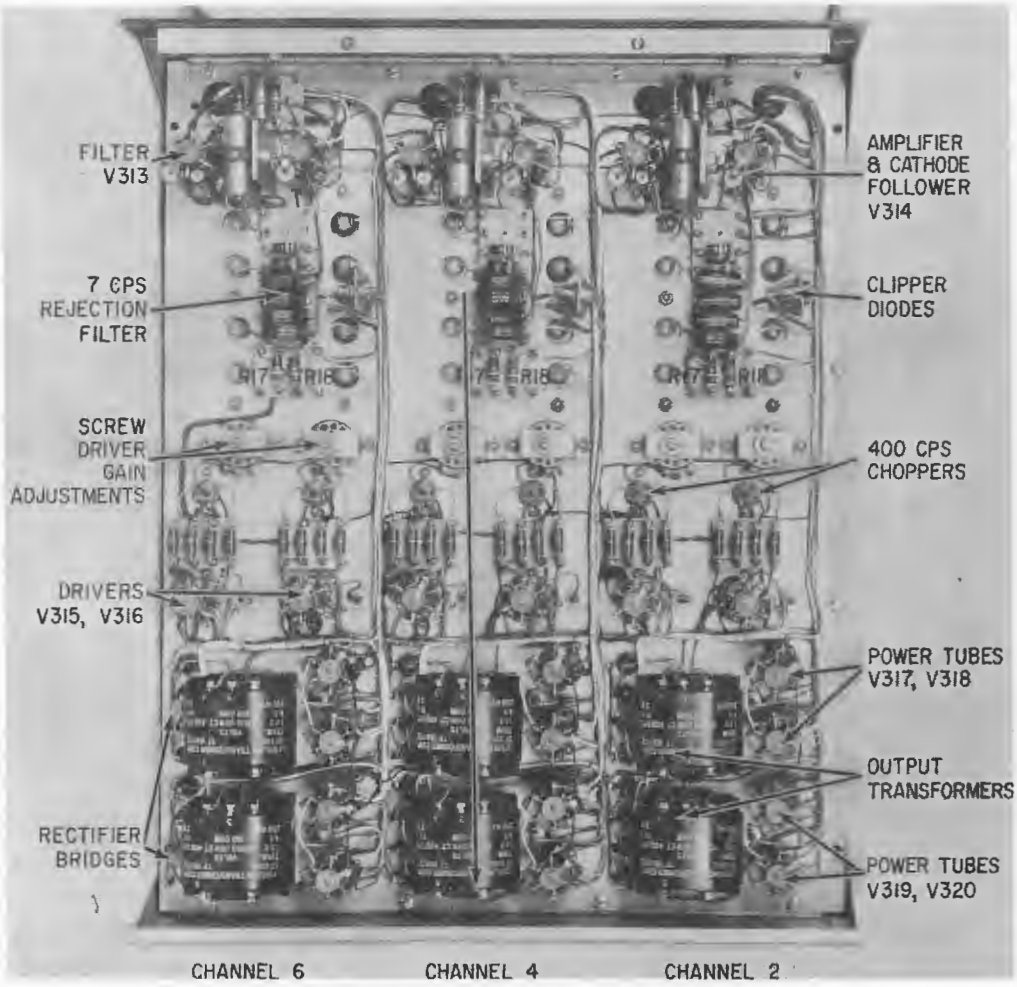

Fig. 44 - Top view of final amplifier [redacted] (unclass)

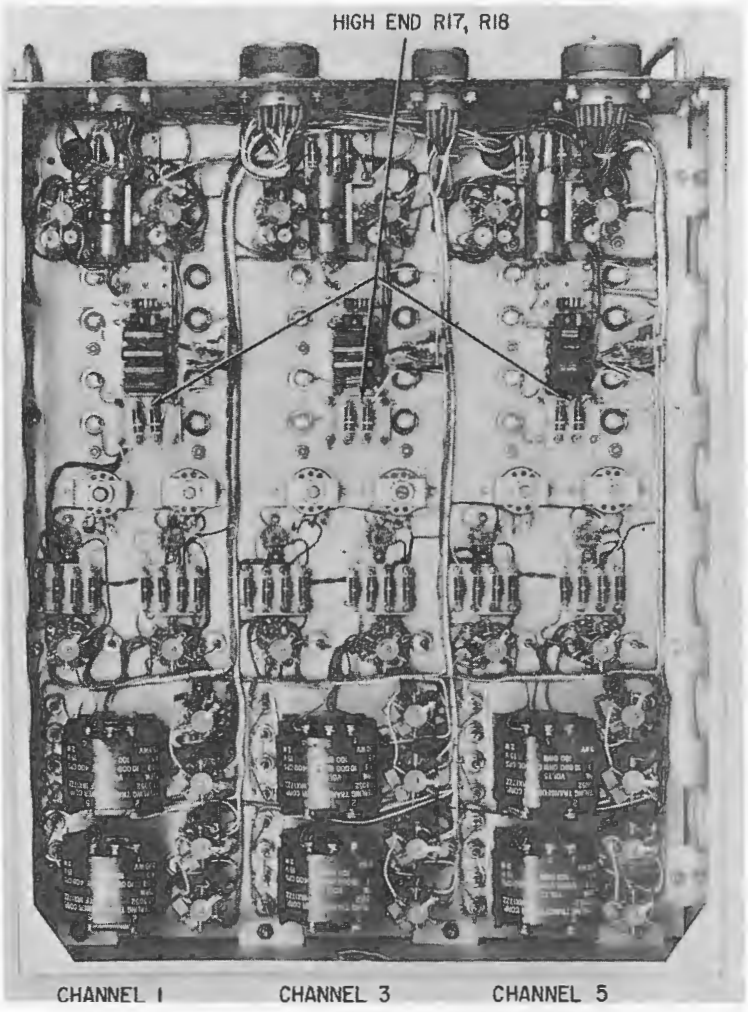

Fig. 45 - Bottom view of final amplifier ([redacted])

(unclass)

[redacted]

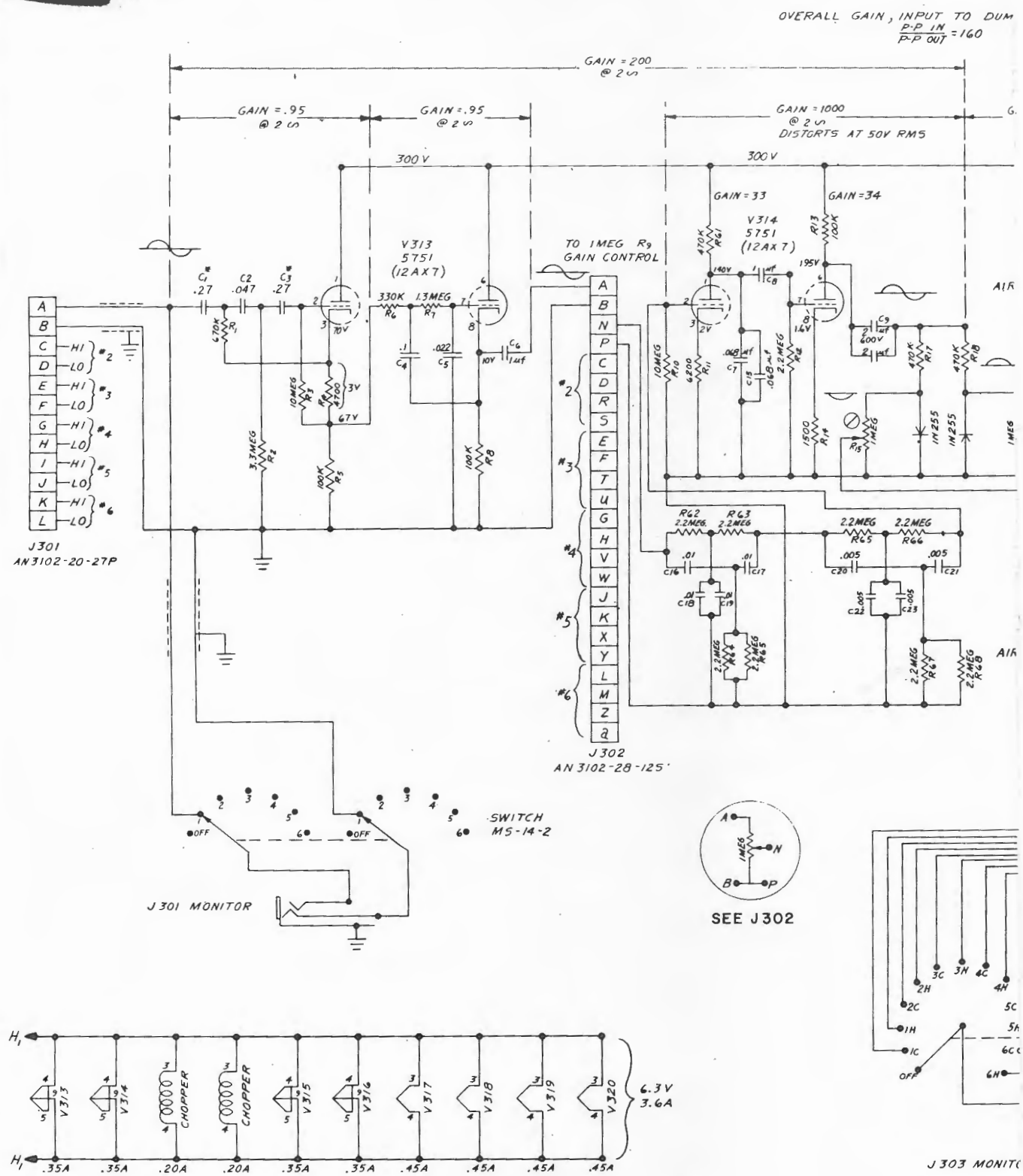

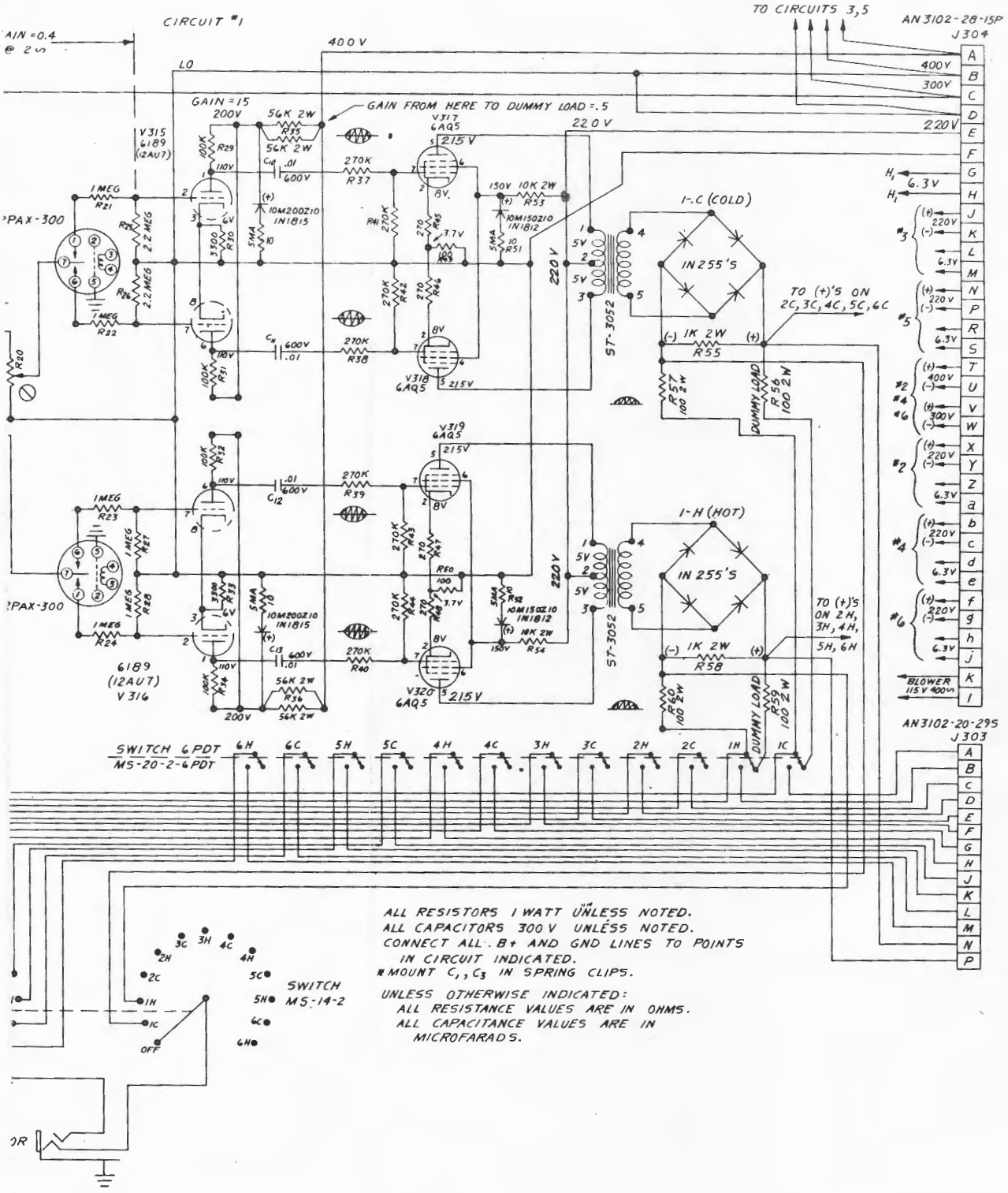

Fig. 46 - Schematic of final amplifier [redacted]
(unclass)

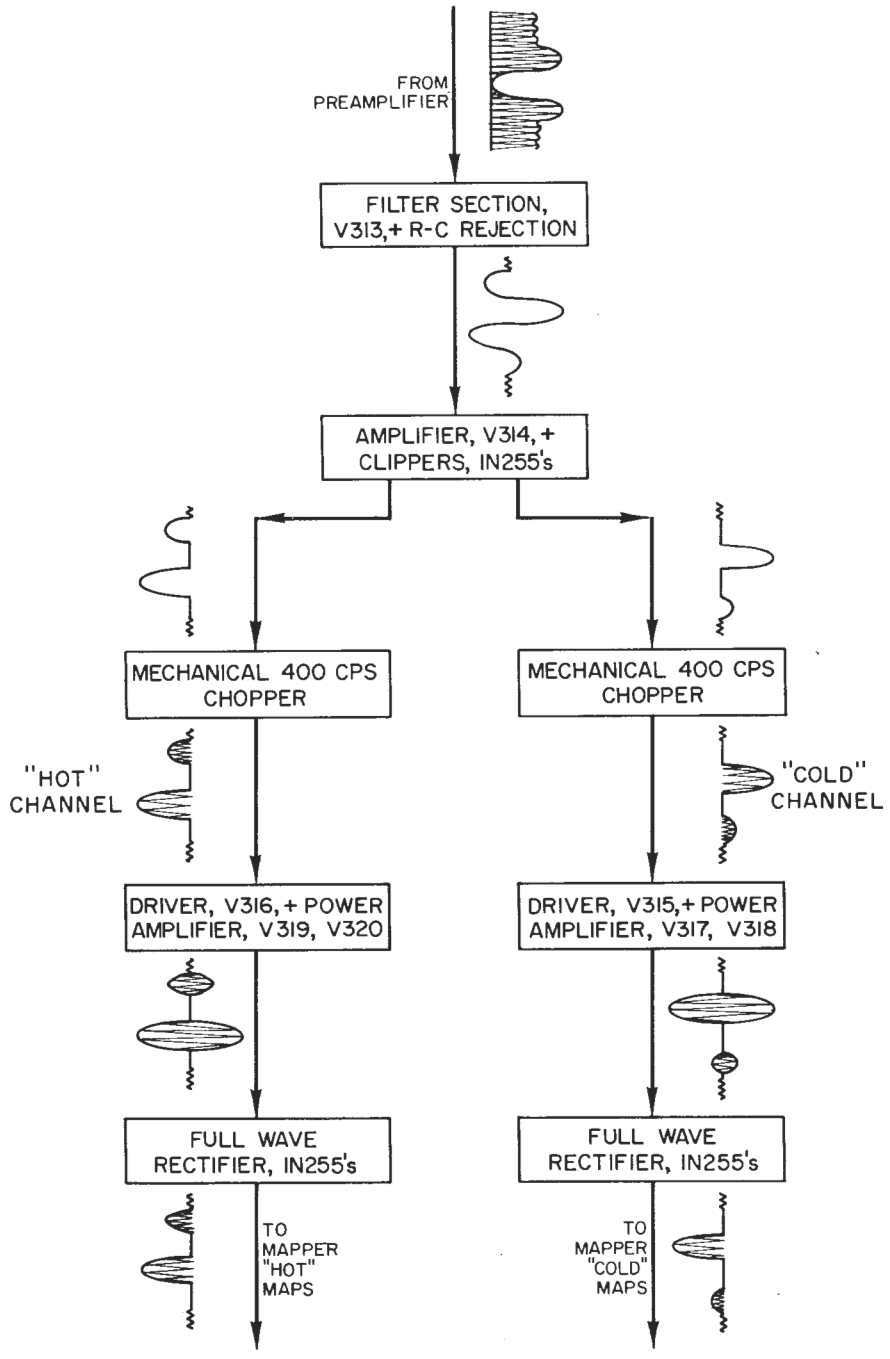

Fig. 47 - Functional diagram for final amplifier ([redacted]) (unclass)

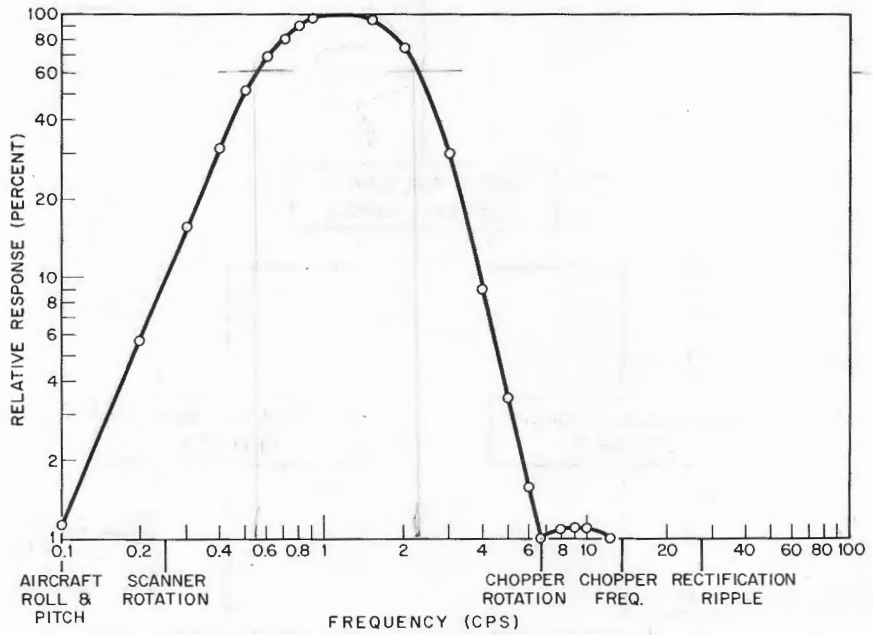

Fig. 48 - Frequency response of final amplifier

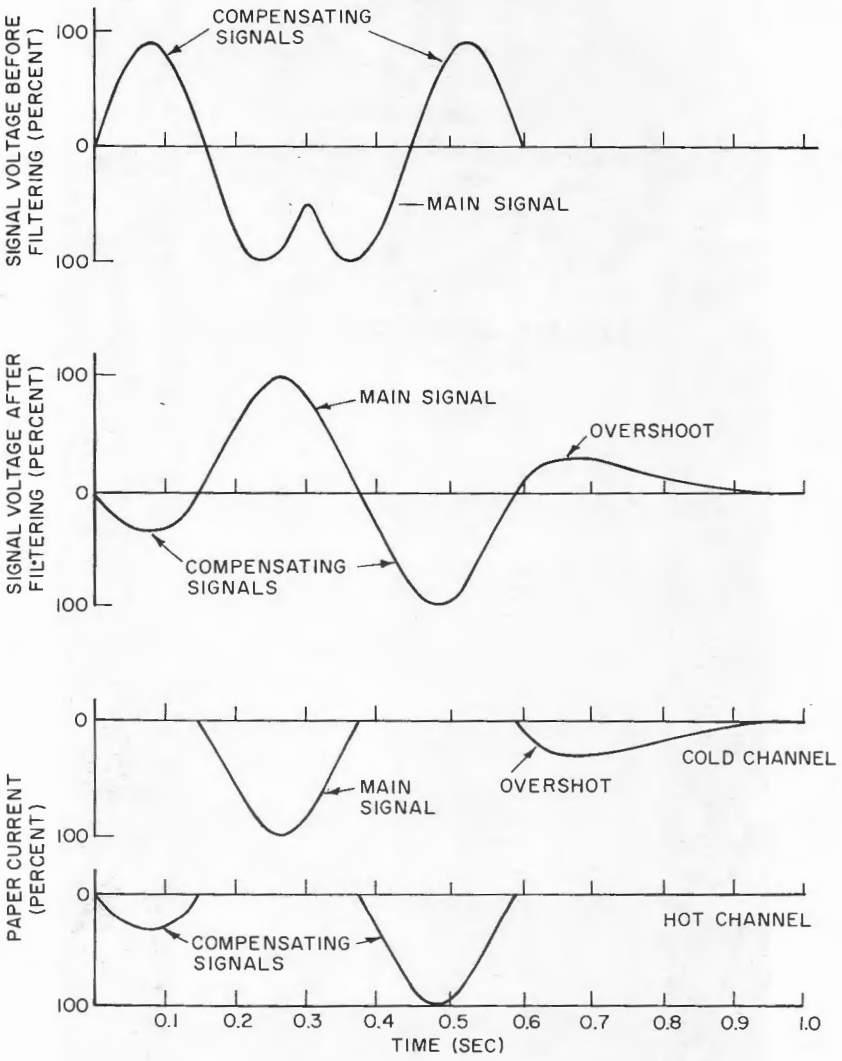

Fig. 49 - Details of a signal pulse from a relatively narrow target before and after filtering and dissection [redacted] (unclass)

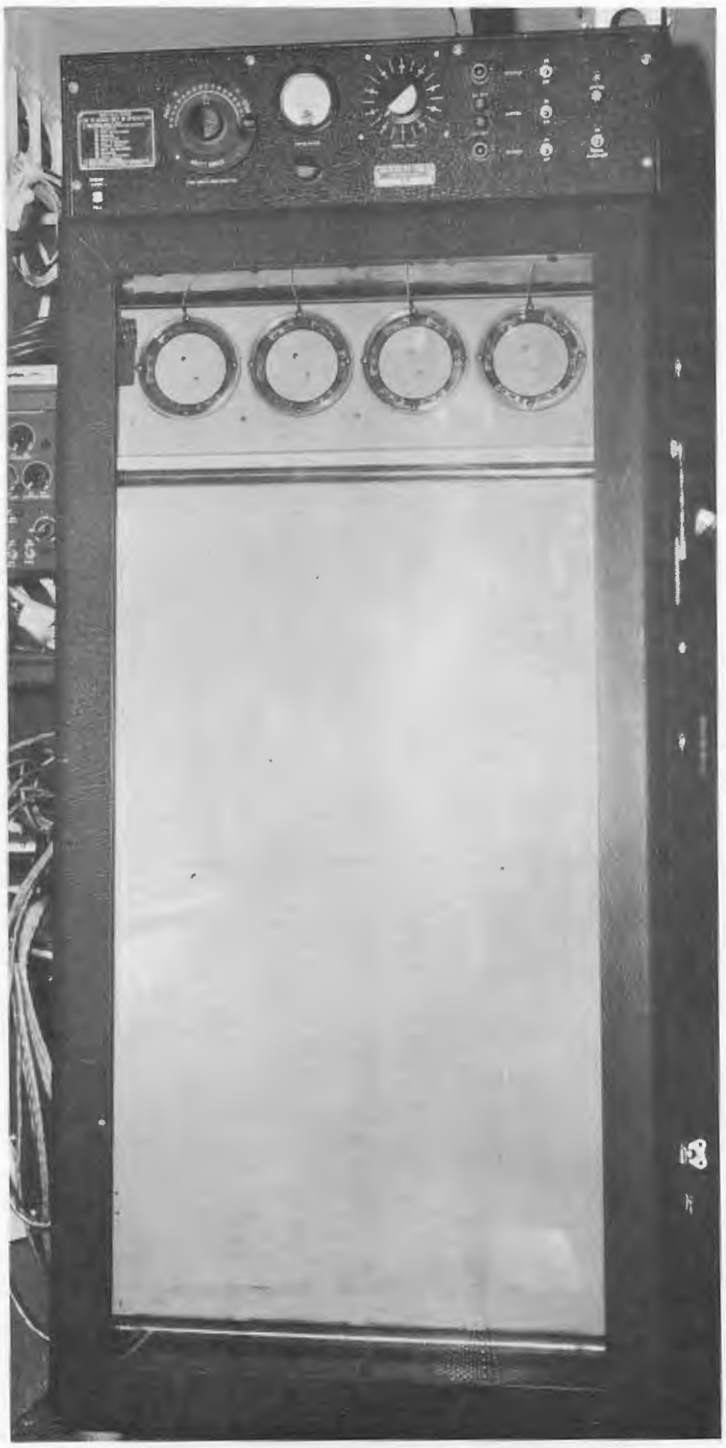

Fig. 50 - Front view of three-coordinate mapper [redacted] (unclass)

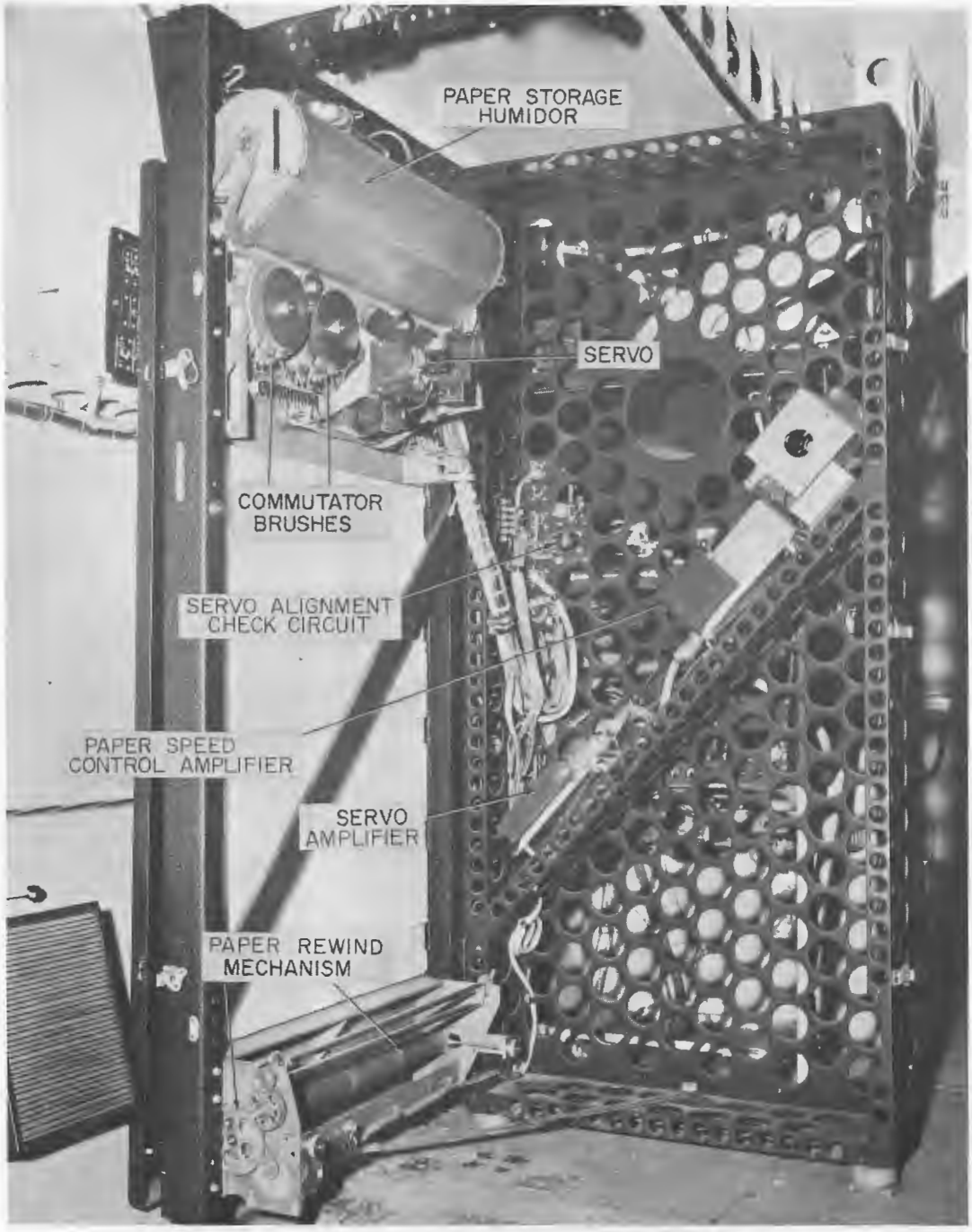

Fig. 51 - Interior of three-coordinate mapper [redacted] (unclass)

[redacted]

Fig. 52 - Writing mechanism in three-coordinate mapper [redacted] (Unclass)

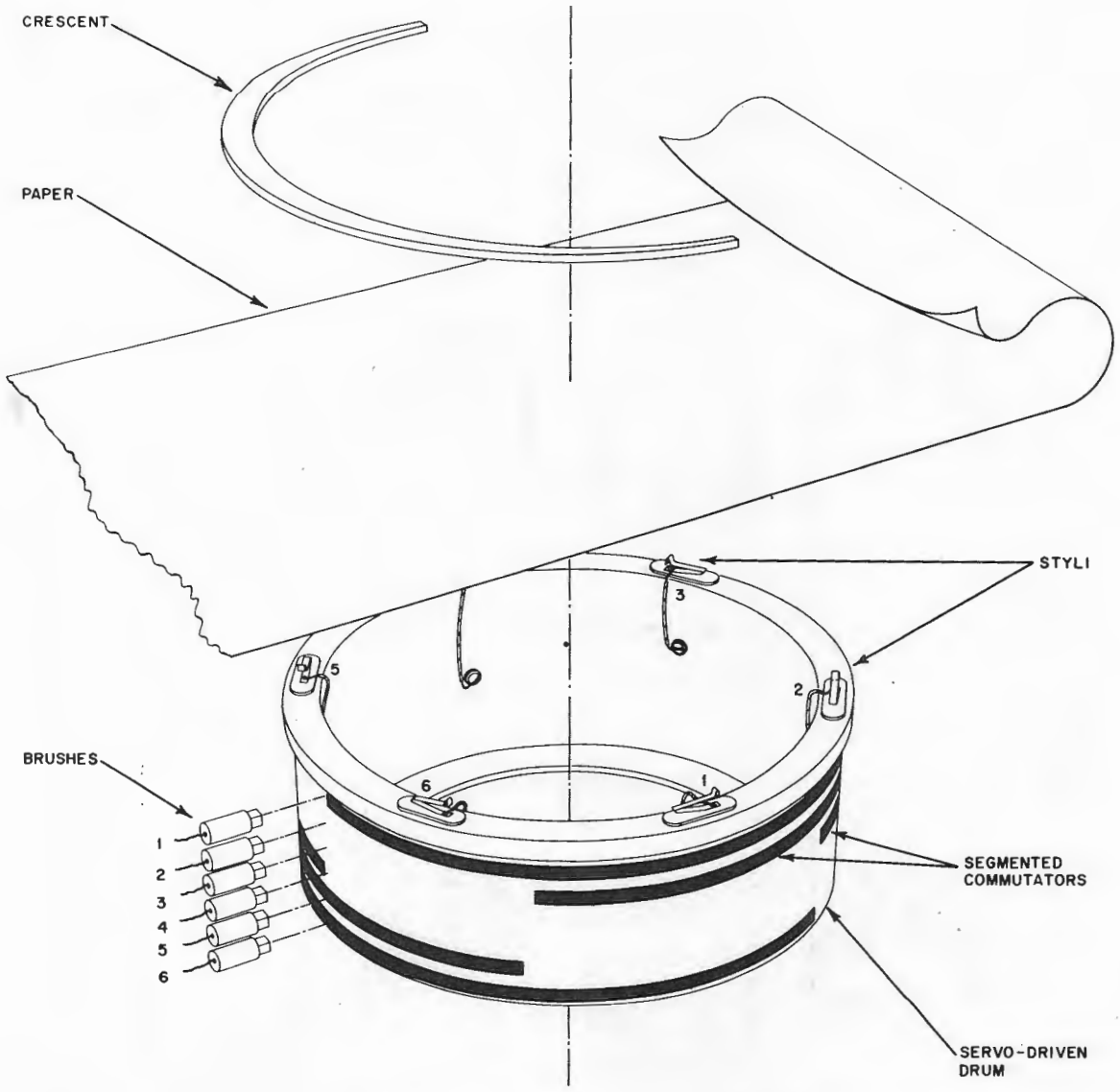

Fig. 53 - Diagram of writing mechanism in three-coordinate mapper [redacted] (Unclass)

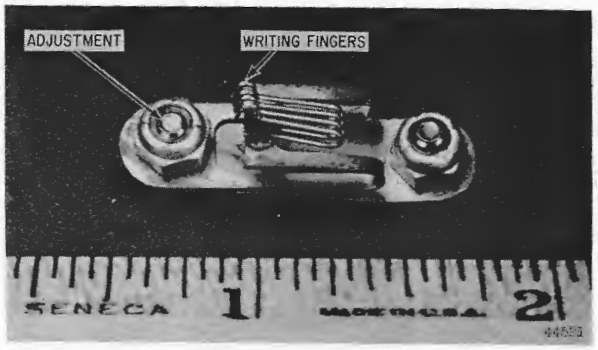

Fig. 54 - Stylus (Unclassified)

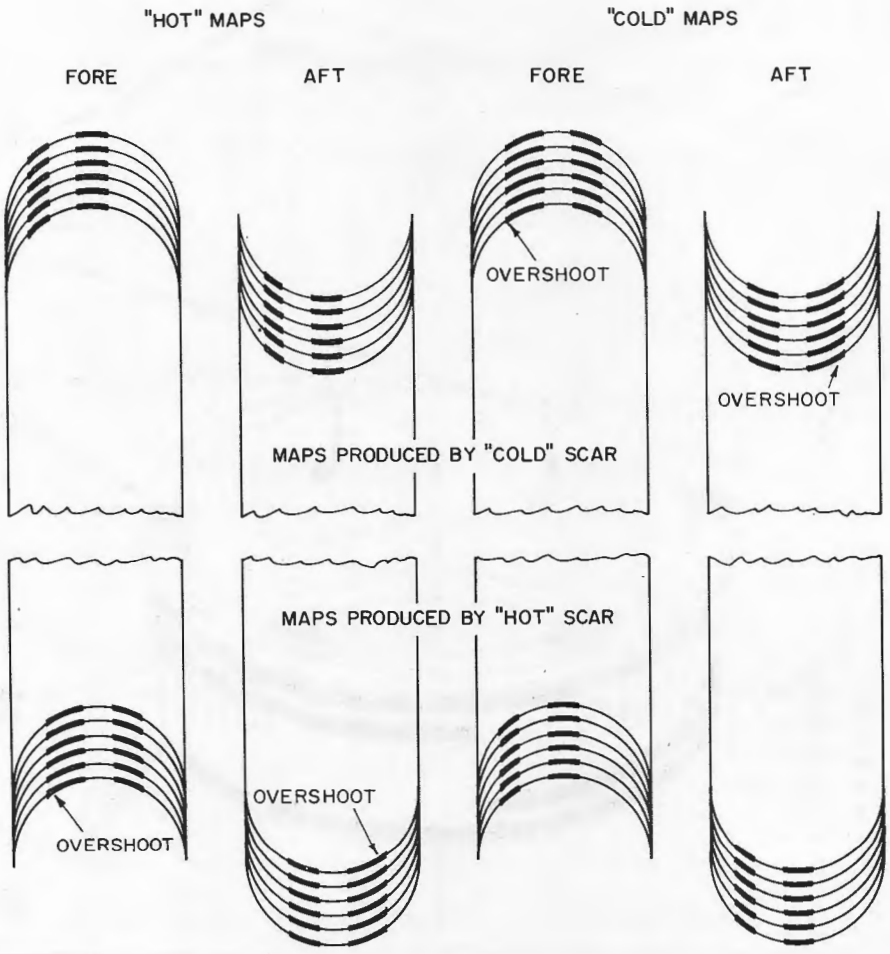

Fig. 55 - Details of the printed signal from a relatively narrow "cold" and "hot" scar ([redacted])

(unclass)

[redacted]

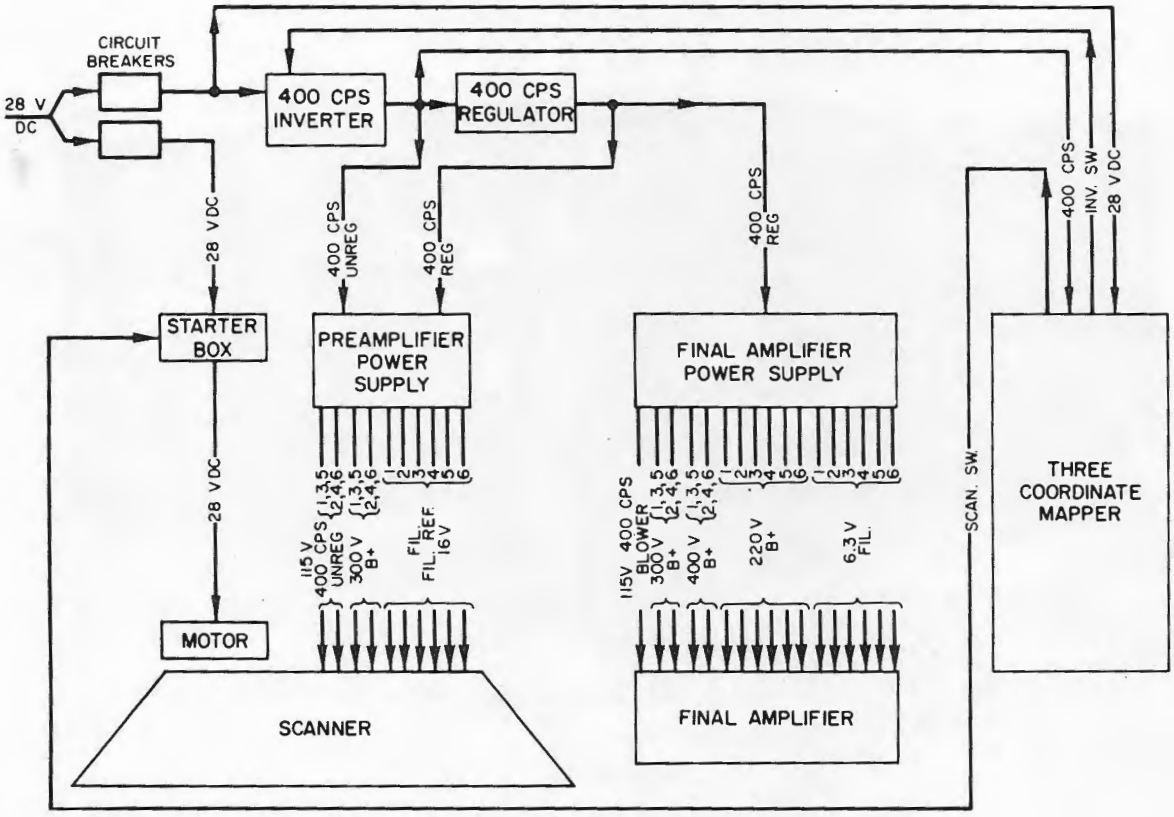

Fig. 56 - Power distribution in AN/AAR-23(XB-1) [redacted]al)

(unclass)

[redacted]

Fig. 57 - Power supply for all six preamplifiers (Unclassified)

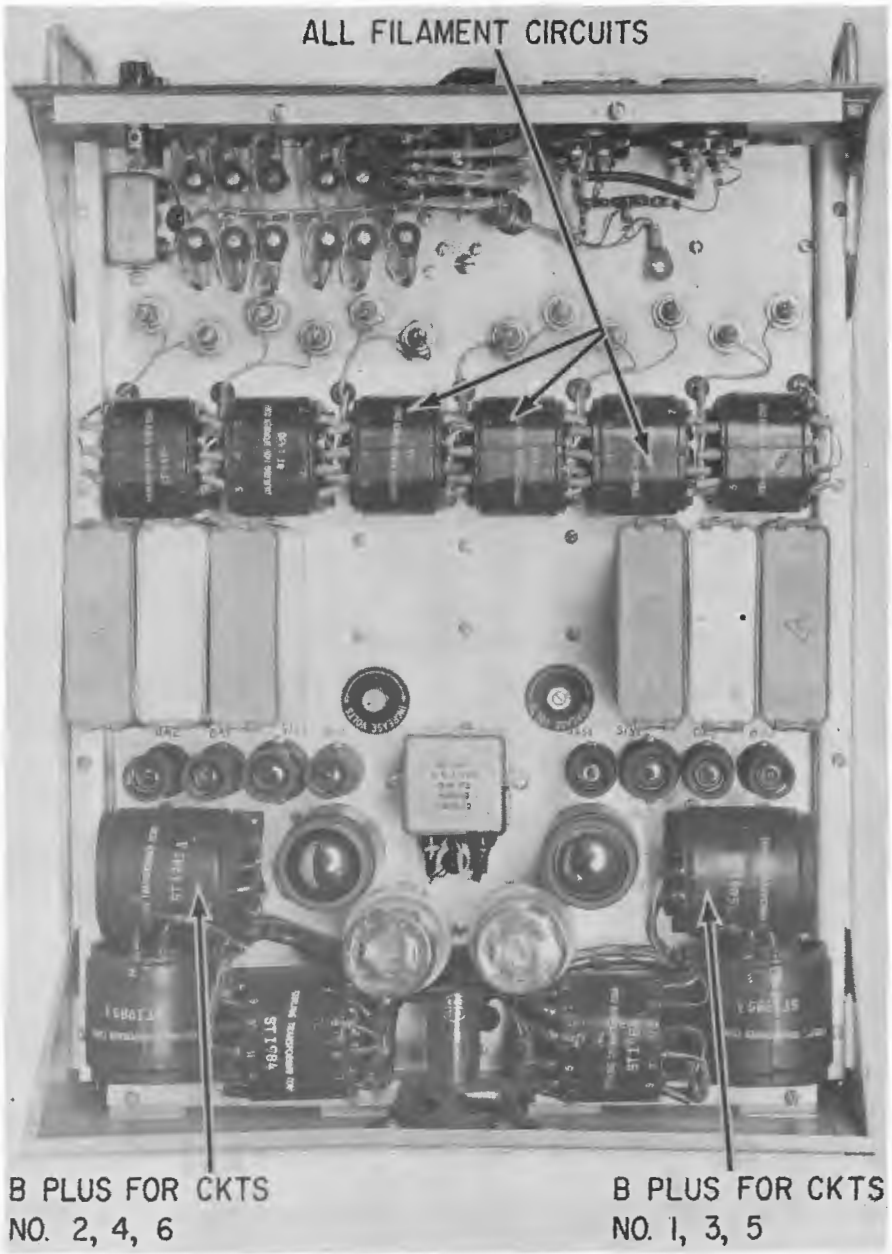

Fig. 58 - Top view of power supply
for preamplifiers (Unclassified)

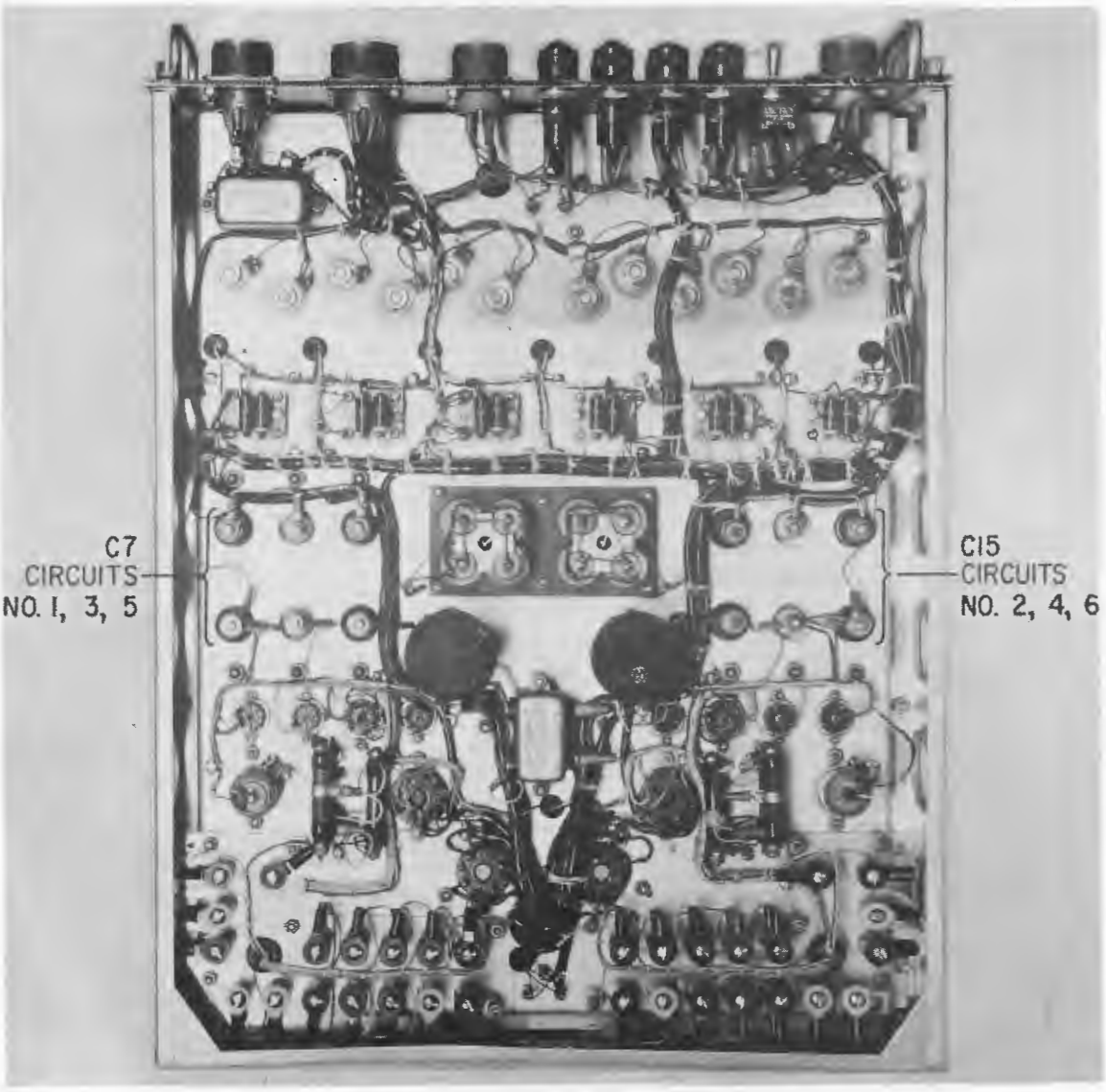

Fig. 59 - Bottom view of power supply for preamplifiers (Unclassified)

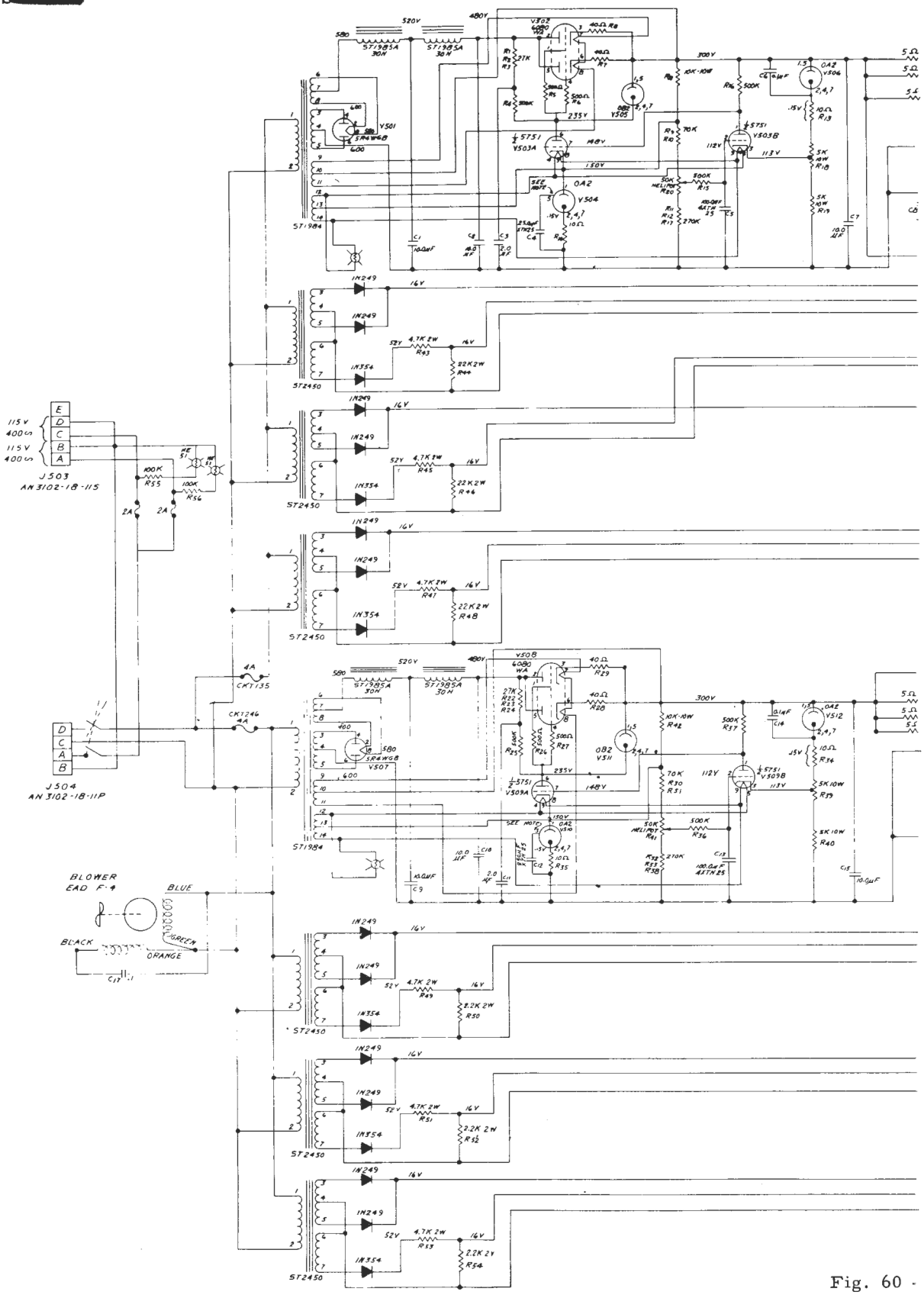

Fig. 60 -

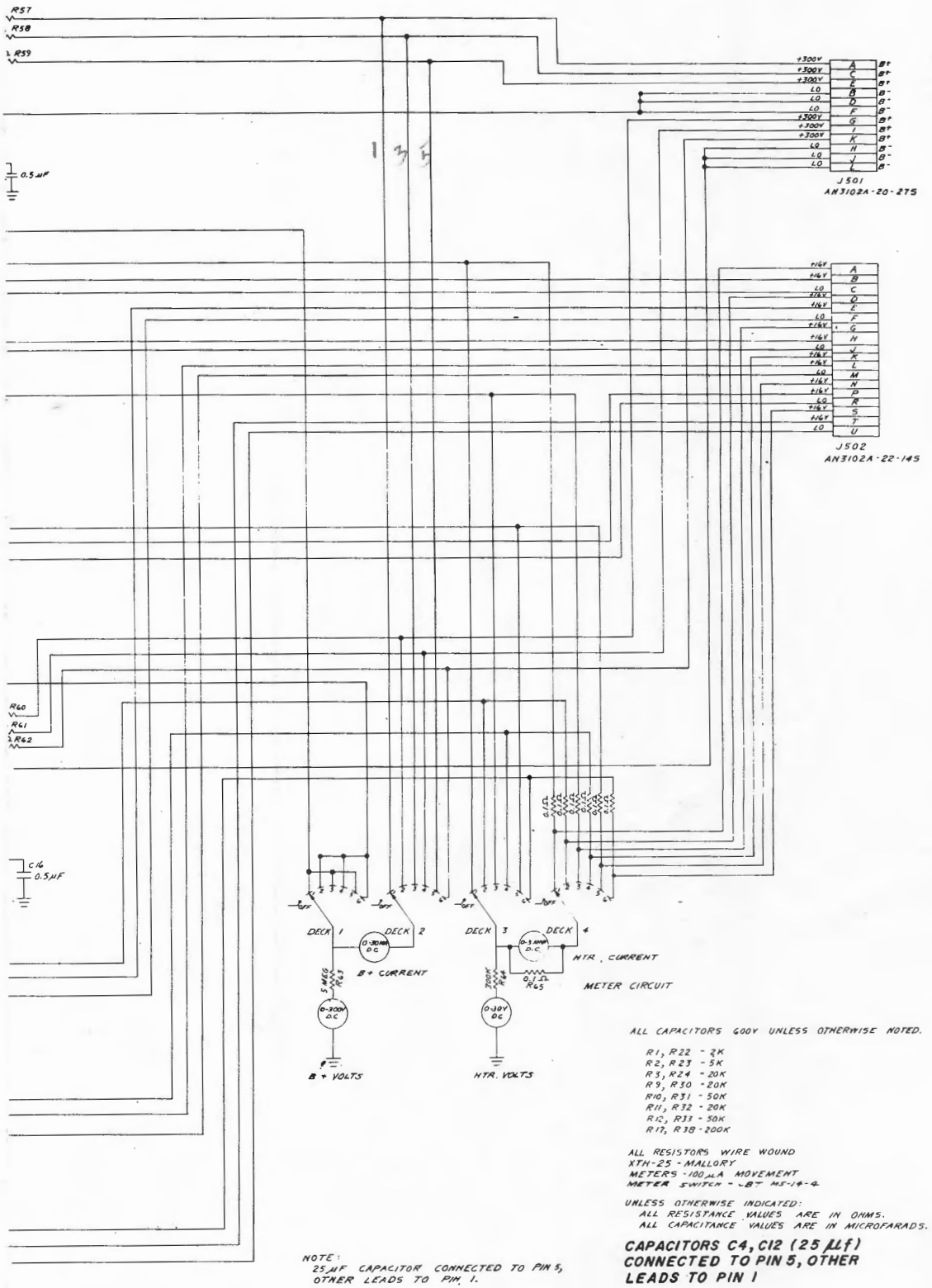

- Schematic of preamplifier power supply. (Unclassified)

Fig. 61 - Power supply for final amplifier (Unclassified)

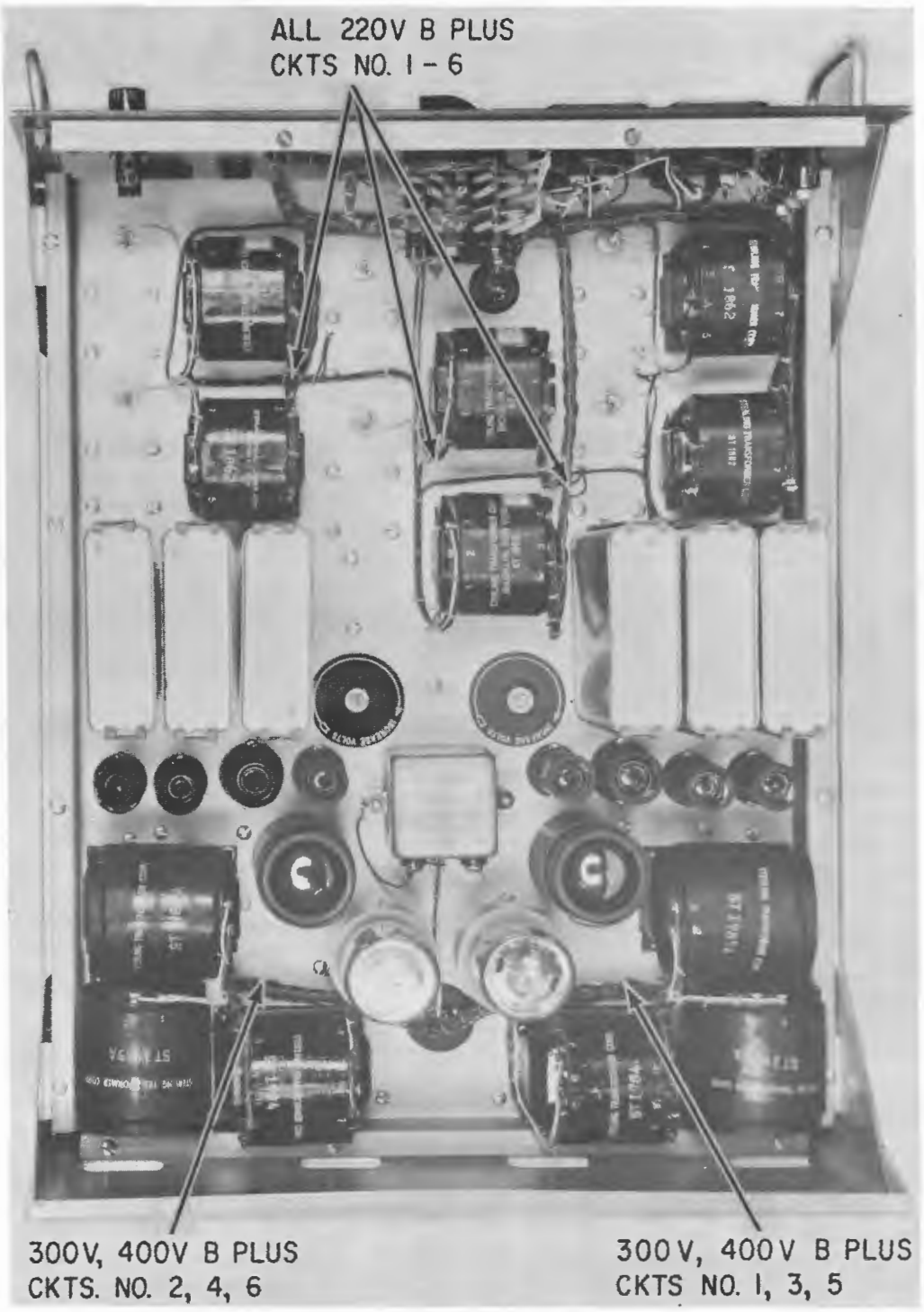

Fig. 62 - Top view of power supply for final amplifier (Unclassified)

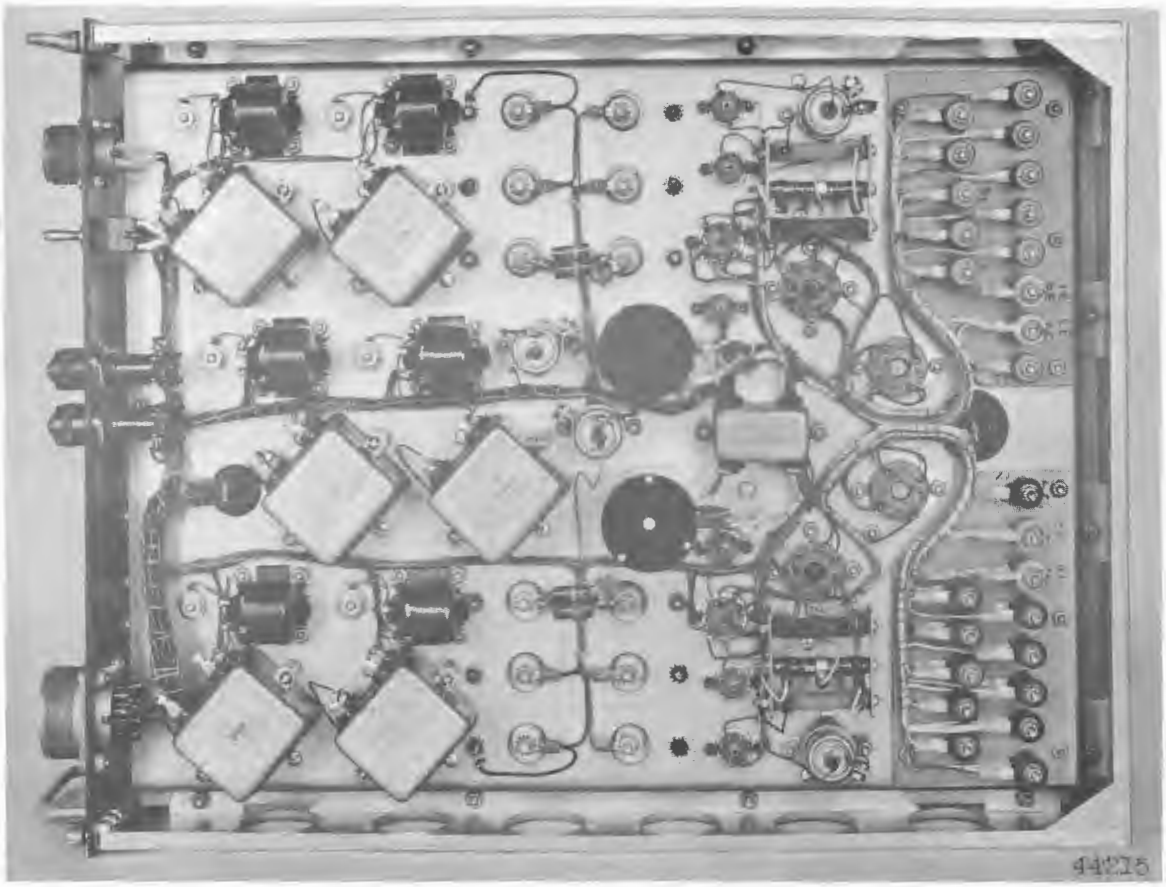

Fig. 63 - Bottom view of power supply for final amplifier (Unclassified)

[redacted]

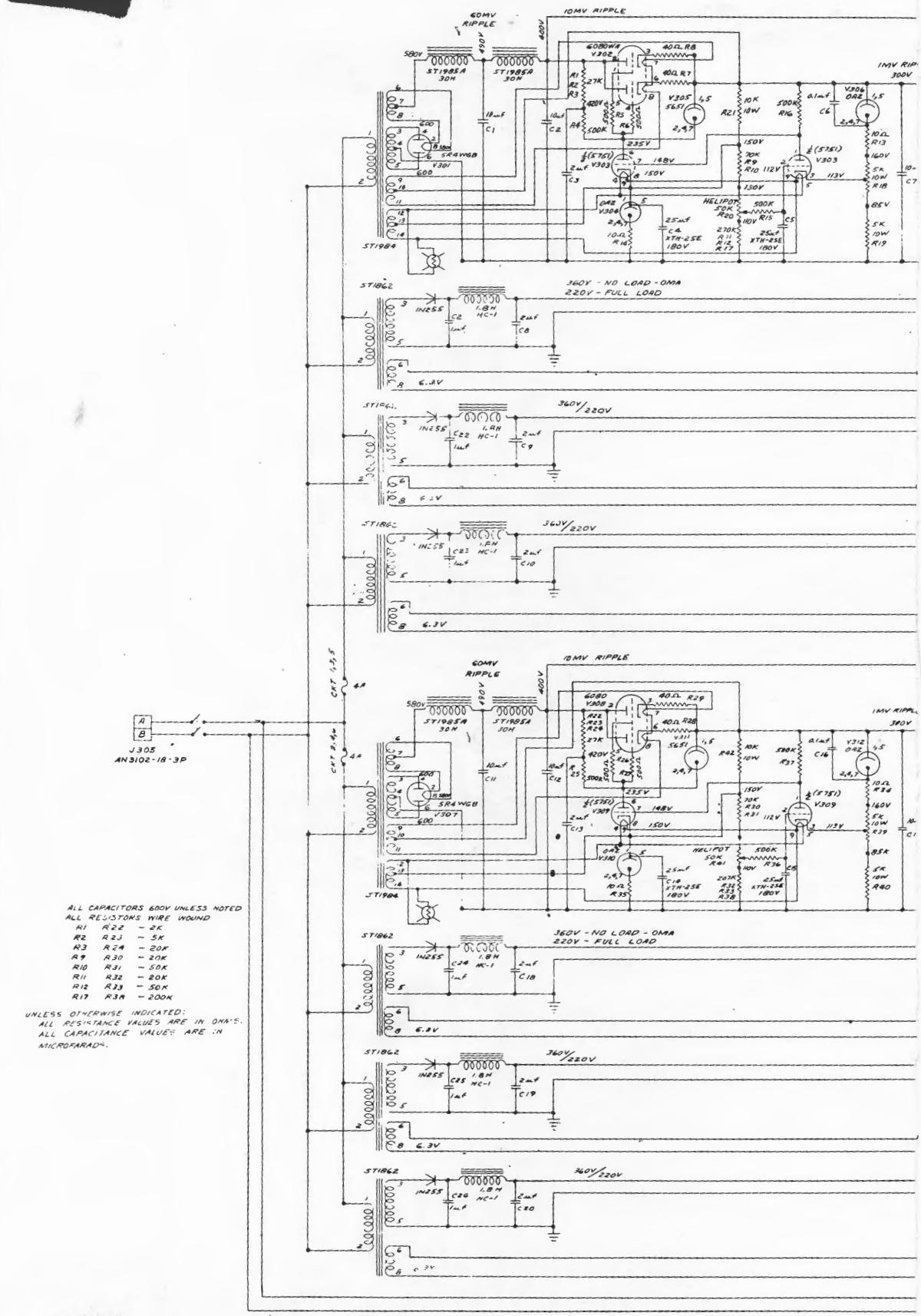

ALL CAPACITORS 600V UNLESS NOTED
ALL RESISTORS WIRE WOUND

R1	R22	– 2K
R2	R23	– 5K
R3	R24	– 20K
R9	R30	– 20K
R10	R31	– 50K
R11	R32	– 20K
R12	R33	– 50K
R17	R34	– 200K

UNLESS OTHERWISE INDICATED:
ALL RESISTANCE VALUES ARE IN OHMS.
ALL CAPACITANCE VALUES ARE IN MICROFARADS.

[redacted]

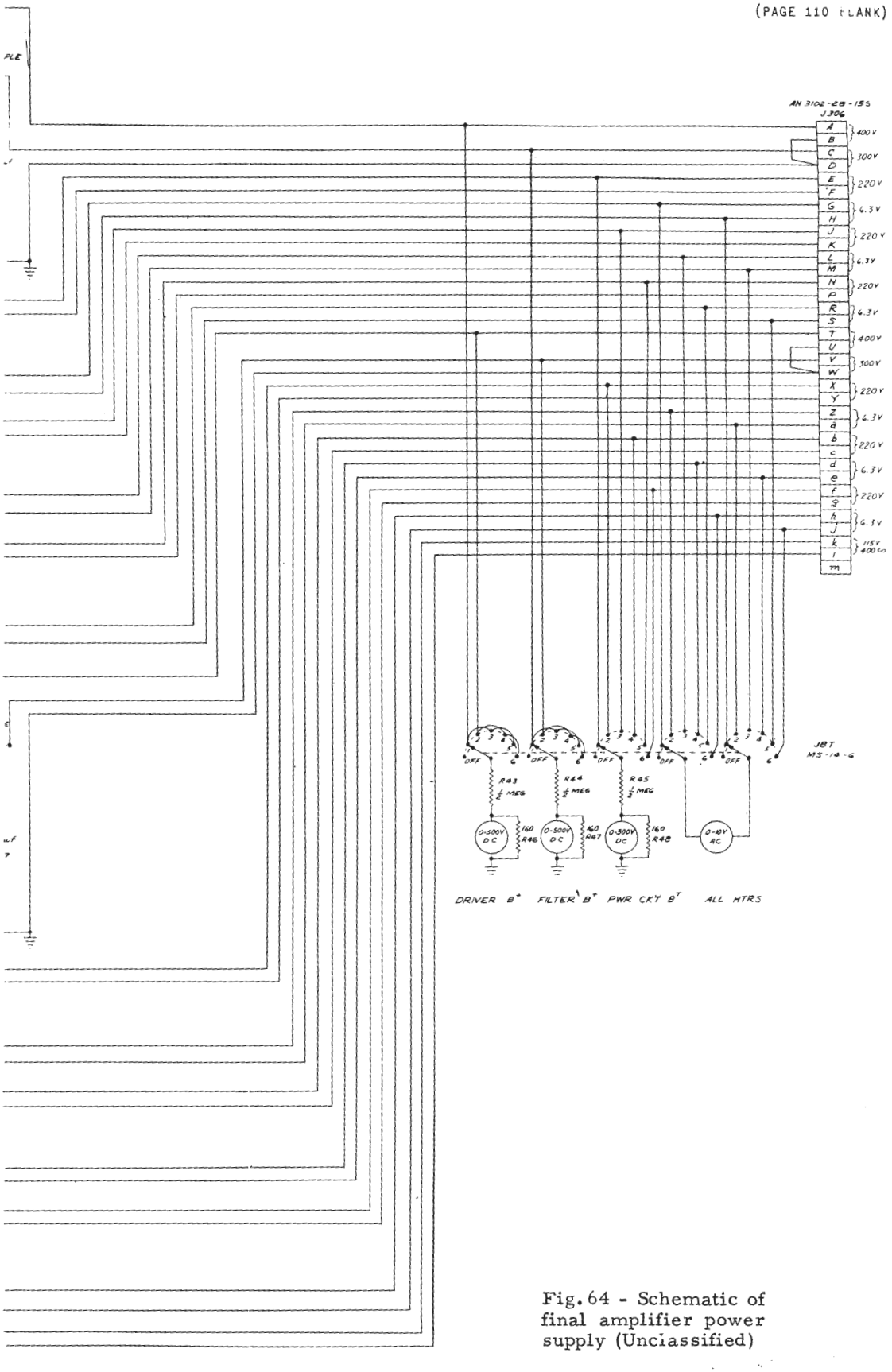

Fig. 64 - Schematic of final amplifier power supply (Unciassified)

Fig. 65 - ZPG-2 airship with AN/AAR-23(XB-1) installation (Unclassified)

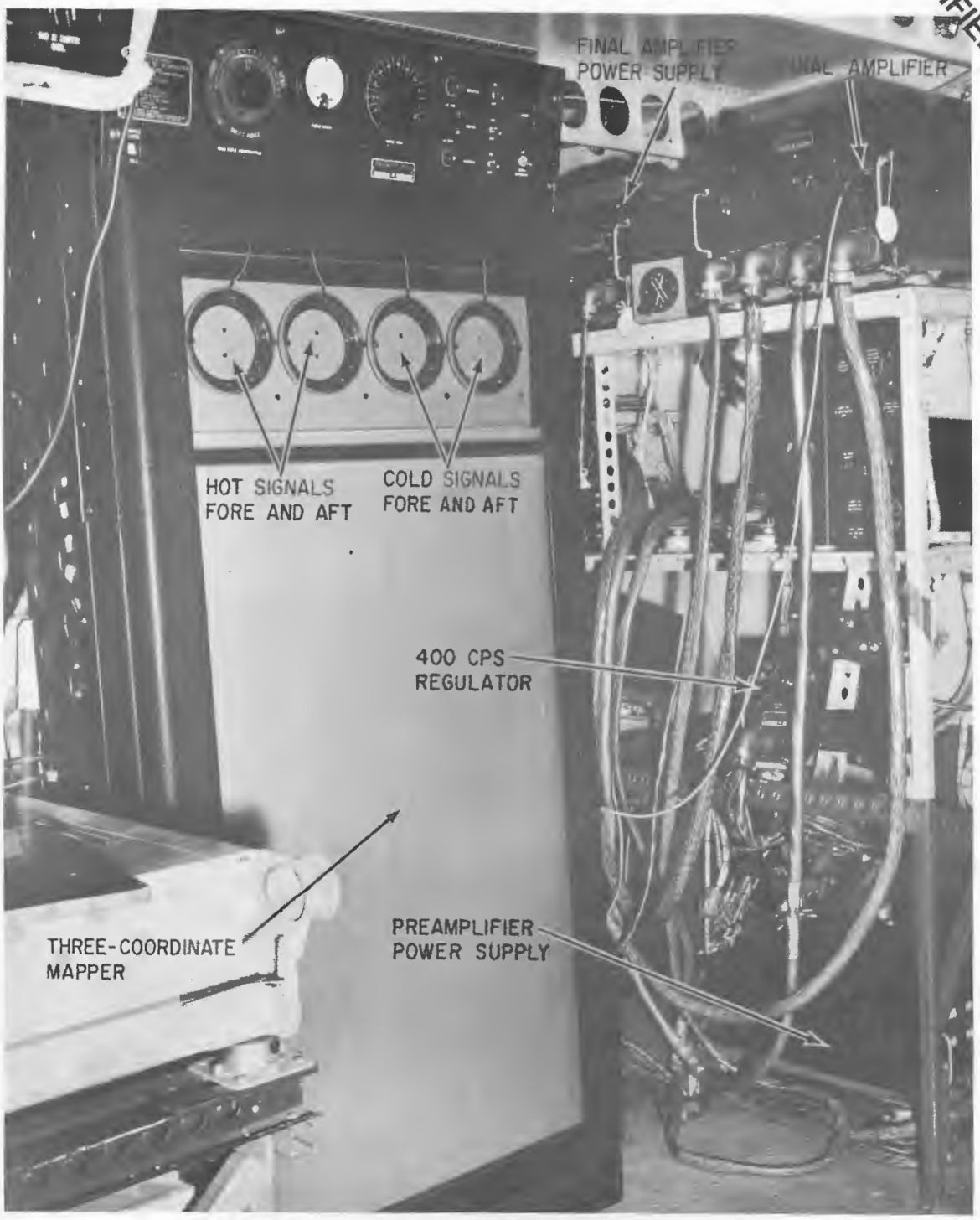

Fig. 66 - Electronic units and three-coordinate mapper installed in airship ([redacted]) (unclass)

[redacted]

Fig. 67 - Inverter installation in airship engine room. Only one 400-cps inverter is required. Spare 400-cps unit and 60-cps unit for monitoring instruments were installed for the NRL tests. (Unclassified)

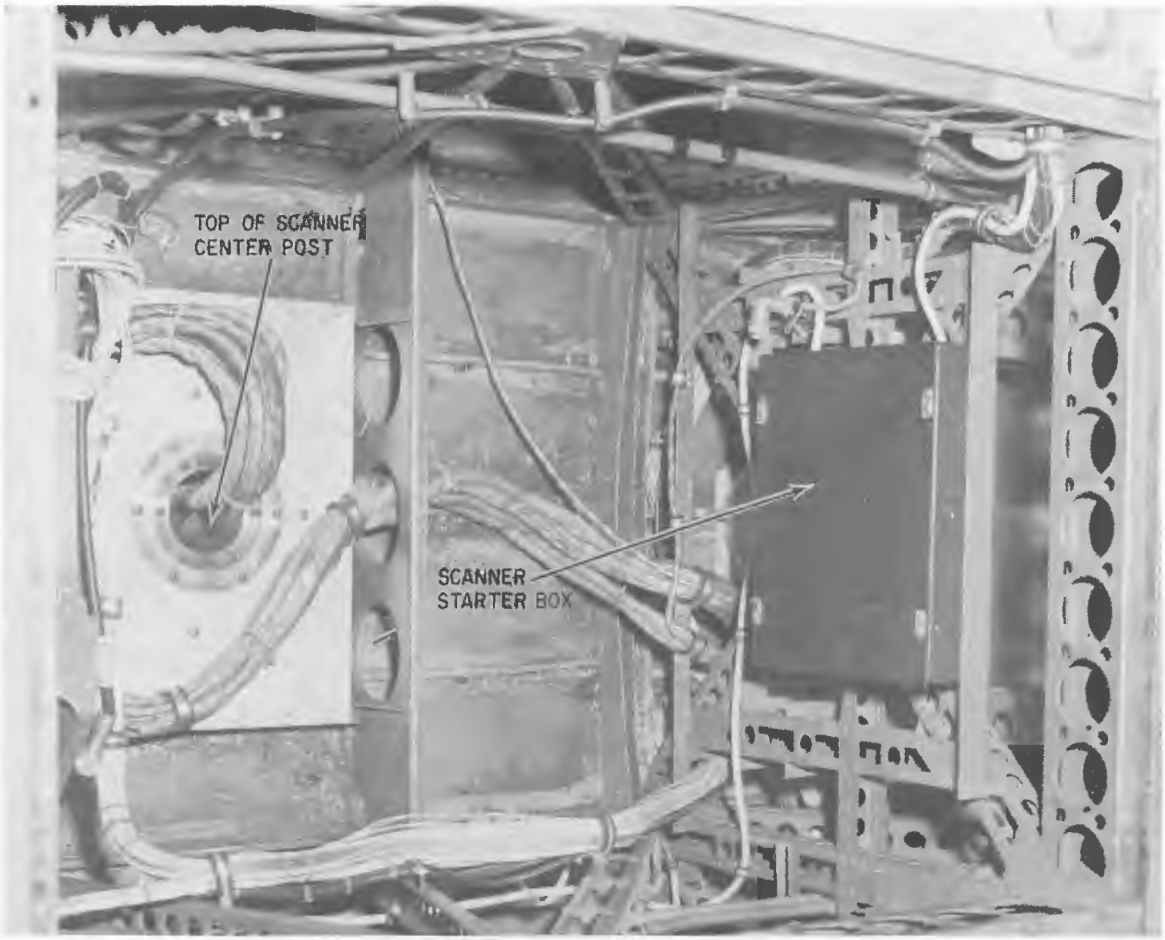

Fig. 68 - Bilge area under mechanic's compartment, showing scanner starter box (Unclassified)

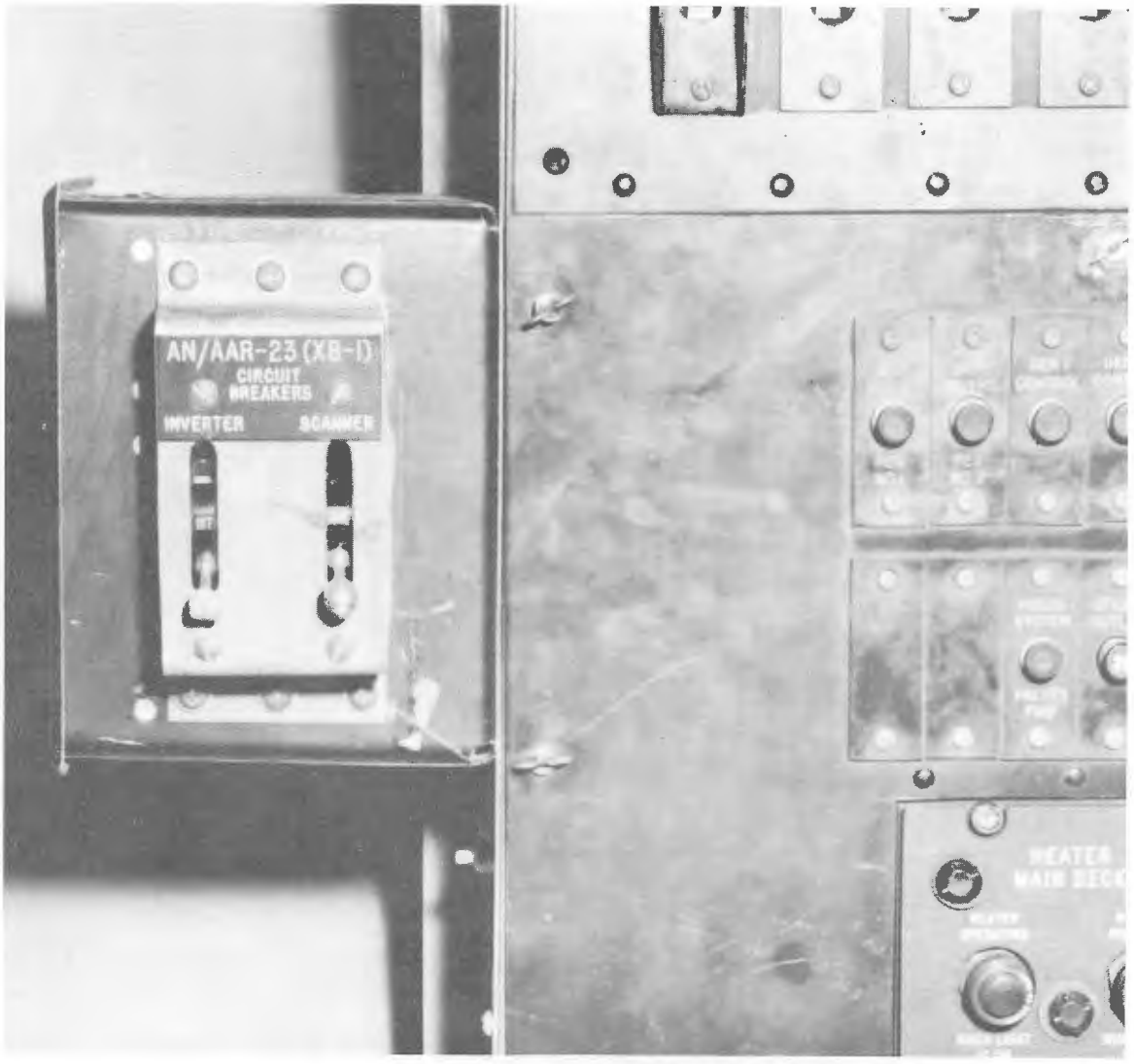

Fig. 69 - Circuit-breaker installation in mechanic's compartment (Unclassified)

Fig. 70 - Aerodynamic fairing added to existing APS-20B radome for AN/AAR-23(XB-1) installation (Unclassified)

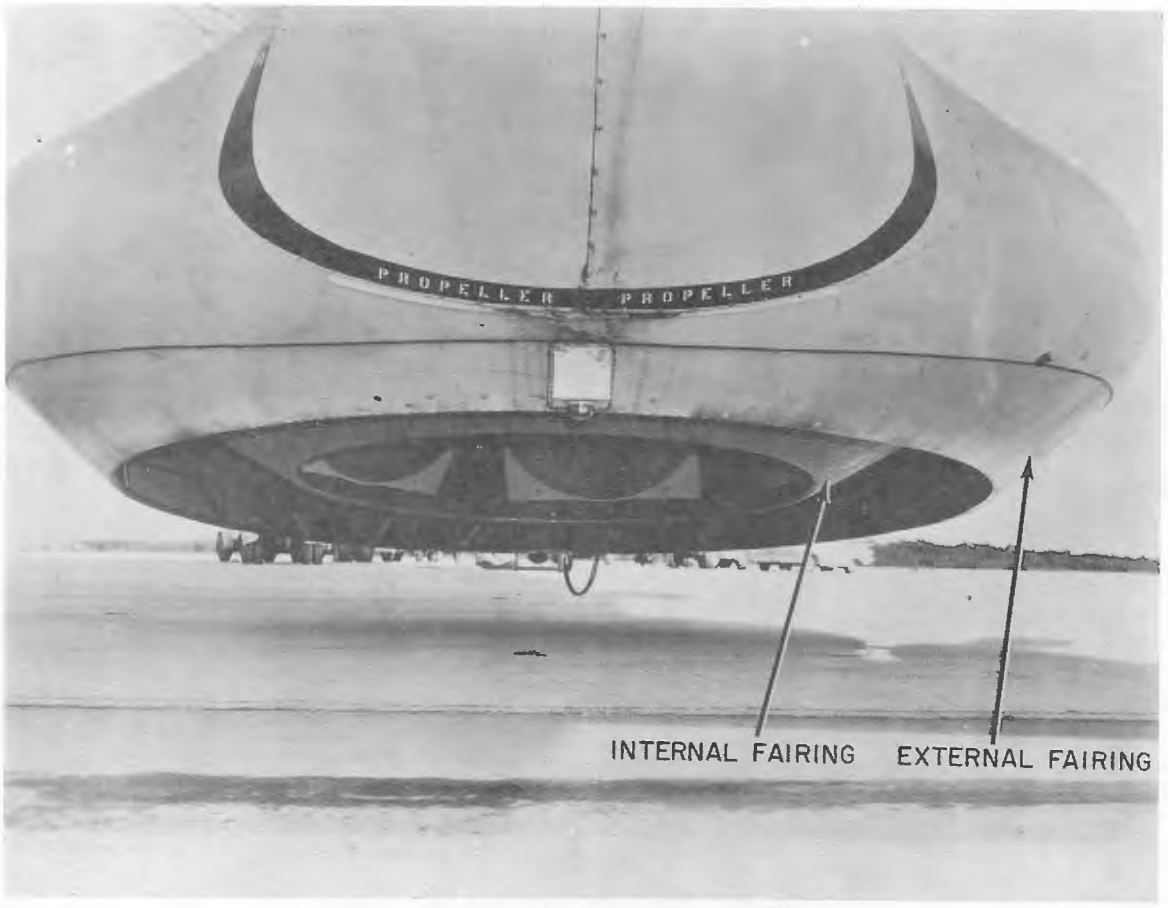

Fig. 71 - Rear view of scanner installation, showing external radome fairing and internal fairing attached to scanner ([redacted])
(unclass)

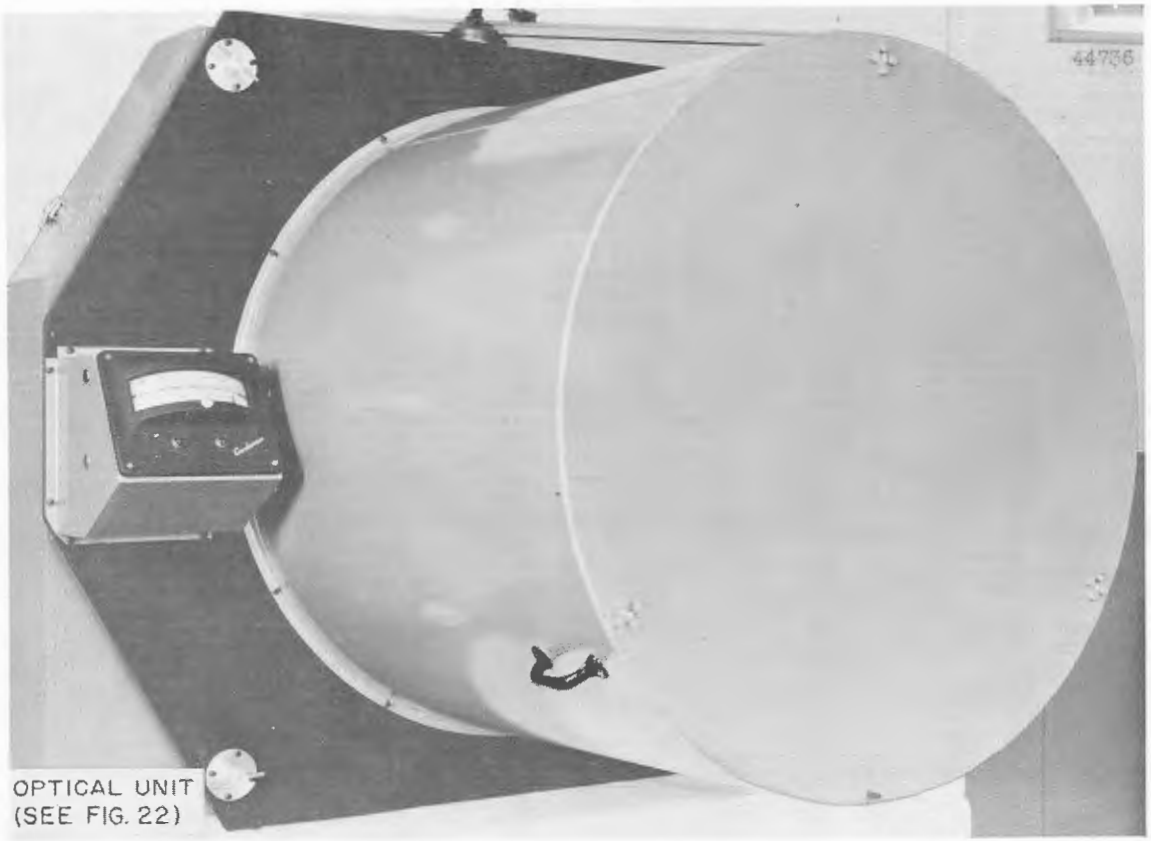

Fig. 72 - Thermal calibrator mounted on an optical unit ready for a calibration run ([redacted])

(unclass)

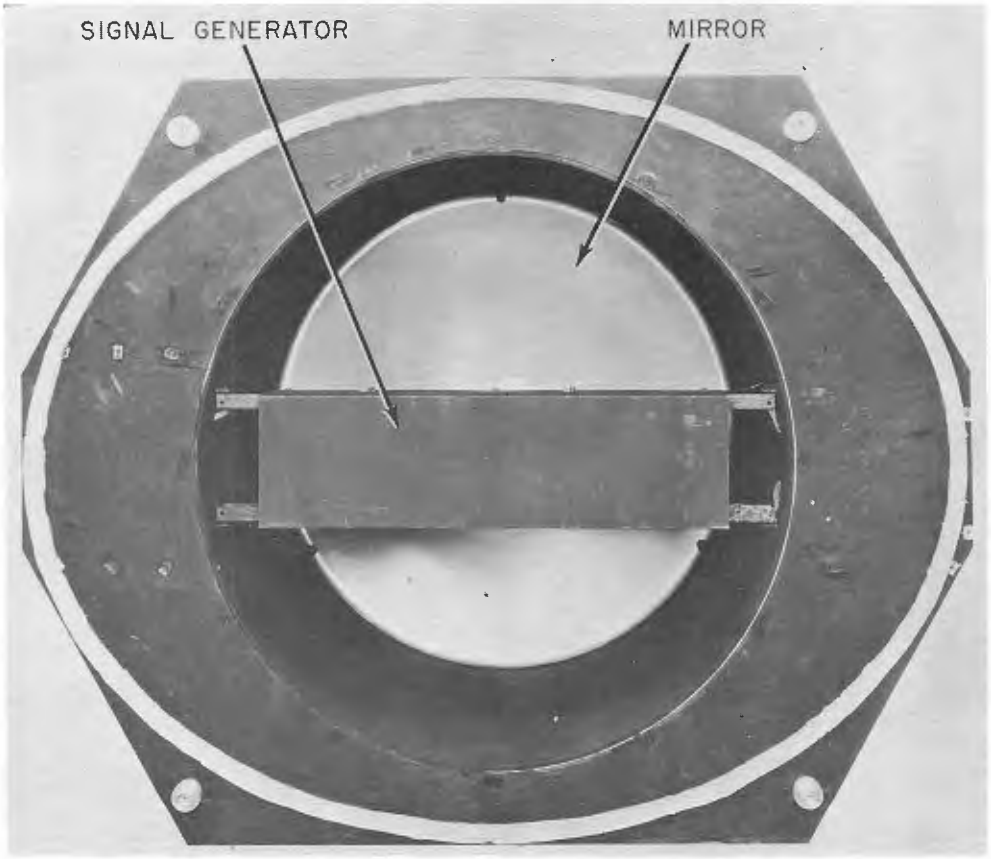

Fig. 73 - Front view of thermal calibrator with mesh attenuator removed, showing thermal signal generator mounted in focal plane of mirror ~~(Confidential)~~ (Unclass)

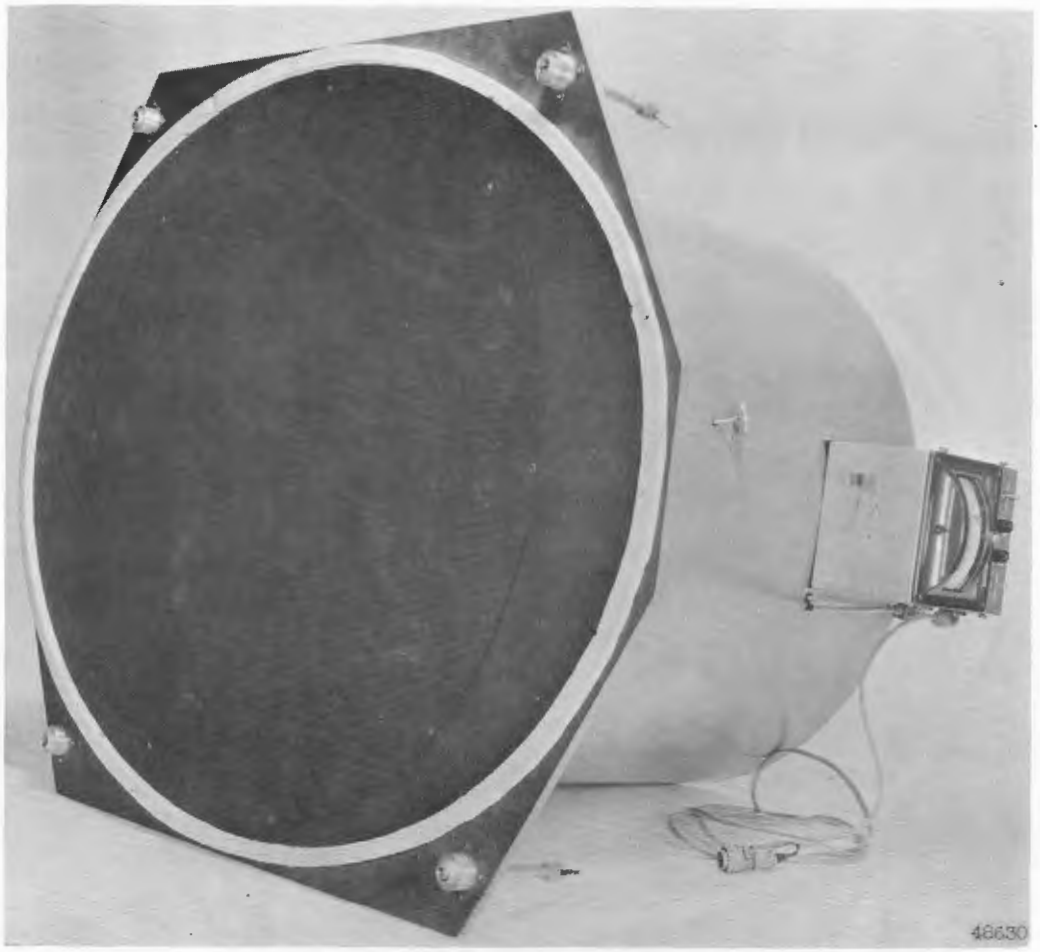

Fig. 74 - Front view of thermal calibrator, showing mesh attenuator ([redacted] (unclass)

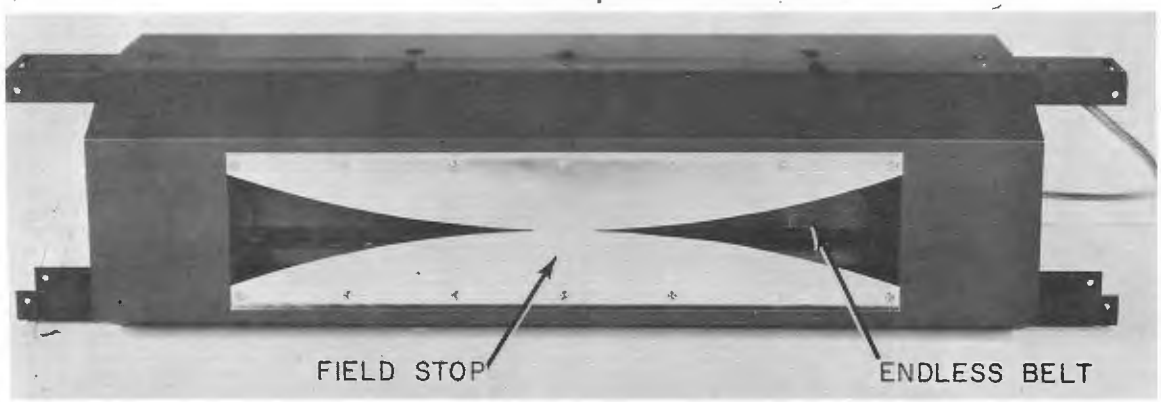

Fig. 75 - Thermal signal generator, showing field stop shaped to compensate for vignetting produced by calibrator's enclosure ([redacted]) (unclass)

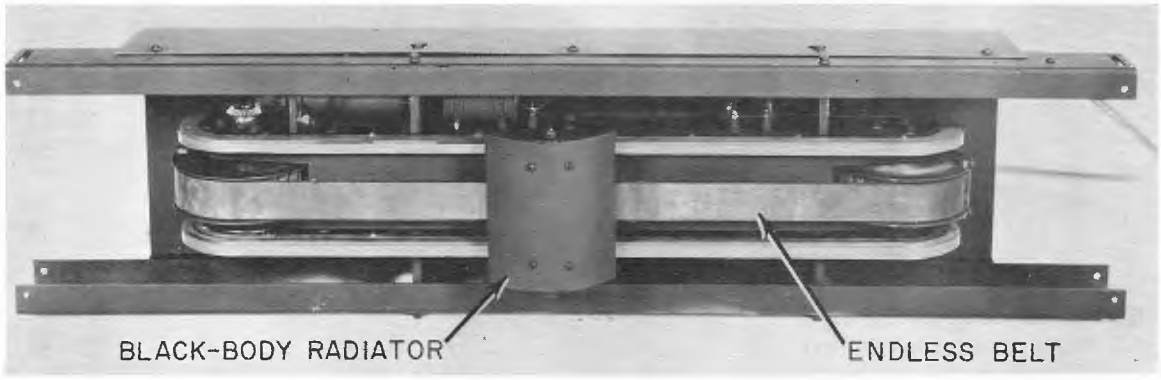

Fig. 76 - Thermal signal generator with field stop removed, showing black-body radiator mounted on endless belt ([redacted]) (unclass)

* * *